

**Guanghui Zhang**

**Methods to extract multi-dimensional  
features of event-related brain activities  
from EEG data**

July 4, 2021

Dissertation draft manuscript



## ABSTRACT

Zhang, Guanghui

Methods to extract multi-dimensional features of event-related brain activities from EEG data

Jyväskylä: University of Jyväskylä, 2021, 76 p. (+included articles)

(JYU Dissertations

ISSN 2489-9003; 404)

ISBN 978-951-39-8746-6 (PDF)

Cognitive processes are studied, among others, by analyzing event-related potentials/oscillations (ERPs/EROs) with various signal processing techniques. The commonly used processing techniques have, however, various limitations. For example, temporal principal component analysis (t-PCA) assumes, contrary to the actual situation, that waveforms of the PCA-extracted component for all subjects are the same. Also, several PCA-extracted components cannot be analyzed simultaneously since their amplitudes and polarities are diversiform. Moreover, conventional time-frequency analysis (TFA) can not efficiently distinguish between evoked EROs mixed in temporal and spectral domains. Additionally, induced EROs are usually investigated using TFA, which ignores the interactions of induced EROs in temporal, spectral, and spatial domains.

This thesis develops some EEG analysis algorithms and provides novel frameworks to investigate the cognitive mechanisms of ERPs/EROs. Specifically, in the first study, to address the problems in t-PCA, we introduce back-projection theory into t-PCA for solving the problem that several extracted components fail to be analyzed simultaneously. ERPs are extracted from single-trial EEG of an individual subject to address the unreasonable hypothesis in the group PCA analysis. In the second study, we explore evoked EROs to study some cognitive process stages that have not been explained accurately before. This is achieved by first extracting the ERPs of interest in the time domain using t-PCA and then transforming the reconstructed waveforms of ERPs into time-frequency representations (TFRs). In the third study, we exploit canonical polyadic tensor decomposition to analyze the multi-domain features of induced EROs from the fourth-order tensor formed by TFRs of single-trial EEG data. This enables us to reveal potential interactions of different modes in induced EROs.

In conclusion, the thesis introduces some new signal processing techniques and novel frameworks to study the dynamics of ERPs/EROs efficiently, which are validated using actual and synthetic EEG/ERP data.

**Keywords:** Event-related potentials/oscillations, principal component analysis, time-frequency analysis, tensor decomposition.

## TIIVISTELMÄ (ABSTRACT IN FINNISH)

Zhang, Guanghui

Menetelmiä moniulotteisten piirteiden tunnistamiseen herätevasteisiin littyvien aivotoimintojen EEG-mittauksista

Jyväskylä: University of Jyväskylä, 2021, 76 s. (+artikkelit)

(JYU Dissertations

ISSN 2489-9003; 404)

ISBN 978-951-39-8746-6 (PDF)

Kognitiivisia prosesseja tutkitaan muun muassa analysoimalla signaalinkäsittelyn keinoin erilaisia EEG:ssä havaittuja vasteita ulkoisiin ärsykkeisiin (ns. ERP/ERO, event-related potential/oscillation). Yleisimpiin menetelmiin liittyy kuitenkin selkeitä rajoitteita. Esimerkiksi ajallinen pääkomponenttianalyysi (t-PCA) olettaa, vastoin todellisuutta, että eri yksilöillä vasteajat ja -muodot ovat samat ja vain amplituudi vaihtelee. Pääkomponenttianalyysi ei myös soveltu usean rinnakkaisen vasteen analysointiin, koska vasteiden polariteetit vaihtelevat. Perinteinen aika-taajuusanalyysi (TFA) ei puolestaan tunnista ajan ja taajuuden suhteen sekottuneita herätevasteita. Sama pätee myös herätevasteiden indusoimien vasteiden analyysiin. Vasteiden useampiulotteisia vuorovaikutuksia ajan, taajuuden ja paikan suhteen ei voida erittää.

Tässä työssä kehitetään EEG analyysimenetelmiä ja uusia viitekehysiä, joilla voidaan tutkia ERP ja ERO signaaleihin liittyviä kognitiivisia mekanismeja. Ensimmäisessä osatutkimuksessa sovelletaan takaisinprojisioinnin tekniikkaa ajalliseen pääkomponenttianalyysiin (t-PCA) ja mahdollistetaan näin useamman samanaikaisen vasteen erottelu. Lisäksi osoitetaan, että menetelmää voi soveltaa ilman rajoittavaa oletusta vasteiden samankaltaisuudesta eri yksilöiden välillä. Toisessa tutkimuksessa yhdistettiin t-PCA menetelmä ja sen avulla rekonstruoidut vasteet aika-taajuus analyysiin (TFR). Näin pystytettiin saamaan tarkempaa tietoa herätteen aiheuttaman värähtelyn (ERO) dynamiikasta ja edelleen tämän taustalla olevista kognitiivisista prosesseista. Kolmannessa tutkimuksessa sovellettiin moniulotteista tensorihajotelmaa (canonical polyadic tensor decomposition) neliulotteiseen aika-taajuus muotoiseen EEG-dataan. Näin pystytettiin analysoimaan herätteiden indusoimia värähtelyjä (ERO) yhtäaikaisesti useamman tekijän suhteen ja tunnistamaan eri tekijöiden yhteisvaikutuksia aiempaa paremmin.

Yhteenvedona työssä esiteltiin uusia signaalinkäsittelytekniikoita ja lähestymistapoja ERP/ERO signaalien dynamiikan tehokkaaseen analyysiin. Uudet menetelmät validoitiin sekä synteettisellä että todellisella EEG-datalla.

Avainsanat: Aika-taajuusanalyysi, pääkomponenttianalyysi, herätepontiaali, herätevärähtely, tensorihajotelmat

<b>Author</b>	Guanghui Zhang Faculty of Information Technology University of Jyväskylä Finland
<b>Supervisors</b>	Timo Tiihonen Faculty of Information Technology University of Jyväskylä Finland
	Fengyu Cong School of Biomedical Engineering Dalian University of Technology China Faculty of Information Technology University of Jyväskylä Finland
	Zheng Chang Faculty of Information Technology University of Jyväskylä Finland
	Tapani Ristaniemi Faculty of Information Technology University of Jyväskylä Finland
<b>Reviewers</b>	Li Hu Department of Psychology University of Chinese Academy of Sciences China
	Zhiguo Zhang School of Biomedical Engineering Shenzhen University China
<b>Opponent</b>	Danilo Mandic Department of Electrical and Electronic Engineering Imperial College London United Kingdom



## ACKNOWLEDGEMENTS

I would like to thank the people who are always with me during my doctoral research. Without their help, encouragement, and support, it is impossible to achieve this dissertation.

First of all, I would like to give my most sincere gratitude to my supervisors: Prof. Tapani Ristaniemi, Prof. Fengyu Cong, Docent Zheng Chang, and Prof. Timo Tiihonen, for their selfless guidance and support to my doctoral research in the past three years. I feel so lucky that they are my supervisors. Their ingenious suggestions, rich life experiences, and unparalleled knowledge, have a substantial effect on making progress in both my academic career and my life.

Thanking Tapani for providing me with such an opportunity to study at the University of Jyväskylä to pursue my doctoral degree. In the first half of the duration of my doctoral study, he always responded my demands in time and gave valuable comments and suggestions for my reports. This work is dedicated to the memory of Prof. Tapani Ristaniemi whose integrity, wisdom, and grace should be remembered and missed.

Fengyu is the guider of my academic career. He patiently taught me how to search and read articles, how to combine the theory with basic stuff, and how to use some platforms (e.g., MATLAB) to analyze ERP data, etc. All in all, he helped me establish a solid foundation of the building of my work. We frequently discussed the issues in my work and he could always give me informative feedback even on the weekend and holiday. Moreover, he also encouraged and supported me to attend advanced seminars and conferences to learn novel ideas and thoughts from other researchers. Besides academic issues, he taught me how to get along with our cooperators and overcome troubles in daily life.

Zheng and Timo are named as my supervisors in the last stage (2020.09-2021.06) of my doctoral study. To Zheng, he is like an older brother rather than a supervisor, and he always shares his personal research experiences with me and gives straightforward and efficient suggestions for my academic and life issues. Timo always gives me rapid responses in time whenever I send an email to him. He taught me how to handle a methodology topic and how to organize the outline, what really counts is to tell a remarkable 'story' to other researchers about our work at the stage of drafting. He also reminded me to follow out all the stages for preparing the thesis pre-examination and final defense in time and gave me useful help to my graduation. His strict and responsible attitude towards academics and life inspires me a lot as well. Additionally, I would like to thank him to help me translate the abstract and summary parts of my dissertation into Finnish.

I thank my cooperators, Dr. Yingzhi Lu, Dr. Xiawen Li, Dr. Jiacheng Chen, Dr. Yingying Wang, and Dr. Xue Xia from Shanghai University of Sport, for sharing their EEG datasets with me. I also would like to thank Associate Prof. Peng Li from Shenzhen University for his patient answers to my questions in the cognitive field and EEG data sharing. Furthermore, I would like to thank

Associate Prof. Xueyan Li and Prof. Shuo Cao from the Dalian University of Technology for helping me to improve the quality of the included articles so that the papers are more logical and readable.

I am also grateful to the reviewers of my dissertation, Prof. Li Hu and Prof. Zhiguo Zhang, for their valuable suggestions and constructive comments. I give my sincere appreciation to Prof. Danilo P. Mandic for accepting the invitation and being my opponent in my public defense.

Furthermore, I am extremely grateful to Deqing Wang, Reza Mahini, Xulin Wang, Antti-Jussi Lakanen, Ville Isomottonen, Dongdong Zhou, Xiaoshuang Wang, Huashuai Xu, Zhonghua Chen, Wenya Liu, Jia Liu, Rui Yan, Yongjie Zhu, Lili Tian, Yalin Sun, Wei Qi, Xichu Zhu, Xiaobang Sun, and many other friends, who are accompanied with me in Jyväskylä so that the life is lovely and interesting. Moreover, giving my thanks to Fan Li, Guoqiang Hu, Rao Fu, Liting Song, Ying Li, Yuxing Hao, Xiaoyu Wang, Wei Zhao, and all other members of ASAP laboratory at the Dalian University of Technology for their support and help during my doctoral study.

I would like to thank the China Scholarship Council for providing funding to support me in for studying my Ph.D. degree at the University of Jyväskylä (No.20180606165) and I am also extremely grateful to the University of Jyväskylä for providing such a critical training platform.

Last but not least, I give my most profound appreciation to my parents, my older sister, my younger brother, my grandpa, and all the other family members for their endless love and support. Also, I would like to thank my girlfriend, Dingding Feng, who always accompanied me every day so that I do not feel lonely in such a coronavirus situation. She always takes some actions to cheer me up when I can not focus on my research, and she also tells some funny stories to make me feel happy and joyful when I was depressed. With the help and support from my family, I can finally achieve my Ph.D. study without any pressure.

To myself, go ahead and never stop.

Jyväskylä, June 2021  
Guanghui Zhang

## LIST OF ACRONYMS

<b>EEG</b>	Electroencephalogram
<b>ERP</b>	Event-related potential
<b>TFA</b>	Time-frequency analysis
<b>PCA</b>	Principal component analysis
<b>ICA</b>	Independent component analysis
<b>SNR</b>	Signal-to-noise ratio
<b>ANOVA</b>	Analysis of variances
<b>ERO</b>	Event-related oscillation
<b>PSD</b>	Power spectral density
<b>FFT</b>	Fast Fourier transform
<b>AFC</b>	Amplitude-frequency characteristic
<b>ADHD</b>	Attention-deficit hyperactivity disorder
<b>TFR</b>	Time-frequency representation
<b>PCs</b>	Principal components
<b>STFT</b>	Short time Fourier transform
<b>CMCWT</b>	Complex Morlet continuous wavelet transform
<b>ICs</b>	Independent components
<b>NCPD</b>	Nonnegative canonical polyadic decomposition
<b>BSS</b>	Blind source separation
<b>CMW</b>	Complex Morlet wavelet
<b>CMT</b>	Continous wavelet transform
<b>ERD/ERS</b>	Event-related desynchronization/synchronization
<b>ERSP</b>	Event-related spectral perturbation
<b>CPD</b>	Canonical polyadic decomposition
<b>RD</b>	Reading disability
<b>AD</b>	Attention deficit
<b>MMN</b>	Mismatch negativity
<b>MEG</b>	Magnetoencephalography

## LIST OF FIGURES

FIGURE 1	Some widely used techniques for the extraction of ERP/ERO ...	16
FIGURE 2	Illustrations of conventional time-domain analysis and spectral analysis.....	18
FIGURE 3	Illustrations of the applications of PCA and ICA on EEG data...	21
FIGURE 4	Illustration of time-frequency analysis based on the complex Morlet continuous wavelet transform .....	22
FIGURE 5	Example of two-component NCPD for a third-order tensor .....	24
FIGURE 6	Methods and data types are used in three studies .....	26
FIGURE 7	Example of blind source separation model for a temporal concatenated matrix .....	29
FIGURE 8	The example of estimating source number (PCA).....	31
FIGURE 9	An example for the application of PCA on ERP data .....	33
FIGURE 10	Example for calculation of evoked and induced oscillations .....	37
FIGURE 11	Example for the time-frequency representations using different mother wavelets .....	39
FIGURE 12	The example for the applications of three common used baseline correction techniques on TFRs .....	41
FIGURE 13	An example for the application of TFA on ERP data .....	42
FIGURE 14	An example of NCPD for a fourth-order tensor of ERP data.....	48
FIGURE 15	An example of Tucker decomposition with nonnegative constraint for a fourth-order tensor of ERP data .....	49

# CONTENTS

## ABSTRACT

TIIVISTELMÄ (ABSTRACT IN FINNISH)

## ACKNOWLEDGEMENTS

## LIST OF ACRONYMS

## LISTS OF FIGURES

## CONTENTS

## LIST OF INCLUDED ARTICLES

1	INTRODUCTION .....	15
1.1	Single-way component analysis techniques.....	15
1.1.1	Conventional time-domain analysis .....	16
1.1.2	Spectral analysis .....	17
1.1.3	Limitations.....	19
1.2	Two-way component analysis techniques .....	19
1.2.1	Principal/Independent component analysis.....	20
1.2.2	Time-frequency analysis .....	21
1.2.3	Limitations.....	23
1.3	Multi-way component analysis techniques.....	23
1.4	Research aims/solutions .....	24
1.5	Dissertation structure .....	26
2	METHODS TO MEASURE CHARACTERISTICS OF EVENT-RELATED POTENTIALS/OSCILLATIONS .....	27
2.1	Theory and procedure of PCA/ICA to extract ERPs .....	27
2.1.1	Mathematical model for PCA.....	27
2.1.2	PCA procedure for ERPs extraction .....	30
2.1.2.1	Arranging ERP/EEG data into a matrix .....	30
2.1.2.2	Estimating the number of sources.....	31
2.1.2.3	Selecting the rotation method.....	32
2.1.2.4	Identifying the PCA-extracted components of in- terest .....	32
2.1.2.5	Analyzing the identified PCA-extracted compo- nents .....	34
2.1.3	Model of ICA and its application.....	35
2.2	Theory and procedure of complex Morlet continuous wavelet transform to extract EROs .....	36
2.2.1	The theory of complex Morlet continuous wavelet trans- form for ERP data analysis .....	36
2.2.2	CMCWT procedure for EROs extraction .....	39
2.2.2.1	TFR calculation.....	39
2.2.2.2	ERO identification and analysis.....	41
2.3	Theory and procedure of tensor decomposition to extract EROs....	42
2.3.1	Mathematical models for tensor decomposition.....	43

2.3.1.1	The definition of canonical polyadic decomposition	43
2.3.1.2	The definition of Tucker decomposition .....	44
2.3.1.3	The differences between CPD and Tucker decom- position .....	45
2.3.2	Applications of tensor decomposition on ERP datasets.....	45
2.3.2.1	Determining the number of extracted components for tensor decomposition .....	46
2.3.2.2	Canonical polyadic decomposition of tensor of ERP datasets.....	46
2.3.2.3	Tucker decomposition of tensor of ERP datasets ....	49
3	SUMMARIES OF STUDIES AND AUTHOR CONTRIBUTIONS.....	51
3.1	Study 1: Measuring temporal and spatial properties of the de- sired ERPs from individual subject's data by temporal-PCA .....	51
3.1.1	Motivation .....	51
3.1.2	Methods .....	52
3.1.3	Results.....	52
3.1.4	Conclusion and discussion .....	53
3.1.5	Author contributions .....	53
3.2	Study 2: Objectively measuring temporal and spectral properties of evoked EROs via temporal-PCA and TFA .....	53
3.2.1	Motivation .....	54
3.2.2	Methods .....	54
3.2.3	Results.....	55
3.2.4	Conclusion and discussion .....	55
3.2.5	Author contributions .....	56
3.3	Study 3: Measuring multi-domain properties of induced EROs using tensor decomposition.....	56
3.3.1	Motivation .....	56
3.3.2	Methods .....	57
3.3.3	Results.....	57
3.3.4	Conclusion and discussion .....	57
3.3.5	Author contributions .....	58
4	CONCLUSION AND DISCUSSION.....	59
4.1	Overview.....	59
4.2	Research limitations.....	60
4.3	Future directions .....	61
	YHTEENVETO (SUMMARY IN FINNISH) .....	63
	REFERENCES.....	64
	INCLUDED ARTICLES	

## LIST OF INCLUDED ARTICLES

- PI Guanghui Zhang, Xueyan Li, Yingzhi Lu, Timo Tiihonen, Zheng Chang, and Fengyu Cong. Single-trial-based Temporal Principal Component Analysis on Extracting Event-related Potentials of Interest for an Individual Subject. *To be submitted*, 2021.
- PII Guanghui Zhang, Lili Tian, Huaming Chen, Peng Li, Tapani Ristaniemi, Huili Wang, Hong Li, Hongjun Chen, and Fengyu Cong. Effect of Parametric Variation of Center Frequency and Bandwidth of Morlet Wavelet Transform on Time-frequency Analysis of Event-related Potentials. In: *Jia Y., Du J., Zhang W. (eds) Proceedings of 2017 Chinese Intelligent Systems Conference. CISC 2017. Lecture Notes in Electrical Engineering, vol 459, pp. 693-702*, [https://doi.org/10.1007/978-981-10-6496-8\\_63](https://doi.org/10.1007/978-981-10-6496-8_63), 2018.
- PIII Guanghui Zhang, Xueyan Li, and Fengyu Cong. Objective Extraction of Evoked Event-Related Oscillation from Time-Frequency Representation of Event-Related Potentials. *Neural Plasticity*, vol. 2020, Article ID 8841354, 20 pages, <https://doi.org/10.1155/2020/8841354>, 2020.
- PIV Guanghui Zhang, Chi Zhang, Shuo Cao, Xue Xia, Xin Tan, Lichengxi Si, Chenxin Wang, Xiaochun Wang, Chenglin Zhou, Tapani Ristaniemi, and Fengyu Cong. Multi-domain Features of the Non-phase-locked Component of Interest Extracted from ERP Data by Tensor Decomposition. *Brain Topography* 33, 37–47, <https://doi.org/10.1007/s10548-019-00750-8>, 2020.
- PV Guanghui Zhang, Xueyan Li, Xiulin Wang, Wenya Liu, Yongjie Zhu, Xiaoshuang Wang, Reza Mahini, Rao Fu, Zheng Chang, Timo Tiihonen, and Fengyu Cong. Signal Processing Techniques for Event-related Potentials: from Single-way to Multi-way Component Analysis. *To be submitted*, 2021.



# 1 INTRODUCTION

Electroencephalogram (EEG) can be categorized into three different types based on the types of external stimuli: (*a*) the first type is spontaneous EEG recorded without any external stimuli, for example, in the open/close eye resting state; (*b*) the second one is event-related potential (ERP), which is elicited by the controlled stimuli, such as repeated pictures (Luck, 2014; Handy, 2005); (*c*) the third one is ongoing EEG, which is elicited by natural stimuli, e.g., watching movies and listening music (Rogenmoser et al., 2016; Zhu et al., 2020).

Compared with the other two types of EEG, ERP brain signals collected by the controlled stimuli enable researchers to study specific cognitive processes of event-related brain activities efficiently (Luck, 2014; Handy, 2005). Therefore, ERP signals have been widely used to investigate the specific cognitive functions of brain activities for both neuropsychiatric disease patients and normal people (Luck, 2014; Handy, 2005). In order to efficiently extract event-related brain activities and study related mechanisms of brain activities better, different signal processing techniques have been developed.

The following sections briefly introduce some widely used signal processing techniques (see *Figure 1*), such as conventional time-domain analysis (Luck, 2014), spectral analysis (Bruns, 2004; Başar et al., 2016a), time-frequency analysis (TFA) (Tallon-Baudry and Bertrand, 1999; Herrmann et al., 2014; Roach and Mathalon, 2008), principal/independent component analysis (PCA/ICA) (Huster and Raud, 2018; Dien, 2012; Eichele et al., 2011; Onton et al., 2006), tensor decomposition (Cong et al., 2015a), etc, to extract the properties of event-related brain activities in different dimensions.

## 1.1 Single-way component analysis techniques

Either temporal or spectral amplitudes of event-related brain activities are measured from the single-way representatives (i.e., time-series or frequency-series). The related procedures are correspondingly named conventional time-domain

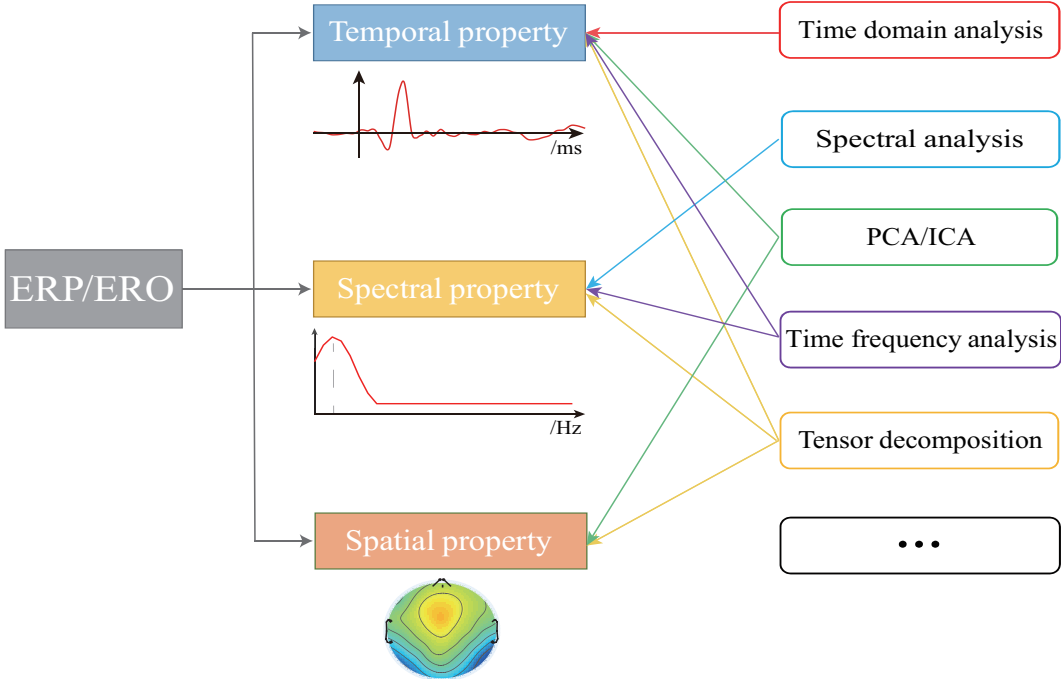


FIGURE 1 Some widely used techniques for the extraction of event-related potential/oscillation (ERP/ERO). PCA/ICA: principal/independent component analysis.

analysis and spectral analysis.

The following contents briefly introduce the applications of both single-way component analysis techniques and then discuss about their limitations in current ERP/EEG data analysis.

### 1.1.1 Conventional time-domain analysis

Since magnitudes of ERPs (e.g., several microvolts) are significant smaller than those of artifacts (e.g., tens or hundreds of microvolts), some preprocessing steps are performed on the raw EEG data to improve the signal-to-noise ratio (SNR) for measuring ERPs of interest better. The preprocessing procedure commonly contains the following steps: re-reference (Yao et al., 2019; Hu et al., 2019), filtering (de Cheveigné and Nelken, 2019; de Cheveigné, 2020; Widmann et al., 2015), using ICA to remove eye activity artifacts (Winkler et al., 2011; Mognon et al., 2011; Jung et al., 2000), segmentation, and baseline correction (Alday, 2019), and so forth.

Hereinafter, 'EEG data' represents the preprocessed single-trial signals and 'ERP data' are the preprocessed trial-averaged signals.

Based on the preprocessed EEG data, the waveforms of ERPs, which are related to the specific events (i.e., different stimuli), are obtained by averaging the single-trial EEG data (Luck, 2014; Handy, 2005). This averaging procedure is based on the three following assumptions: (a) Artifacts, such as sensor noise, eye activities, muscle movement, are significantly removed during the preprocessing

procedure; (b) Spontaneous brain activities are significantly canceled out since they are uncorrelated between samples of different trials; (c) The numbers and the orders of sources for all single-trial EEG data are the same.

Usually, there are several different ERPs in the trial-averaged waveforms, and those ERPs are characterized by their polarities, peak latencies, and topographical distributions (Luck, 2014; Handy, 2005). For instance, N100 (or N1) is a negative-going ERP which is mainly found in fronto-central regions about 80-120 ms (Vogel and Luck, 2000; Näätänen and Picton, 1987). N2 is a negative-going ERP and its peak latency occurs within time window from 200-350 ms after stimulus-onset at anterior sites (Patel and Azzam, 2005; Folstein and Van Petten, 2008). P3 is a positive-going ERP whose peak latency locates in about 250 - 500 ms, and it is primarily found in parietal lobe sites (van Dinteren et al., 2014; Polich, 2007).

Different ERPs might be used to explain different cognitive processes. For example, the changes of N2 in amplitude, topography, latency obtained by using conventional time-domain analysis are used to study the executive cognitive functions (Folstein and Van Petten, 2008). Likewise, the related cognitive functions in decision-making processes based on the amplitude, topography, and latency of P3 can also be studied (Polich, 2007). Some researchers have investigated the functions of inhibitory control deficits in schizophrenia by comparing the amplitude of N100 obtained from EEG data of schizophrenia patients and control health people (Hughes et al., 2012). The N100 reduction is used to study the influence of medicine on schizophrenia patients (Rosburg et al., 2008).

When using conventional time-domain analysis, the amplitudes of ERPs are firstly measured from the averaged ERP data within an experimenter-defined time window at the selected electrodes. The identification of the time window and the selection of electrodes are often based on both the findings in previous reports and the visual inspection of the grand averaged waveforms for ERPs of interest. Afterwards, the differences between/among different experimental conditions for the measured amplitudes of ERPs are identified by means of statistical analysis techniques, for example, repeated-measurement analysis of variances (rm-ANOVA), t-test, and non-parametric permutation test (see *Figure 2 (a) → (b)*).

### 1.1.2 Spectral analysis

Similar to the measurement of ERPs (the salient part within a short defined time window) in the time domain, spectral analysis measures the amplitudes of salient parts in specific frequencies (see *Figure 2 (a) → (c) → (d)*) (Gross, 2014; Başar et al., 2016a). In principle, one desired ERP can be considered as a superposition of several oscillations in different frequencies. The term of event-related oscillations (EROs) is used to represent the salient parts at specific frequency bands elicited by controlled stimuli (or cognitive tasks) (Başar et al., 2016a; Başar, 2013; Güntekin and Başar, 2016; Başar et al., 2001; Karakaş et al., 2000). Therefore, like the definition of an ERP in time-domain, the salient part in a specific frequency band

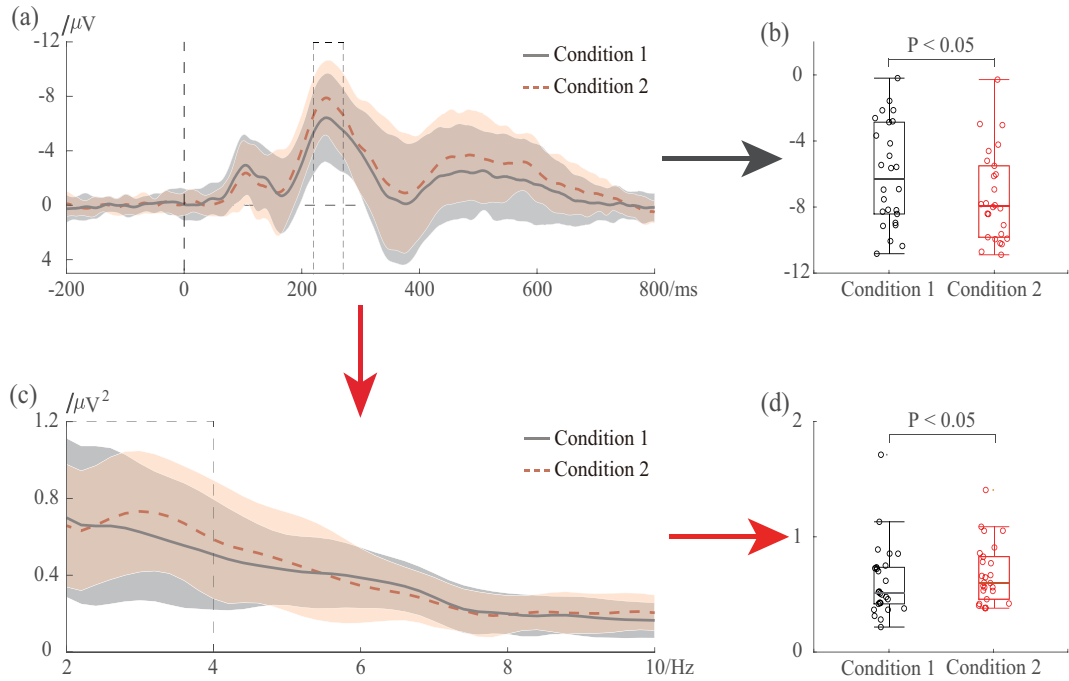


**FIGURE 2** Illustrations of conventional time-domain analysis ((a) → (b)) and spectral analysis ((a) → (c) → (d)). (a) The grand averaged waveforms for two experimental conditions at some typical electrodes. (b) The amplitudes of ERPs (i.e., N2) for different individual subjects within time window from 220 to 270 ms. (c) The grand averaged power spectral density (PSD) of two different experimental conditions at typical electrodes. (d) The energies of different individual subjects of higher evoked delta (2-4 Hz) oscillation. The details of data used in current figure are available in (Lu et al., 2017)

(e.g., theta band: 4-8 Hz) is interpreted as the preferred ERO.

EROs are classified into varied frequency bands, namely, delta (1-4 Hz), theta (4-8 Hz), alpha (8-12 Hz), beta (13-30 Hz), and gamma (30-70 Hz) (Başar et al., 2016a; Başar, 2013; Başar et al., 2001; Başar and Güntekin, 2008). EROs can be obtained by performing spectral analysis techniques on the trial-averaged ERP data, and these are called evoked EROs that are strictly phase-locked and time-locked to events. Based on spectral analysis, EROs can also be generated from single-trial EEG data and they are named induced EROs which are non-phase locked and time-locked to events, and they are the automatic responses to cognitive tasks (Başar et al., 2016a; Başar, 2013).

Several techniques, such as fast Fourier transform (FFT), Hilbert transform, and wavelet transform, have been developed and widely used to transform the time-domain signals of either trial-averaged ERP or single-trial EEG into contents in frequency domain (amplitude-frequency characteristics, i.e., AFCs) (Başar et al., 2016a; Başar, 2013). Bruns (2004) has demonstrated that there are no differences among the results of the three techniques in practical applications on actual neuronal datasets. With those techniques, the cognitive mechanisms can be investigated based on event-related activities for cognitive disorder patients, such as

attention-deficit hyperactivity disorder (ADHD), bipolar disorders, Alzheimer's, mild cognitive impairment, schizophrenia, and alcoholism patients (Başar, 2013; Başar and Güntekin, 2008; Başar et al., 2016a,b)

### 1.1.3 Limitations

For both the conventional time-domain analysis and spectral analysis, the statistical analysis results are usually influenced by the experimenter-determined time window/frequency range, which tends to be a subjective method. Additionally, the characteristic of ERPs/EROs is merely interpreted in one dimension. Therefore, for conventional time-domain analysis, it is challenge to know how the ERPs of interest change along with frequencies. Likewise, the temporal characteristic of EROs is inevitably neglected in spectral analysis. Furthermore, ERPs/EROs of interest are generally mixed with others of non-interest in temporal, spatial, and spectral domains. As a result, the features of EROs/ERPs might not be explored entirely using single-way component analysis techniques.

To tackle the problem in the selection of time window for ERPs, some researchers (Michel and Koenig, 2018; Murray et al., 2008; Mahini et al., 2020) have attempted to use clustering analysis to determine an optimal time window for ERPs of interest. However, the overlapping between components might prevent the proper clustering of the components in this types of technique. For example, unrelated time points may be classified as a part of the desired ERPs when topographies corresponding to those time points (which do not belong to the time range of ERPs in the time domain) are highly similar to that of ERPs of interest. Such a bias selection may also happen when performing clustering analysis on the yields of spectral analysis to determine a frequency range for EROs.

In order to address the other problems in single-way component analysis techniques, different advanced techniques are available, for example, TFA (Herrmann et al., 2014; Roach and Mathalon, 2008), PCA/ICA (Huster and Raud, 2018; Dien, 2012; Barry and De Blasio, 2018; Eichele et al., 2011), and tensor decomposition (Cong et al., 2015a). In the following section, the applications and limitations of those advanced techniques are separately discussed.

## 1.2 Two-way component analysis techniques

To address the problem that ERPs of interest are mixed with others, PCA and ICA (Huster and Raud, 2018; Dien, 2012; Eichele et al., 2011) can be employed to extract ERPs of interest from the mixed ERP/EEG data. Additionally, the brain activities can also be extracted from time-frequency representations (TFRs) to study their temporal and spectral dynamics (Tallon-Baudry and Bertrand, 1999; Roach and Mathalon, 2008; Cohen, 2014; Herrmann et al., 2014).

In the following, the applications of PCA/ICA and TFA on the ERP/EEG data are firstly discussed, and then the shortcomings of these two-way compo-

nent analysis techniques are clarified.

### 1.2.1 Principal/Independent component analysis

The recorded EEG data are often represented by a matrix (i.e., channels are in rows and time points are in columns) in some popular toolboxes, like EEGLAB (Delorme and Makeig, 2004). In an ERP experiment, the preprocessed multiple EEG/ERP datasets can also be arranged into a big-size matrix along either time samples or channels (see *Figure 3*) (Dien, 2012; Dien et al., 2005, 2007). Consequently, matrix decomposition algorithms, like PCA and ICA, can be conducted to extract and preserve the shared characteristics of ERPs of interest among different subjects. Meanwhile, ERPs of non-interest and artifacts can be removed (Dien, 2012; Dien et al., 2005, 2007).

In PCA technique, there are two different ways to extract ERPs of interest. Herein, the application of group PCA on the trial-averaged ERP data is taken as an example (see *Figure 3*). In the first way, ERPs are extracted from temporal-stacked matrix (i.e., electrodes  $\times$  (time samples  $\times$  conditions  $\times$  subjects)) and the related PCA-decomposition is called as spatial-PCA (see *Figure 3 (a)*) (Dien, 2012; Dien et al., 2005). In the spatial-PCA, electrodes are variables, and the products of time samples, conditions, and subjects are observations. Spatial-PCA assumes that the spatial components (i.e., factor loadings) for all subjects share the same topography but different in amplitudes of temporal components (i.e., factor scores, see the waveforms of extracted components in *Figure 3 (a)*) (Dien, 2012). For the other one, the PCA decomposition of spatial-concatenation matrix (i.e., time samples  $\times$  (electrodes  $\times$  conditions  $\times$  subjects)) is named as temporal-PCA (see *Figure 3 (b)*). The underlying idea is that the waveforms of temporal components (i.e., factor loadings) for all subjects are the same and the amplitudes of spatial components are different (i.e., topographies, which are also called factor scores) (Dien, 2012).

Noticeably, due to volume conduction, all ERPs and artifacts are mixed in spatial domain to some degree (Dien, 2012). It is, therefore, usually recommended to use temporal-PCA to obtain the desired ERPs rather than spatial-PCA (Dien, 2012). The previous study also confirmed that temporal-PCA yields better overall results than those of spatial-PCA (Dien, 1998).

To capture the temporal and spatial characteristics of ERPs of interest, most researchers have obtained ERPs from the trial-averaged ERP data of all subjects (Widmann et al., 2018; Bonmassar et al., 2020; Steele et al., 2016; Gentsch et al., 2013). Moreover, others have attempted to extract the ERPs of interest from the single-trial EEG data of all subjects at the group level (Rushby et al., 2005; MacDonald et al., 2015; MacDonald and Barry, 2017; Rushby and Barry, 2009).

The main difference between ICA and PCA is that ICA ensures the extracted components are independent but rotated principal components (PCs) obtained by PCA plus rotation method are related. Moreover, the applications of ICA can also be categorized into temporal-ICA and spatial-ICA based on the forms of the matrices (see *Figure 3*) (Huster and Raud, 2018; Eichele et al., 2011). Addition-

ally, the features of ERPs of interest in temporal and spatial domains can also be extracted from both the single-trial EEG data and trial-averaged ERP data of all subjects via ICA decomposition (Cong et al., 2010; Van Dinteren et al., 2018; Huster et al., 2020). Rissling et al. (2014) had attempted to use ICA to extract ERPs of interest from individual subject's data.

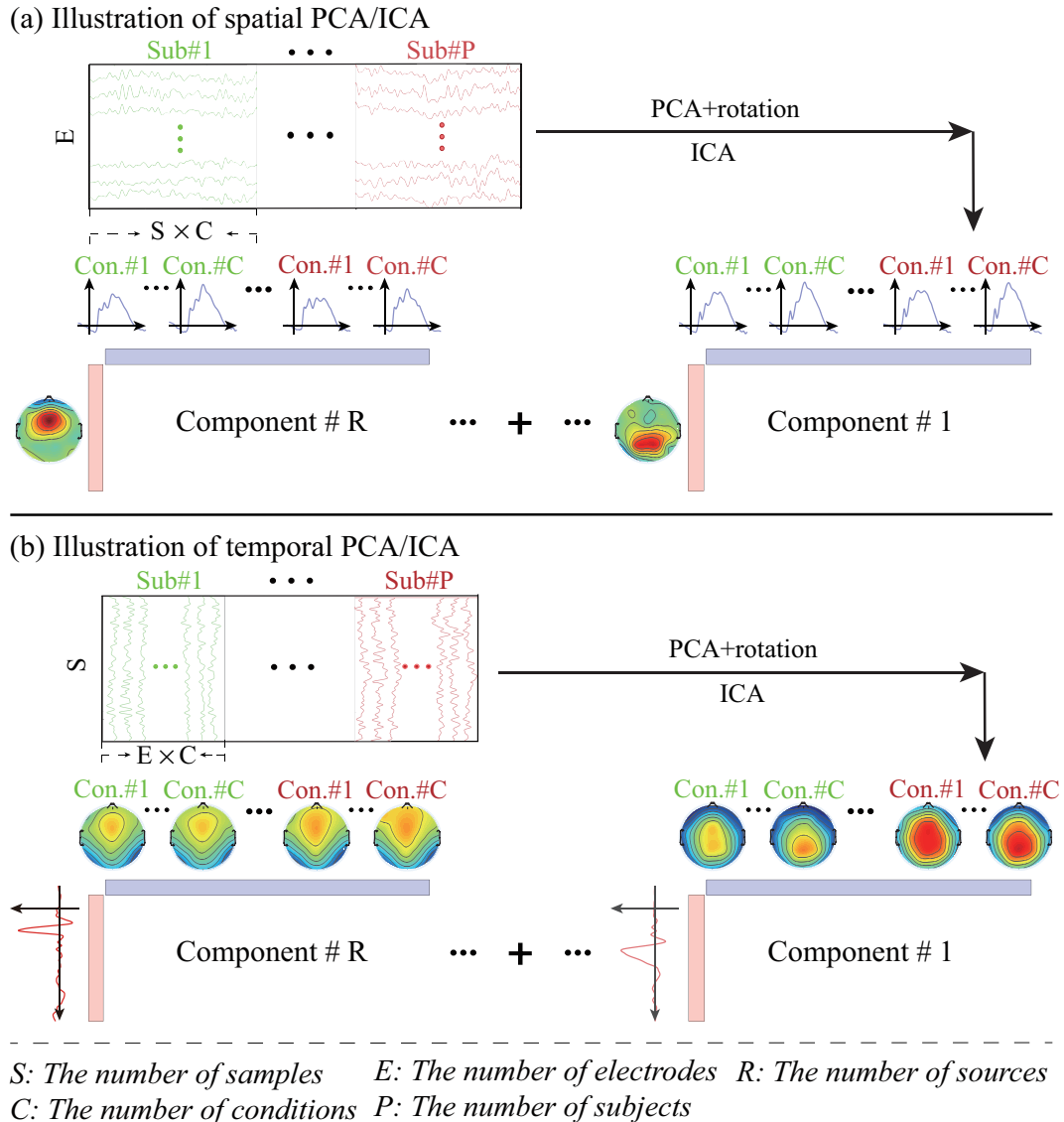


FIGURE 3 Illustrations of the applications of PCA and ICA on EEG data. (a) Spatial PCA/ICA analysis. (b) Temporal PCA/ICA analysis.

### 1.2.2 Time-frequency analysis

After the time-domain EEG/ERP data are transformed into time-frequency signals (i.e., TFRs), the dynamics of event-related brain activities in temporal and spectral domains can be captured simultaneously (see *Figure 4*) (Cohen, 2014; Herrmann et al., 2014; Tallon-Baudry and Bertrand, 1999). As in spectral analysis

of event-related brain activities, the temporal and spectral dynamics response to events are also named as EROs. Those EROs are divided into varied frequency bands, e.g., delta, alpha, theta, gamma, and beta bands (Başar et al., 2001).

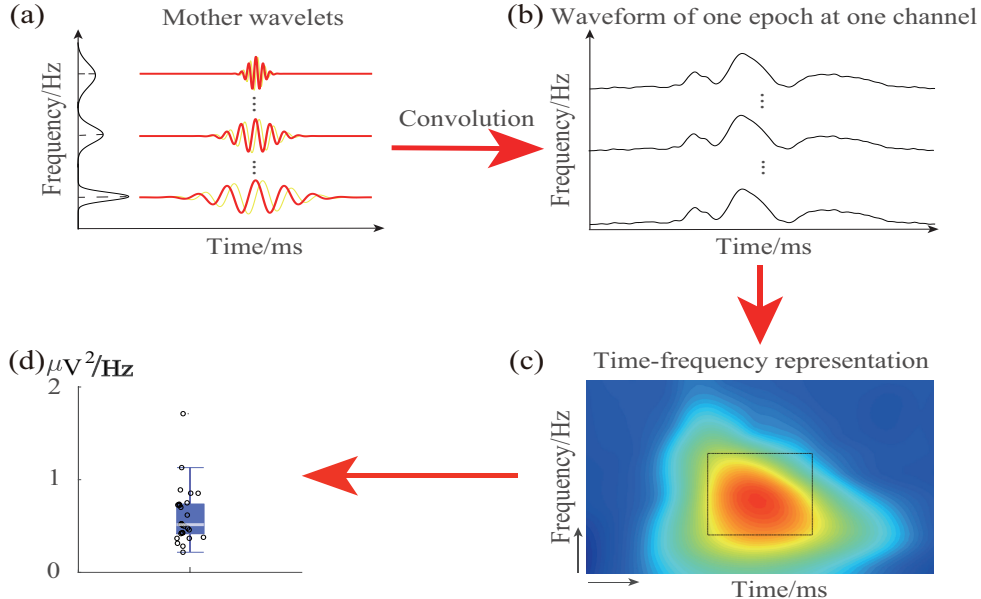


FIGURE 4 | Illustration of time-frequency analysis based on the complex Morlet continuous wavelet transform. (a) Complex Morlet mother wavelets. (b) The waveform of one-epoch EEG data at one channel. (c) The time-frequency representation of the time-domain signal in (b). (d) The power of ERO of interest (marked by black rectangle) in (c).

There are two different strategies to compute EROs (Herrmann et al., 2014; Tallon-Baudry and Bertrand, 1999). In the first strategy, TFRs are obtained from the trial-averaged ERP data using some TFA algorithms, and the obtained EROs in such TFRs are time-locked and phase-locked to event onset (i.e., evoked EROs). In the second strategy, TFRs of single-trial EEG data are firstly calculated, and then the TFRs of single-trial EEG data are averaged to obtain total brain activities that consist of both evoked and induced EROs. Induced EROs are non-phase locked to stimulus onset, and they will be significantly canceled out during the averaging procedure in the time domain (Tallon-Baudry and Bertrand, 1999; Herrmann et al., 2014).

To obtain EROs and study the temporal-spectral dynamics of EROs, different TFA algorithms, e.g., short-time Fourier transform (STFT), complex Morlet continuous wavelet transform (CMCWT), Hilbert-Huang transform, Z-transform, and Wigner-Ville distribution, have been developed (Roach and Mathalon, 2008; Wacker and Witte, 2013; Cohen, 2014). Some algorithms have been nested in free available toolboxes, for example, EEGLAB (Delorme and Makeig, 2004), ERP-WAVELAB (Mørup et al., 2007), and Brainstorm (Tadel et al., 2011), which allow researchers to study EROs easily. Compared with other algorithms, CMCWT is frequently used to investigate EROs because it provides superior time resolution

and frequency resolution of TFRs.

### 1.2.3 Limitations

Regarding the current applications of temporal-PCA, there are two main challenges. Since the latencies and phases of the waveforms of an ERP for all individuals are vary to some degree, the waveform of an ERP of interest is often decomposed into several components by PCA (Zhang et al., 2020a; Cao et al., 2020; Li et al., 2019). The biggest challenge is that those PCA-extracted components decomposed from the waveforms of an ERP for different subjects cannot be analyzed simultaneously since their polarities and amplitudes may be different. This limitation means that only the partial information of one desired ERP is involved and analyzed if not all of PCA-extracted components, which come from the same ERP, are not considered. The other limitation of group temporal-PCA is that the waveforms of one ERP of interest for all subjects are assumed to be the same, and this assumption is contrary to actual waveforms of ERPs.

For ICA, two issues need to be concerned. The first issue is that the extracted independent components (ICs) are assumed to be independent of each other, which are not in accord with the actual ERP sources, and those ERP sources are correlated to some extent due to volume conduction. The second issue is that the extracted ICs may be variant in different runs (Cong et al., 2011b).

Concerning the applications of TFA, the TFRs are usually obtained from the original preprocessed ERP/EEG data, and the desired EROs in the obtained TFRs may still be highly blended or mixed with others of non-interest. Consequently, the properties of EROs cannot be fully explored and some cognitive functions cannot be accurately explained. To tackle this, Bernat and colleagues suggested that applying PCA on the TFRs to extract the EROs (Bernat et al., 2005, 2007; Harper et al., 2014; Bowers et al., 2018), the core step is to calculate weightings between the PCA-extracted components obtained from TFRs with the original TFRs. In such a technique, the weighted TFRs are still compound demonstrated by using synthetic data in our recent work (Zhang et al., 2020a). It should be noted that a mother wavelet needs to be firstly defined by a set of bandwidth and center frequency before using CMCWT. Setting of bandwidth and center frequency directly affects on the time resolution and frequency resolution of the obtained TFRs (Zhang et al., 2018a, 2020b). Therefore, different sets of bandwidth and center frequency need to be attempted to obtain relative optimal TFRs.

## 1.3 Multi-way component analysis techniques

After time-domain EEG/ERP data are converted into time-frequency signals, in a typical ERP experiment, at least five modes (i.e., dimensions) are included, namely, time sample, electrode, frequency, condition, and subject modes. Therefore, TFRs of multi-condition and multi-subject can be presented by a multi-array

(i.e., tensor, the size of its dimensions is more than two). Figure 5 shows an example of two-component nonnegative canonical polyadic decomposition (NCPD) for a third-order tensor.

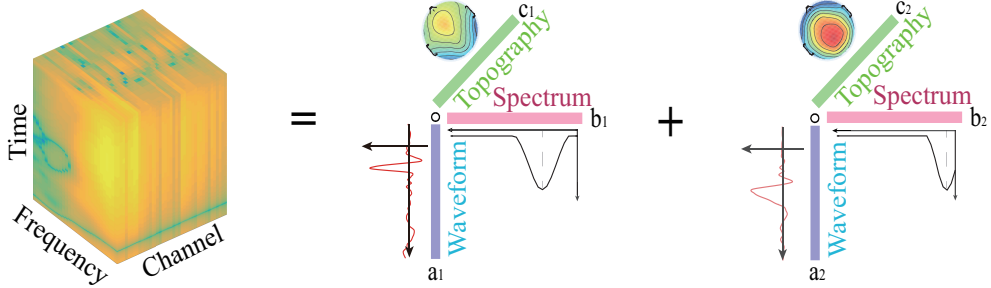


FIGURE 5 Example of two-component NCPD for a third-order tensor.

Canonical polyadic and Tucker are two widely used models in the tensor decomposition (Cong et al., 2015a), which bring us a new sight to investigate the dynamics of brain activities in temporal, spectral, and spatial domains, and study the potential interactions of EROs among those modes. Similar to the assumption in the applications of PCA/ICA, brain activities corresponding to event onset for all subjects share the spectrum in the frequency domain, the waveform in the time domain, and the topographical distribution in the space domain. The differences of EROs among all subjects are expressed in the features of subject-condition mode.

According to different study purposes, different forms of tensors with varied dimensions can be organized. For example, to extract the multi-mode features of evoked EROs in temporal, spatial, and spectral domains, a fourth-order tensor with temporal, spatial, spectral, and subject-condition modes is generated (Cong et al., 2013b, 2014; Yu et al., 2020; Zhang et al., 2020b). Some researchers tried to dig out potential interaction of EROs from some merged modes (e.g., subject and condition are merged into one mode in a fourth-order tensor) using tensor decomposition to decompose a fifth-order tensor (time samples  $\times$  frequency bins  $\times$  electrodes  $\times$  subjects  $\times$  conditions) (Wang et al., 2018; Mørup et al., 2006).

However, these applications of tensor decomposition mainly focused on studying the dynamics of the evoked EROs; the investigations of induced EROs by using tensor decomposition are seldom carried out.

## 1.4 Research aims/solutions

This thesis aims to develop essential signal processing techniques and introduce novel frameworks to study the cognitive dynamics of brain activities in temporal, spatial, and spectral domains from the EEG/ERP data. Specific solutions are provided to overcome the shortcomings in the two-way (*Articles I, II, and III*) and

multi-way component analysis techniques (*Article IV*) as described in *Subsections 1.2.3 and 1.3*.

The detailed object and solution of each included article are listed as below:

*Article I:* We conduct the back-projection theory into temporal-PCA application to analyze several PCA-extracted components, which are derived from the waveforms of the same ERP, simultaneously. In order to address the unreasonable hypothesis of temporal-PCA that all subjects' waveforms of ERPs are the same, we extract the ERPs of interest from the individual subject's EEG data collected from an emotional ERP experiment with two factors. The results of the proposed techniques are also compared with other alternative techniques (conventional time-domain analysis and group temporal-PCA [single-trial and trial-averaged] analysis).

*Article II:* To investigate how the complex Morlet mother wavelet affects on the time-frequency results, we firstly calculate TFRs of the same ERP data using 80 different complex Morlet mother wavelets (determined by a set of bandwidth and center frequency). Afterwards, we compute the statistical analysis results of the same evoked EROs for TFRs of different mother wavelets.

*Article III:* To fill the gap that evoked EROs may fail to be explored entirely since they overlap with others in temporal and spectral domains, a novel framework that combines temporal-PCA and TFA is proposed to extract evoked EROs objectively. We firstly extract ERPs of interest in the time domain using temporal-PCA plus Promax rotation and reconstruct the waveforms of the interesting ERPs. Next, the reconstructed waveforms of ERPs of interest are converted into time-frequency signals via the CMCWT algorithm. The proposed technique is validated by a set of synthetic ERP data and an actual EEG of a simple gambling task. The comparable methods are conventional TFA and TFA-PCA.

*Article IV:* To address the problem that the interactions of induced EROs among different modes are inevitably lost in conventional TFA, tensor decomposition is conducted to extract the temporal, spatial, and spectral characteristics of induced EROs from fourth-order tensor in a go/nogo paradigm task. The conventional TFA is also conducted to extract induced EROs.

*Article V:* During the study we notice that there is no systematic source that would have covered the various signal processing techniques used for ERP analysis. To fill in this gap, we summarize the theories and procedures of the techniques related to extraction of ERPs/EROs more widely than is needed to explain the methods used in this thesis. This article grew out from preparing the Study 3 but will not be discussed independently in the following section.

This thesis consists of three studies. Study 1: Measuring temporal and spatial properties of the desired ERPs from individual subject's data by temporal-PCA (*article I*). Study 2: Objectively measuring temporal and spetral properties of evoked EROs via temporal-PCA and TFA (*articles II and III*). Study 3: Measuring multi-domain properties of induced EROs using tensor decomposition (*article IV*). The details of the used methods and data types in different studies are described in *Figure 6*.

Additionally, the developed PCA algorithm is used in both *articles I and*

III. In the articles III and IV, the selected set of bandwidth and center frequency is used to define the mother wavelet for calculating evoked and induced EROs, respectively, based on the work in the article II.

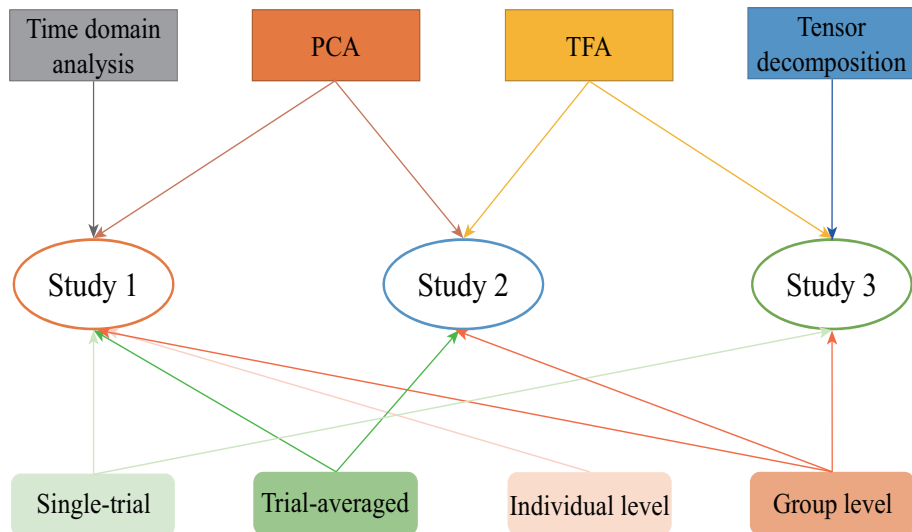


FIGURE 6 Methods and data types are used in three studies. PCA: principal component analysis; TFA: time-frequency analysis.

## 1.5 Dissertation structure

The details of the dissertation structure are described as following:

Chapter 1 briefly introduces the applications and limitations of some widely used techniques, and the aim of this dissertation is also clarified.

Chapter 2 describes the mathematical theories and procedures on extracting ERPs/EROs for the some techniques.

Chapter 3 briefly summarizes the contents of the included articles and lists the authors' contributions in each article.

Chapter 4 summarizes the conclusions and limitations in current thesis, and potential directions for future investigation are also discussed.

## 2 METHODS TO MEASURE CHARACTERISTICS OF EVENT-RELATED POTENTIALS/OSCILLATIONS

This chapter firstly introduces the fundamental theories of PCA/ICA, CMCWT, and tensor decomposition. Afterwards, it describes the basic steps of these techniques for the extraction of ERPs/EROs.

### 2.1 Theory and procedure of PCA/ICA to extract ERPs

The recorded EEG signals are considered as the sum of products between source signals in cortex and weighting factors, and the model is called blind source separation (BSS) model (see *Figure 7*). PCA/ICA aims to estimate the underlying source signals and weighting factors.

In this section, the model and applications of PCA/ICA are detailed in order.

#### 2.1.1 Mathematical model for PCA

The application of temporal-PCA is firstly described using BSS model, and the difference between temporal-PCA and spatial-PCA under this model is discussed.

In application of temporal-PCA, for a spatial concatenated matrix  $\mathbf{X} \in \Re^{N \times M}$  (see *Figure 3 (b)*).  $N$  and  $M$  respectively represent the number of time samples and the number of electrodes by subjects by conditions. The matrix can be expressed by using the linear transformation model as below (Cong et al., 2011a,c; Zhang et al., 2020a, 2021).

$$\mathbf{X} = \mathbf{H}\mathbf{S}_1 + \mathbf{E} = \mathbf{H}(\mathbf{S}_1 + \mathbf{S}_2) = \mathbf{H}\mathbf{S}. \quad (1)$$

In the above equation,  $\mathbf{H}$  denotes a mixing matrix with full ranks and its each column is the weighting value from  $r^{th}$  source in the brain cortex to  $m^{th}$  electrode along the brain scalp;  $\mathbf{S} = \mathbf{S}_1 + \mathbf{S}_2 (\mathbf{S} \in \Re^{R \times M})$ ,  $\mathbf{E} = \mathbf{H}\mathbf{S}_2$ ,  $\mathbf{S}_1$  is the unknown source matrix in brain cortex, and  $\mathbf{S}_2$  is the sensor-noise source matrix.

Usually, the model in *Eq. 1* is regarded as an over-determined model (Cong et al., 2011a) since the number of the observed signals  $N$  is considered to be larger than that of the source signals  $R$ . Therefore, some approaches, such as cumulative explained variance (Huster and Raud, 2018; Van Dinteren et al., 2018; Huster et al., 2020; Zhang et al., 2020a), can be used to estimate the number of sources (i.e.,  $R$ ). Afterwards, the overdetermined model in *Eq. 1* is transformed into determined one as below:

$$\mathbf{D} = \mathbf{V}^T \mathbf{X} = \mathbf{V}^T \mathbf{HS} = \mathbf{AS}, \quad (2)$$

where  $\mathbf{D} \in \Re^{R \times M}$ ;  $\mathbf{V}^T \in \Re^{R \times N}$  is dimensionality reduction matrix obtained by applying PCA on  $\mathbf{X}^T$ ;  $\mathbf{A} \in \Re^{R \times R}$  is regarded as the mixing matrix.

Both  $\mathbf{A}$  and  $\mathbf{S}$  are unknown. Therefore, BSS algorithm is used to seek an unmixing matrix  $\mathbf{W}$  (Comon and Jutten, 2010). In detail, in the applications of PCA on EEG,  $\mathbf{W}$  is usually obtained by using some rotation algorithms, e.g., Promax, Infomax, etc (Abdi and Williams, 2010; Richman, 1986). And then, through this unmixing matrix, the related component matrix can be linearly estimated as below (Cong et al., 2011a; Zhang et al., 2020a, 2021):

$$\mathbf{Y} = \mathbf{WD} = \mathbf{WAS} = \mathbf{CS}, \quad (3)$$

where  $\mathbf{Y}$  represents the estimation of unknown source matrix in *Eq. 2* and its rows are the topographical distributions of the estimated components; The amplitudes and polarities of the estimated components are indeterminate and  $\mathbf{C} = \mathbf{WA}$  is the global matrix. The inverse matrix  $\mathbf{B} = \mathbf{W}^{-1}$  of the unmixing matrix is used to estimate the mixing matrix  $\mathbf{A}$  (Cong et al., 2011a).

Under the determined model condition in *Eq. 2*, in order to analyze those extracted components of interest in microvolts, the component of interest is projected back to the electrode fields. This procedure is described as following ( i.e., back-projection) (Makeig et al., 1997, 1999; Cong et al., 2011a,c; Onton et al., 2006).

$$\mathbf{Q}_r = \mathbf{b}_r \circ \mathbf{y}_r, \quad (4)$$

herein,  $\mathbf{Q}_r \in \Re^{R \times M}$  represents the projected waveforms of ERPs of interest at all electrodes for  $r^{th}$  component;  $\mathbf{b}_r$  is the relative projection strength of  $r^{th}$  component onto all electrodes, and  $\mathbf{y}_r$  is the  $r^{th}$  row of the estimated component matrix  $\mathbf{Y}$ ; ‘ $\circ$ ’ is the outer product between two vectors.

In practice, we pursue an ideal solution (i.e., global optimization condition) that uses one estimated component to uniquely represent the information of one source in *Eq. 2*. That is to say, only one nonzero element in each row and each column of  $\mathbf{C}$  can be obtained. Thus, the procedure, i.e., using an estimated component to unique denote one source in *Eq. 2*, can be defined as:

$$\mathbf{Q}_r = \mathbf{b}_r \circ \mathbf{y}_r = \mathbf{a}_j \circ \mathbf{s}_j, \quad (5)$$

here,  $\mathbf{a}_j$  is  $j^{th}$  column of the mixing matrix  $\mathbf{A}$ , and  $\mathbf{s}_j$  is  $j^{th}$  row of the source matrix  $\mathbf{S}$  in *Eq. 2*. ‘ $\circ$ ’ denotes the outer product of two vectors.

Back to the original overdetermined model in *Eq. 1*, the back-projection of the  $r^{th}$  component generated from the matrix  $\mathbf{X}$  is expressed as:

$$\underline{\mathbf{X}}_r = \mathbf{u}_r \circ \mathbf{y}_r, \quad (6)$$

$$\mathbf{U} = \mathbf{VB}, \quad (7)$$

where  $\mathbf{u}_r$  represents the  $r^{th}$  column of  $\mathbf{U}$  and it is the time course (i.e., waveform) for  $r^{th}$  extracted component. The outer product between the inverse matrix  $\mathbf{B}$  and the dimensionality reduction matrix  $\mathbf{V}$  is conducted to denote  $\mathbf{U}$ , which is the estimation of the weighting matrix  $\mathbf{H}$  in *Eq. 1*.

In the applications of PCA on EEG/ERP data to extract ERPs of interest, several PCA-extracted components derived from the waveforms of one ERPs need to be selected to project to all electrodes simultaneously for correcting their amplitude and polarity indeterminacies so that they can be analyzed in microvolt level (Comon and Jutten, 2010). The procedure of back-projection of several components is implemented as following:

$$\begin{aligned} \underline{\mathbf{X}} &= \left[ \mathbf{u}_{r_1}, \dots, \mathbf{u}_{r_i} \right] \left[ \mathbf{y}_{r_1}, \dots, \mathbf{y}_{r_i} \right]^T \\ &= \mathbf{u}_{r_1} \circ \mathbf{y}_{r_1} + \dots + \mathbf{u}_{r_i} \circ \mathbf{y}_{r_i}, \end{aligned} \quad (8)$$

where,  $r_1, \dots, r_{i-1}$ , and  $r_i$  ( $1 \leq r_i < R$ ) are used to represent the sequences of the selected components; The size of the matrix  $\underline{\mathbf{X}}$  is the same to  $\mathbf{X}$ .

Noticeably, for spatial-PCA (see *Figure 7*), the rows and columns of  $\bar{\mathbf{X}}$  are channels and time samples, respectively. Here,  $\bar{\mathbf{X}}$  is used to represent the matrix, which is to be decomposed, for avoiding confusion with that in temporal-PCA. The  $\mathbf{u}_r$  and  $\mathbf{y}_r$  are the topography and waveform of  $r^{th}$  estimated component, respectively.

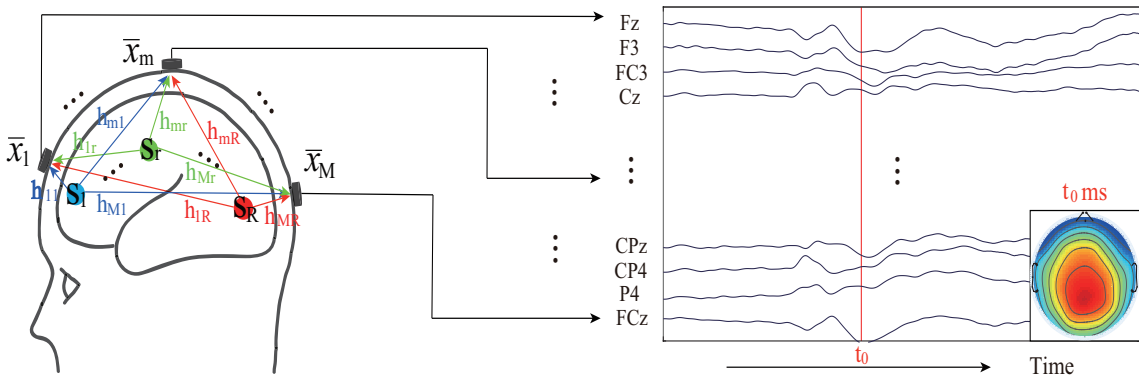


**FIGURE 7** Example of blind source separation (BSS) model for a temporal concatenated matrix  $\bar{\mathbf{X}} = \left[ \bar{\mathbf{x}}_1, \dots, \bar{\mathbf{x}}_m, \dots, \bar{\mathbf{x}}_M \right]^T = \sum_{m=1}^M \sum_{r=1}^R \mathbf{h}_{mr} \mathbf{s}_r$  (i.e., electrode  $\times$  time sample).  $\bar{\mathbf{x}}_m$  is collected waveform at  $m^{th}$  electrode;  $\mathbf{s}_r$  is the  $r^{th}$  source signal;  $\mathbf{h}_{mr}$  is the weighting value from  $r^{th}$  source to  $m^{th}$  electrode.

### 2.1.2 PCA procedure for ERPs extraction

This subsection introduces the procedure of PCA for extracting ERPs of interest from the preprocessed EEG/ERP data. Herein, the following steps are involved in the ERP extraction: arranging ERP/EEG data into a matrix, estimating the number of sources, selecting the rotation method, identifying the components of interest, and analyzing the identified components.

#### 2.1.2.1 Arranging ERP/EEG data into a matrix

In multi-subject and multi-condition ERP experiments, two different strategies are usually used to extract ERPs of interest when using PCA.

On the one hand, ERPs of interest are usually extracted from the waveforms of all subjects simultaneously and this strategy is referred to as group PCA analysis. In the group PCA analysis, all subjects' data are connected to form a matrix, i.e.,  $\mathbf{X} = [\mathbf{X}(1), \dots, \mathbf{X}(p), \dots, \mathbf{X}(P)]$  (here, P is used to represent the number of subjects). As a result, the mixing matrices in *Eq. 1* are considered to be the same for different subjects:  $\mathbf{H} = \mathbf{H}(1) = \dots = \mathbf{H}(p) = \dots = \mathbf{H}(P)$ . Moreover, both the sequences ( $\mathbf{S}_r = \mathbf{S}(1)_r = \dots = \mathbf{S}(p)_r = \dots = \mathbf{S}(P)_r$ , r is the source order which is smaller than M) and the numbers ( $R = R(1) = \dots = R(p) = \dots = R(P)$ ) of the sources for different subjects are also invariable.

On the other hand, the interesting ERPs can be explored from single-trial EEG data of individual subject (i.e., individual-subject PCA analysis). In such a strategy, to obtain a better performance of PCA, the channels of single-trial EEG for each subject under different experimental conditions are concatenated to form a matrix separately (Zhang et al., 2021). By contrast with the assumptions in the first strategy, the mixing matrices for different subjects are allowed to be varied in this strategy. Moreover, the orders and the numbers of the sources for different subjects might be different (Zhang et al., 2021). Furthermore, the waveforms/topographies (corresponding to temporal-PCA and spatial-PCA, respectively) of ERPs of interest for different single trials within one subject's EEG data are assumed to be the same.

For both group and individual-subject PCA analysis strategies, there are at least four modes for multi-subject and multi-condition ERP datasets, namely, time sample (S), electrode (E), experimental condition (C), and subject (P). Therefore, two different types of matrices (see *Figure 3*) can be formed, both of which contain variables and observations (Dien, 2012; Dien et al., 2007, 2005). Herein, the application of PCA on trial-averaged ERP data is taken as an example. For the first type of matrix, the averaged ERP data are stacked over electrodes of all subjects of all conditions to generate a matrix  $\mathbf{X}$  with the size of  $S \times (E \times P \times C)$ . In such a matrix, the variables are time samples, and observations are the products of electrodes, conditions and subjects. For the second type of matrix, the matrix  $\mathbf{X}$  with the size of  $E \times (P \times C \times S)$  can be organized over time samples for all subjects under different conditions. In this type of matrix, the electrodes are considered to be variables and the waveforms (the combinations of time samples,

conditions, and subjects) at all electrodes are the observations.

In conclusion, before using PCA, we have to confront two questions. One is how to extract ERPs of interest from all subjects' or individual subject's EEG/ERP data. The other is how to form a matrix connecting EEG/ERP data across electrodes or time samples. The suggested solution is to extract ERPs of interest from the spatial-stacked matrix of an individual EEG data separately. One reason for the solution is that it is challenging to keep all the waveforms of the interesting ERPs for different subjects are unvaried, even those data are strictly recorded under the same experimental environment. For the other reason, ERPs of interest overlap with others of non-interest to some extent in the spatial domain (i.e., their topographies are mixed) because of volume conduction. As a result, it is challenging to separate ERPs of interest from the temporal-concatenated matrix (i.e., by using spatial-PCA).

### 2.1.2.2 Estimating the number of sources

This step aims to use fewer variables to represent the whole information of the original matrix and convert the original over-determined model into the determined model (i.e., from *Eq. 1* to *Eq. 2*).

Typically, the number of sources can be estimated based on the eigenvalues of the extracted components. The eigenvalues are obtained from the covariance matrix  $\mathbf{C}_X = \mathbf{XX}^T$  or  $\mathbf{C}_X = \mathbf{X}^T\mathbf{X}$  in a descending order (one eigenvalue corresponds to one PCA-extracted component).

$$\lambda_1 \geq \dots \geq \lambda_l = \dots = \lambda_L = \sigma^2. \quad (9)$$

In above equation,  $\{\lambda_l\}_{l=1}^L$  represent the eigenvalues of matrix  $\mathbf{C}_X$  and  $L = \min\{M, N\}$ . It is noted that the first PCA-extracted component explains the largest percentage ratio of total variance because its eigenvalue is highest (as shown in *Figure 8 (a)*).

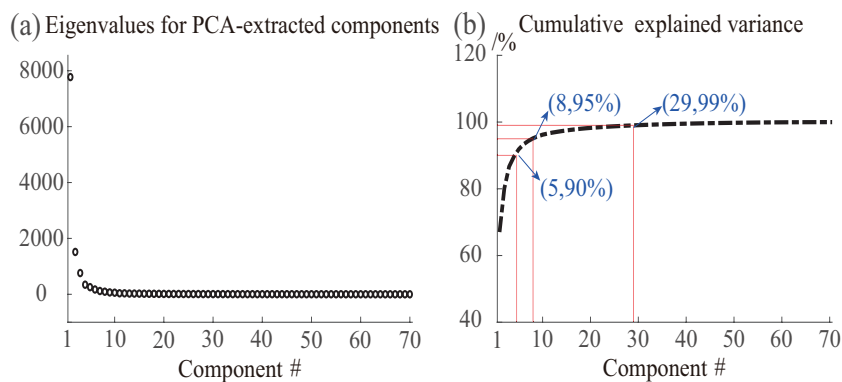


FIGURE 8 The example of estimating source number (PCA). (a) Eigenvalues for the first 70 PCA-extracted components. (b) The cumulative explained variance.

Several approaches, for example, Parallel test (Dien, 2010a; Horn, 1965), cumulative explained variance (Huster and Raud, 2018; Van Dinteren et al., 2018;

Huster et al., 2020; Zhang et al., 2020a), and gap measure (Cong et al., 2013a; He et al., 2010), have been developed to assess the source number. Here, the theory of the cumulative explained variance is supplemented. In practice, the cumulative explained variance is obtained by computing the percentage ratio (PR) of the sums of the first  $R$  eigenvalues over the sums of all eigenvalues.

$$PR = \frac{\sum_{r=1}^R \lambda_r}{\sum_{l=1}^L \lambda_l} \times 100\%, \quad (10)$$

where  $R$  denotes the estimated source number;  $L$  is the number of variables,  $L \geq R$ . Once PR is defined by using a specific value, such as 90%, 95%, and 99%, the number of sources will be estimated. For example, if PR is defined as 99% and the first 29 components explain this ratio of the total variance, these components are then chosen for next procedure (see *Figure 8 (b)*).

#### 2.1.2.3 Selecting the rotation method

The rotation method is targeted at rearranging the structures of the original extracted components into simple and interpretable structures (Dien, 2012). Two different types of rotation are widely used in the applications of ERP analysis. The first type is orthogonal rotation and it requires the PCA-decomposed components to be orthogonal to each other. The second one, i.e., oblique rotation, allows different PCA-decomposed components to be correlated with each other (Dien, 2012). Although the orthogonal rotation (e.g., Varimax) has been applied to extract ERPs of interest, and could yield better results (Dien et al., 2005; Dien, 1998), many previous studies more agreed that Promax rotation is most suited for t-PCA, Infomax rotation is most efficient for spatial-PCA (Dien, 2012; Dien et al., 2007; Dien, 2010b).

#### 2.1.2.4 Identifying the PCA-extracted components of interest

Even artifacts are significantly removed during the preprocessing procedure, the PCA-extracted components can be categorized into four different types at least, namely, components of interest, spontaneous brain activities, components of non-interest, and noise activities. Noticeably, only several PCA-extracted components, which are considered to be separated from the waveforms of ERPs of interest, are selected and used for the following procedure.

Commonly, only the properties of the PCA-extracted components in the temporal and spatial domains conform to the ERPs of interest, those components are then used for next procedure. The following two aspects are served as criteria for selecting the PCA-extracted components of interest (Zhang et al., 2020a; Barry et al., 2020; Karamacoska et al., 2019): (1) The polarity and peak latency of temporal component; (2) The polarity and topographical distribution of the spatial component.

*Figure 9* shows an example for the extraction of N2 by using temporal-PCA. Herein, N2 is primarily found in the frontocentral sites within the time window

220 ms to 270 ms (see *Figure 9 (a)*). For the 2<sup>nd</sup> temporal component, the peak latency is about 262 ms and the polarity is positive. And the active area in the corresponded spatial component is found in frontocentral sites and the polarities in those sites are negative. These features reveal that this PCA-extracted component is decomposed from the waveform of N2. Likewise, the 6<sup>th</sup> component is regarded to be separated from the waveform of N2 (see *Figure 9 (b)*).

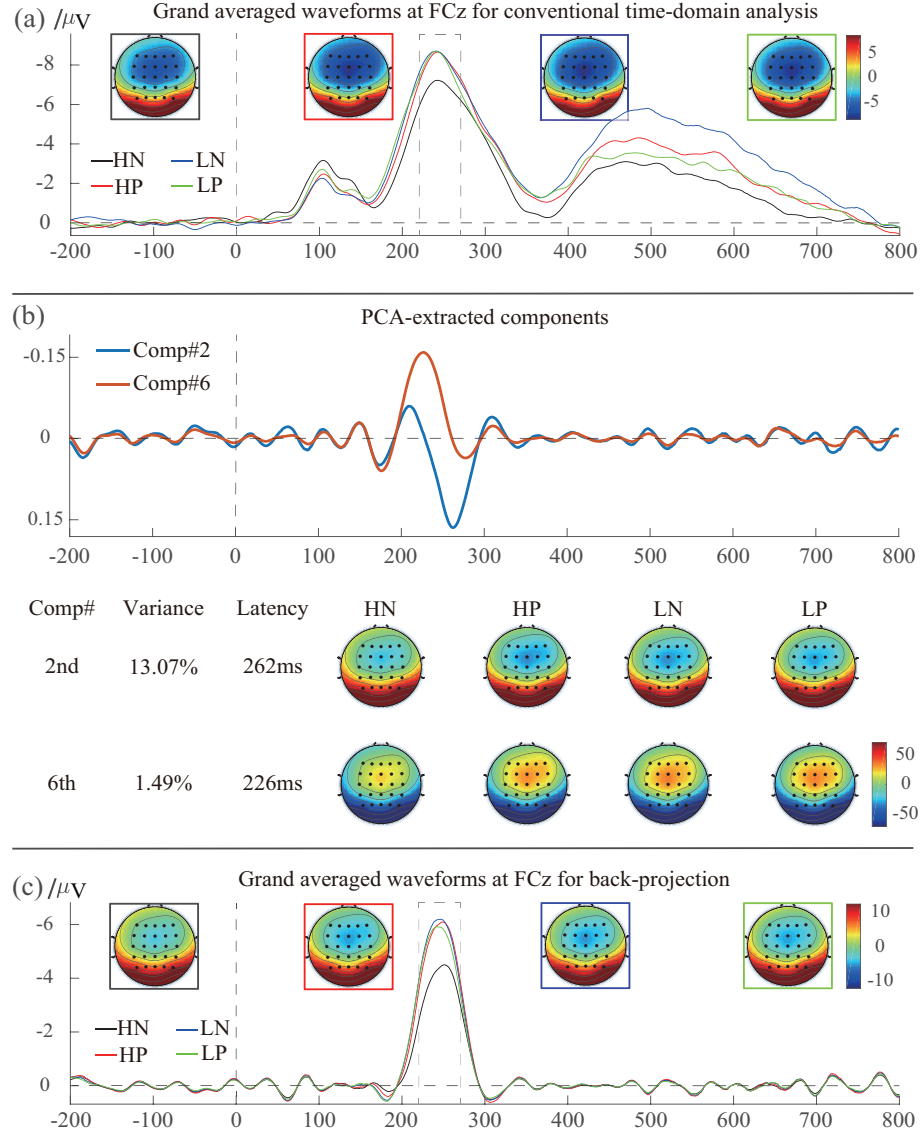


**FIGURE 9** An example for the application of PCA on ERP data. (a) Original ERP data: The grand averaged waveforms (at FCz electrode) and topographies. (b) The temporal and spatial (which were averaged over subjects) features for 2<sup>nd</sup> and 6<sup>th</sup> PCA-extracted components. (c) Back-projected waveforms and related topographies for different conditions.

### 2.1.2.5 Analyzing the identified PCA-extracted components

After the PCA-extracted components are identified, the differences between different experimental conditions are evaluated based on the selected components.

In some previous studies (Male and Gouldthorp, 2020; Delplanque et al., 2005; Widmann et al., 2018; Leue et al., 2009; Hsu et al., 2014), the factor scores obtained by PCA are often fed into statistical analysis methods to examine the differences between/among experimental conditions. In detail, in terms of temporal-PCA, different subjects under different experimental conditions have the common waveform (i.e., factor loadings  $\mathbf{U}_{tPCA}$ ), but the differences are observed in the amplitudes in the related topographies (i.e., factor scores  $\mathbf{Y}_{tPCA}$ ). Therefore, statistical analysis methods are applied to examine the discriminations of the amplitudes for different conditions at some typical electrodes obtained from the selected spatial components. Similarly, in the application of spatial-PCA, a common spatial component is used for spatial characteristic of an ERP for all subjects under different conditions (i.e., refer to factor loadings  $\mathbf{Y}_{sPCA}$ ), whereas the amplitudes of waveforms (i.e., factor scores  $\mathbf{U}_{sPCA}$ ) for all subjects differ from each other. Thus, based on the selected factor score(s), the mean/peak amplitudes within a predefined time window are used as input for statistical analysis methods.

In other investigations, the amplitudes of the interesting ERPs are obtained by calculating the product of factor scores, factor loadings, and standard deviations of the original waveforms (MacDonald and Barry, 2020, 2017; Dien, 2012). However, the latencies of the analyzed ERPs for different subjects in those studies are assumed to be invariant, contrary to actual ERP waveforms. They also do not discuss the situation that how to analyze two or more PCA-extracted components simultaneously, especially for the PCA-extracted components are highly similar in time and space domains.

To fill these gaps, back-projection theory, which has been used in ICA applications (Makeig et al., 1997, 1999; Cong et al., 2011a,c), is conducted to the application of PCA on ERP datasets in our previous studies (Zhang et al., 2020a; Li et al., 2019; Cao et al., 2020; Zhang et al., 2021). The back-projection is to convert the estimated source components into signals at the microvolt level (i.e., electrode fields) by computing the sums of the outer products of the selected temporal and spatial components, as described in *Eq. 8*. Additionally, there are two main advantages when applying back-projection theory to PCA (Zhang et al., 2020a). First, with the back-projection theory, several PCA-extracted components can be analyzed simultaneously. Second, the indeterminacies of the PCA-extracted components in the polarity and the amplitude can be corrected so that the amplitudes of PCA-extracted components can be quantified at the microvolt level.

Furthermore, since one-step PCA (i.e., either temporal-PCA or spatial-PCA) may fail to separate the ERPs, which are highly mixed in temporal and spatial domains, some researchers have attempted to perform two-step PCA on the ERP signals (Dien, 2010b; Spencer et al., 2001; Kamp, 2020; Severo et al., 2020). Two-step PCA is divided into two different types, namely, spatiotemporal and tem-

porospatial. The obtained factor scores from the first step are submitted to the other complementary PCA, for example, spatial-PCA is employed after an initial temporal-PCA. The temporospatial PCA produces better overall results than those of spatiotemporal PCA (Dien, 2012, 2010b).

Herein, an example is given to show how to perform PCA on the trial-averaged ERP data to extract an ERP (i.e., N2) of interest (see *Figure 9*). Noted that the conventional time-domain results for N2 have been reported in this paper (Lu et al., 2017). Moreover, the amplitudes of N2 for four different conditions were measured within the time window 220-270 ms at Fz, FCz, and Cz electrodes (i.e., two factors: Arousal [High vs. Low]  $\times$  Valence [Negative vs. Positive] within-subject experimental design). When using temporal-PCA to extract the N2 of interest, the averaged ERP datasets for all subjects are firstly arranged into a matrix with  $1000 \times 2600$ , i.e., time samples  $\times$  (electrodes  $\times$  subjects  $\times$  conditions). After that, according to the cumulative explained variance method, the percentage ratio is set to be 99%, 29 components are retained and rotated (see *Figure 8 (b)*). Next, based on the characteristics of N2 in the temporal and spatial domains, the 2<sup>nd</sup> and 6<sup>th</sup> components are believed to come from the original waveforms of N2 (see *Figure 9 (b)*). Specifically, the peak latencies of the 2<sup>nd</sup> and 6<sup>th</sup> temporal components are at 262 ms (positive) and 226 ms (negative) separately. Meanwhile, the polarities in frontocentral sites of the related spatial components for both selected components are positive and negative separately. Finally, both components are back-projected to electrode fields see (*Figure 9 (c)*), and the amplitudes of projected N2 are measured at electrode sites Fz, FCz, and Cz.

### 2.1.3 Model of ICA and its application

ICA also follows the BSS model as described in *Subsection 2.1.1*, while an adaptive iteration learning algorithm (Hyvärinen, 1999; Hyvärinen and Oja, 2000) is used to obtain unmixing matrix  $\mathbf{W}$  in the application of ICA. The extracted components by ICA are independent of each other compared with those that are related to each other in PCA and rotation method.

Although ICA has been used to extract ERPs of interest from either spatial- or temporal-stacked trial-averaged/single-trial data (Van Dinteren et al., 2018; Huster et al., 2020; Cong et al., 2010), most researchers would like to use it to remove artifacts from EEG data during the preprocessing procedure (Dimigen, 2020; Winkler et al., 2011; Mognon et al., 2011; Jung et al., 2000). Generally, the raw EEG data of an individual subject ( $\mathbf{X}$  with electrode by time sample) are first decomposed into  $R$  ICs. It should be noted that the number of electrodes is used as the number of the estimated ICs (Onton et al., 2006). This means that the model of BSS in ICA decomposition is a determined model so that only *Eqs. 1 - 5* are involved. In the following, artifacts are identified based on their temporal (i.e., waveform  $\mathbf{y}_k$ ) and spatial (i.e., topography  $\mathbf{w}_k$ ) properties, and then, they are projected back to electrode fields ( $\hat{\mathbf{X}} = \mathbf{w}_{k_1} \circ \mathbf{y}_{k_1} + \dots + \mathbf{w}_{k_i} \circ \mathbf{y}_{k_i}; k_1, \dots, k_{i-1}$ , and  $k_i$  are sequences of ICs associated with artifacts). Finally, ICs associated with artifacts are removed from the raw EEG data ( $\mathbf{X}_{corrected} = \mathbf{X} - \hat{\mathbf{X}}$ ).

## 2.2 Theory and procedure of complex Morlet continuous wavelet transform to extract EROs

As mentioned in *Subsection 1.2.2*, the temporal and spectral modulations of EROs can be explored simultaneously from TFRs (Herrmann et al., 2014; Gross, 2014; Tallon-Baudry and Bertrand, 1999). In reality, each ERP can be regarded to be either an ERO in a specific frequency or a mixture of multiple EROs with varied frequencies (Herrmann et al., 2014).

Many techniques, for instance, STFT, S-transform, CMCWT, and Hilbert transform, have been developed and widely used to calculate TFRs of EEG/ERP data (Roach and Mathalon, 2008; Wacker and Witte, 2013; Gross, 2014). CMCWT is frequently used compared with other techniques since its yields provide an optimal trade-off between time resolution and frequency resolution. That is to say, in the CMCWT technique, the wavelets with shorter length of the time window are conducted at high frequencies and longer wavelets are used at low frequencies (see *Figure 4 (a)*). Consequently, the obtained TFRs have better frequency-resolution at low frequency bands, and better time resolution at high frequency bands (Cohen, 2019; Gross, 2014). Moreover, the TFRs obtained by CMCWT seem to more satisfy the temporal and spectral properties of ERPs of interest because the EROs for the late ERPs (e.g., P300, LPP) are usually located at lower frequency bands, while higher frequency EROs corresponding to some early ERPs (e.g., P1, N1).

In the following, the theory and application of CMCWT on EEG/ERP data are presented.

### 2.2.1 The theory of complex Morlet continuous wavelet transform for ERP data analysis

In the CMCWT, the underlying idea for the calculation of TFRs is to compute the convolutions between ERP signals and complex Morlet wavelets (CMWs or Gabor wavelet) with different lengths derived from the mother wavelet (see *Figure 4 (a) → (b) → (c)*). The convolutions yield the complex-valued series at each frequency band results in the energy (the square of the convolution results) and phase angle (the tangent values between the real part and imaginary part) for EROs can be investigated (Herrmann et al., 2014; Gross, 2014; Makeig et al., 2002; Lachaux et al., 1999; Stam et al., 2007).

As described in *Subsection 1.2.2*, two different types of EROs, i.e., evoked and induced EROs, which response to the stimulus onset, can be obtained from EEG/ERP signals (Herrmann et al., 2014; Roach and Mathalon, 2008; Gross, 2014; Tallon-Baudry and Bertrand, 1999). Evoked EROs are obtained by calculating TFRs of the averaged ERP data (i.e., averaging over single trials, see *Figure 10 (a) → (b) → (c)*). Regarding induced EROs, they are the subtractions between the total brain activities that obtained by averaging TFRs of single trials and the evoked EROs (see *Figure 10 (a) → (d) → (e)*).

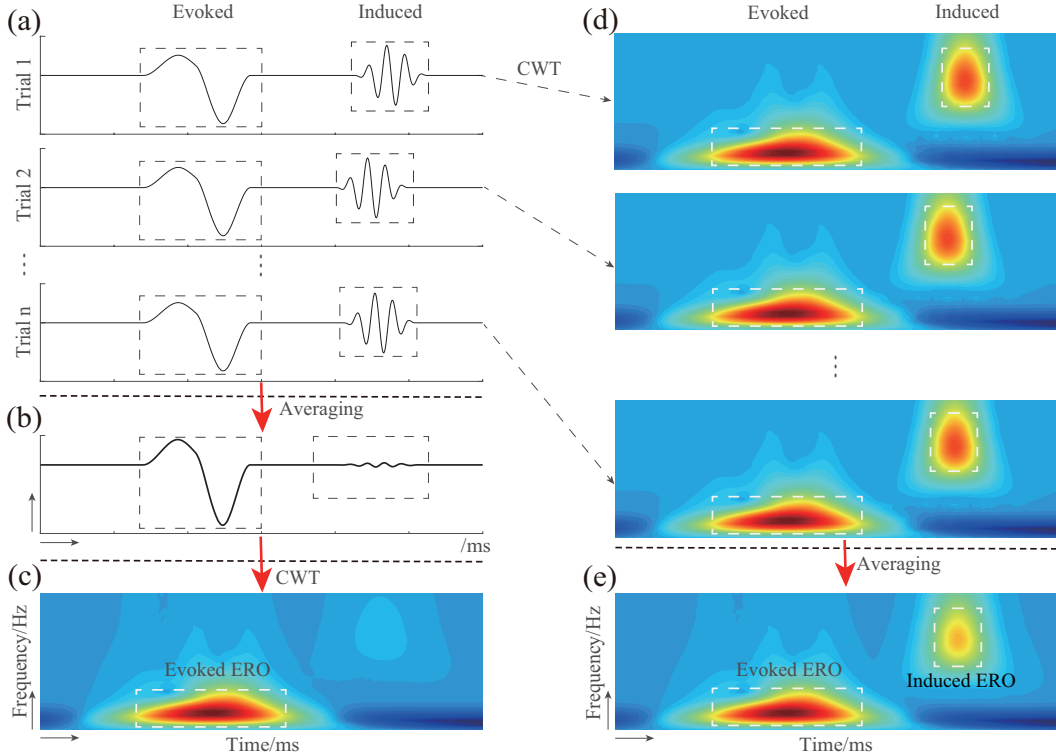


FIGURE 10 Example for calculation of evoked ((a) → (b) → (c)) and induced ((a) → (d) → (e)) oscillations. (a) The waveforms for different trials that contain both evoked and induced brain activities. (b) The averaged waveform over trials in (a) and it should be noted that induced brain activities are cancelled out during averaging procedure. (c) The time-frequency representations (TFRs) of the averaged waveforms in (b), which contains evoked oscillations based on the continuous wavelet transform (CWT). (d) The TFRs of the waveforms for different trials in (a). (e) All brain activities are obtained by averaging the TFRs over trials in (d), including evoked and induced oscillations.

In the following contents, the calculation of the energies for both types of EROs is described.

For a time series  $\mathbf{x}(t)$  with  $N$  points, the related TFRs based on continuous wavelet transform are considered to be the convolutions between time-domain signal  $\mathbf{x}(t)$  and the scaled and shifted mother wavelet  $\psi(\frac{t-t_0}{a})$ . And the related procedure is expressed as below (Herrmann et al., 2005; Zhang et al., 2020b):

$$\mathbf{X}(a, t_0) = \frac{1}{\sqrt{|a|}} \sum_{t=0}^{N-1} \mathbf{x}(t) \psi\left(\frac{t-t_0}{a}\right), \quad (11)$$

where  $\mathbf{x}(t)$  is the waveform at a specific channel;  $a$  and  $t_0$  represent the scaling and shifting parameters, respectively.

Since CMW can govern the trade-off between temporal resolution and frequency resolution, it has been widely used as a mother wavelet (Gross, 2014). The definition of the scaled and unshifted CMW is expressed as (Herrmann et al.,

2005; Zhang et al., 2020b; Tallon-Baudry and Bertrand, 1999):

$$\psi_{CMW} = \frac{1}{\sqrt{\pi\sigma^2}} e^{i2\pi ft} e^{\frac{-t^2}{2\sigma^2}}, \quad (12)$$

where  $f = \frac{f_0}{a}$  ( $f_0$  is the center frequency and  $f$  is the frequency range of interest, e.g., 1-30 Hz) and  $\sigma$  is bandwidth.

A constant ratio (i.e., number of wavelet cycles) is generally used to characterize CMW family and it can be defined as (Zhang et al., 2020b; Tallon-Baudry and Bertrand, 1999):

$$K = \frac{f}{\sigma_f} = 2\pi f \sigma, \quad (13)$$

where,  $\sigma_f = \frac{1}{2\pi\sigma}$ . In practice, this constant ratio is often set to be greater than 5 (Zhang et al., 2020b; Li et al., 2019; Tallon-Baudry and Bertrand, 1999; Xia et al., 2018). Bandwidth  $\sigma$  is inversely proportional to frequency range  $f$  (i.e.,  $\sigma \sim 1/f$ ). As a result, the CMWs have longer lengths at low frequencies and shorter lengths at high frequencies.

Aiming at calculating the energies of evoked EROs, the EEG datasets of single trials for each experimental condition are firstly averaged and then CMCWT is performed on the averaged ERP signal to obtain TFRs. The following equation denotes both steps:

$$\mathbf{X}(t, f)_{Evoked} = \left| \frac{1}{\sqrt{|a|}} \sum_{t=0}^{N-1} \bar{\mathbf{x}}(t) \psi\left(\frac{t-t_0}{a}\right) \right|^2, \quad (14)$$

where  $\bar{\mathbf{x}}(t) = \frac{1}{J} \sum_{j=1}^J \mathbf{x}(t)_j$ , and  $\mathbf{x}(t)_j$  is waveform for  $j^{th}$  single-trial EEG data;  $J$  is the number of single trials.

Likewise, in order to obtain the induced EROs, the total brain activities are firstly computed. In detail, the single-trial EEG data are initially transformed into the time-frequency signals, and then TFRs of single-trial EEG data are averaged. The related procedure is expressed as:

$$\mathbf{X}(t, f)_{Total} = \frac{1}{J} \sum_{j=1}^J \left| \frac{1}{\sqrt{|a|}} \sum_{t=0}^{N-1} \mathbf{x}(t)_j \psi\left(\frac{t-t_0}{a}\right) \right|^2. \quad (15)$$

Afterwards, induced EROs are obtained by subtracting evoked brain activities from the total brain activities.

$$\mathbf{X}(t, f)_{Induced} = \mathbf{X}(t, f)_{Total} - \mathbf{X}(t, f)_{Evoked}. \quad (16)$$

Noted that the similar computation to that of total brain activities is named with different notations in other studies, for example, event-related desynchronization or synchronization (ERD/ERS) (Pfurtscheller and Da Silva, 1999), and event-related spectral perturbation (ERSP) (Delorme and Makeig, 2004).

### 2.2.2 CMCWT procedure for EROs extraction

TFA is targeted at analyzing the energies of prominent parts related to EROs of interest in temporal and spectral domains. In order to realize this purpose, the applications of CMCWT are classified into two main procedures: TFR calculation, and ERO identification and analysis here.

#### 2.2.2.1 TFR calculation

To calculate the TFRs of the preprocessed EEG/ERP data, the following steps are involved: selection of the analyzed ERO type, the definition of the mother wavelet, and baseline correction.

The first step is to select the type of the analyzed ERO. As described in *Subsection 2.2.1*, two strategies are employed to calculate the event-related brain oscillations, and both strategies directly govern which types of EROs will be obtained. Moreover, the selection of the analyzed ERO types also influences the setting of the frequency range to some degree. For example, for evoked oscillations, they are regarded as the responses to events and usually located at frequencies below 30 Hz. Generally, the frequency range is set from 1 Hz to 30 Hz before obtaining evoked EROs (Tallon-Baudry et al., 1996; Villena-González et al., 2018; Musacchia et al., 2017).

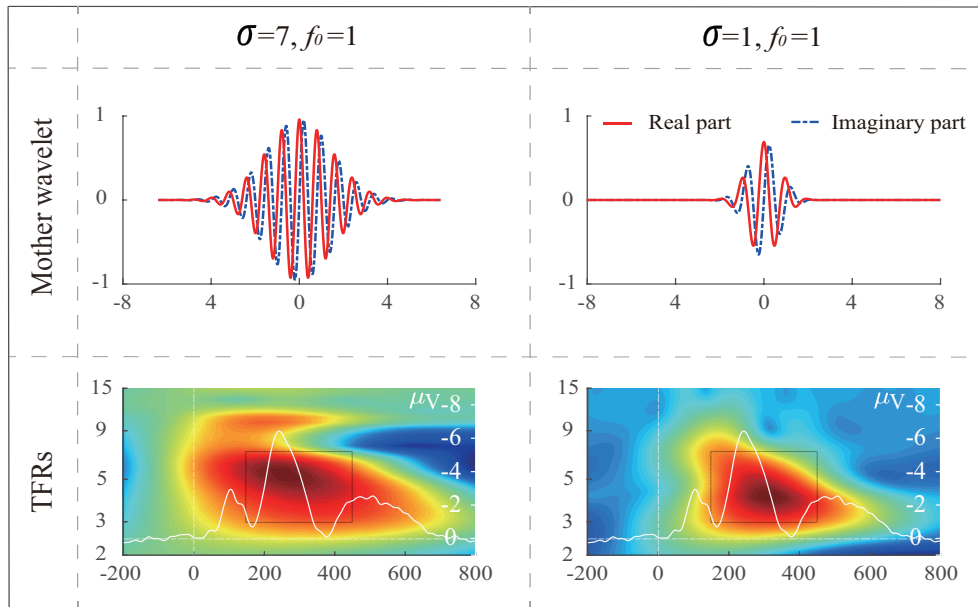


FIGURE 11 Example for the time-frequency representations (TFRs) using different mother wavelets.

The second step is to define the mother wavelet. As displayed in *Eqs. 11* and *12*, the time resolution and frequency resolution of TFRs are affected by the mother wavelet. The mother wavelet is defined by a set of bandwidth  $\sigma$  and center frequency  $f_0$ . Moreover, the findings in previous studies (Zhang et al., 2020b,

2018a) indicated that different parametric settings of center frequency and bandwidth result in divergent time-frequency results (See *Figure 11*). Therefore, we need to select an appropriate set of center frequency and bandwidth from many sets to obtain suboptimal time-frequency results so that the energies of EROs can be observed in a relatively limited time window and a short frequency range.

The third step is to correct baseline effect. Similar to the measurement of ERPs that are seen as the increased or decreased deflections compared with amplitudes in a pre-stimulus time interval, EROs are also considered as the relative changes to a defined baseline in the pre-stimulus period (Gross, 2014; Hu et al., 2014; Grandchamp and Delorme, 2011). Therefore, a relatively appropriate baseline correction approach is needed to help us easily identify and observe EROs in whole frequencies, especially in high frequencies. There are several commonly used approaches for baseline correction, such as the decibel method, the subtraction method, and the percentage method (Roach and Mathalon, 2008) (see *Figure 12*).

Usually, after the TFRs of trial-averaged ERP data are computed (i.e., evoked brain activities  $\mathbf{X}(t, f)_{\text{Evoked}}$ ) or the TFRs of single-trial EEG data are averaged (i.e., total brain activities  $\mathbf{X}(t, f)_{\text{Total}}$ ), the baseline correction step is then achieved by means of subtraction correction approach. In principle, the subtraction method is to calculate the subtractions between the original obtained evoked or total brain activities and the mean power of the defined baseline interval (e.g., from -200 ms to 0 ms) (Li et al., 2016; van den Broeke et al., 2017; Hu et al., 2014).

$$\mathbf{X}(t, f)_s = \mathbf{X}(t, f) - \mathbf{X}(f)_b, \quad (17)$$

where  $\mathbf{X}(f)_b$  is the averaged baseline activities within the defined pre-stimulus baseline interval.

Similarly, in order that EROs can be easily observed, percentage method can also be applied to compute the percentage ratio between the baseline-subtracted TFRs and the mean power of the baseline interval after the TFRs are initially calculated. This approach is expressed as below (Li et al., 2018; Hu et al., 2014):

$$\mathbf{X}(t, f)_p = \frac{\mathbf{X}(t, f) - \mathbf{X}(f)_b}{\mathbf{X}(f)_b} \times 100\%. \quad (18)$$

For the decibel method, it is first to compute percentages between the baseline subtracted TFRs and the mean power within the predefined time window at a specific frequency. Afterwards, these percentages are converted into decibels (dB) and this approach is implemented as (Roach and Mathalon, 2008):

$$\mathbf{X}(t, f)_{dB} = 20 \log_{10} \frac{\mathbf{X}(t, f) - \mathbf{X}(f)_b}{\mathbf{X}(f)_b}. \quad (19)$$

Hu et al. (2014) argued that some bias estimations of EROs are introduced using the percentage baseline correction method but not for subtraction baseline correction method, especially for single-trial analysis. However, there is no specific recommendation which baseline correction approaches enable the EROs

more easily to be identified and visualized, and this is more likely to rely on the specific experimental paradigms and time window length of single trial EEG data (Gross, 2014).

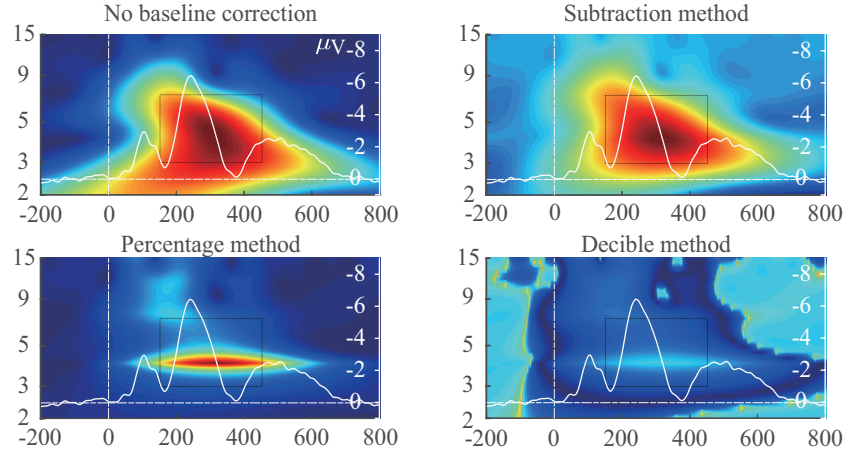


FIGURE 12 The example for the applications of three common used baseline correction techniques on TFRs.

### 2.2.2.2 ERO identification and analysis

Similar to the measurement of an ERP of interest in the time domain, the energies of the desired EROs under different experimental conditions are obtained within a defined region determined by both in time and frequency domains. Generally, according to both the previous findings and the inspection of TFRs in the current study, the region of an ERO are subjectively determined by means of a pre-set time window and a frequency range. This approach is named as conventional rectangle method because of the rectangle-like shape of the predefined region for an ERO of interest.

Noticeably, there are at least two shortcomings in this conventional rectangle method (Zhang et al., 2020a). For the first one, this is a subjective and arbitrary method. For the other one, the features of the other EROs may be involved if the predefined region is too large. Conversely, the partial characteristics of the desired EROs may be neglected.

To solve both problems, different advanced approaches have been attempted in the previous studies. For example, Jia et al. (2015) conducted clustering analysis which was based on similarities of topographies for different frequency bins and time points, to identify the regions of EROs; However, this approach may introduce some features of non-interest when the spatial property (i.e., topography) of the analyzed EROs is highly similar to others. Some researchers have attempted to use PCA to decompose the original TFRs to obtain the EROs of interest and then analyzed the factor scores which were related to EROs of interest (Roach et al., 2021) or analyzed the weightings between factor loadings and the original TFRs (Bernat et al., 2007, 2005; Hu et al., 2015). Noted that the weighted

EROs obtained by the approaches mentioned-above may be still mixture. To further study, Zhang et al. (2020a) firstly employed PCA on the waveforms of ERPs to extract temporal-spatial features of ERPs of interest and then transformed the extracted signals into the time-frequency signals (which is investigated in *Study 2*, see *Section 3.2*).

*Figure 13* is an example of the analysis of evoked theta EROs from a two-factor (Arousal [High vs. Low]  $\times$  Valence [Negative vs. Positive]) emotional ERP experiment based on CMCWT method (the details about experiment can refer to (Lu et al., 2017)). To obtain the theta EROs of interest, the mother wavelet is firstly defined by a set of the bandwidth  $\sigma$  and center frequency  $f_0$ , both of which are equal to 1. Secondly, TFRs are obtained by computing the square of the convolutions between the mother wavelet and preprocessed ERP signals (the values of convolutions are complex numbers). Thirdly, after baseline correction is achieved by using the subtraction method, the grand averaged TFRs are obtained from all subjects under each condition at Fz, FCz, and Cz electrodes (see *Figure 13* (a)). Finally, according to the inspections of grand averaged TFRs and previous studies, the energies of evoked theta oscillations of different conditions are calculated within the time window of 150 - 450 ms, and the frequency band is range 3 Hz to 7 Hz (see *Figure 13* (b)).

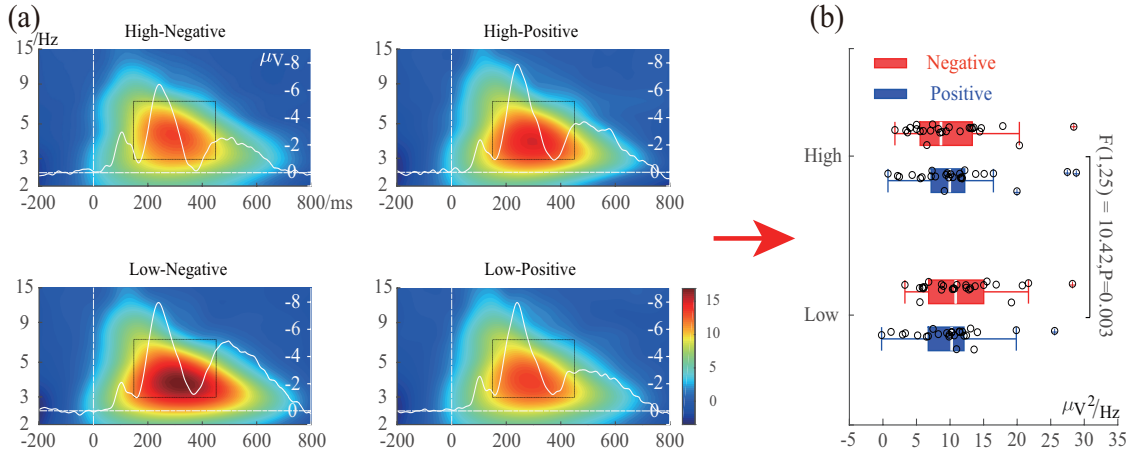


FIGURE 13 An example for the application of TFA on ERP data. (a) The grand averaged time-frequency representations (TFRs) of different experimental conditions at Fz, FCz, and Cz electrodes. (b) The energies of evoked theta oscillation (time window is from 150 ms to 450 ms and frequency range is 3-7 Hz) for different subjects under different conditions.

### 2.3 Theory and procedure of tensor decomposition to extract EROs

In a multi-subject and multi-condition ERP experiment, there exist four modes at least, namely, time, channel, condition, and subject. After the time-domain sig-

nals are transformed into the time-frequency signals, the frequency mode is also included. For the time-frequency results of single-trial EEG data in a between-subject experimental design (at least two groups), seven modes are contained: time, channel, condition, subject, trial, and group. Traditionally, the features of ERPs/EROs are measured in partial modes which result in the interactive effects among all modes that may not be explored. For example, in single-way component analysis techniques, the amplitudes of ERPs/EROs are merely quantified in either time mode or frequency mode.

According to the naturally high-dimensional characteristic of EEG/ERP data, tensor decomposition algorithms, which are based on two commonly used models of canonical polyadic (Hitchcock, 1927) and Tucker (Tucker, 1966), can be used to study the interactive effects among all modes of event-related brain activities.

In this section, only the basic concepts of both models are introduced. The details of mathematical algorithms for both models can be refer to (Cichocki et al., 2009, 2015). Also, their applications in the extraction of event-related brain activities are presented.

### 2.3.1 Mathematical models for tensor decomposition

#### 2.3.1.1 The definition of canonical polyadic decomposition

As described in *Section 2.1*, when using PCA and ICA, the matrix  $\mathbf{X}$  can be decomposed into the sum of R rank-one matrices, which is expressed as below:

$$\mathbf{X} = \sum_{r=1}^R \mathbf{a}_r^{(t)} \circ \mathbf{a}_r^{(c)} + \mathbf{E} = \sum_{r=1}^R \hat{\mathbf{X}}_r + \mathbf{E}, \quad (20)$$

where,  $\hat{\mathbf{X}}_r$  is a rank-one matrix and it is the outer product of  $r^{th}$  temporal component  $\mathbf{a}_r^{(t)}$  and spatial component  $\mathbf{a}_r^{(c)}$ .

Similarly, when using canonical polyadic decomposition (CPD), for a multi-array (i.e., tensor)  $\mathbf{X} \in \Re^{I_1 \times I_2 \times \dots \times I_M}$  with multiple modes, it is decomposed into R tensors (the rank of any tensor is one) plus the error tensor (Cong et al., 2015a, 2013b):

$$\mathbf{X} = \sum_{r=1}^R \mathbf{a}_r^{(1)} \circ \mathbf{a}_r^{(2)} \circ \dots \circ \mathbf{a}_r^{(M)} + \mathbf{E} = \sum_{r=1}^R \hat{\mathbf{X}}_r + \mathbf{E} = \hat{\mathbf{X}} + \mathbf{E} \approx \hat{\mathbf{X}}. \quad (21)$$

*Eq. 21* is also seen as BSS model (Cichocki et al., 2009; De Lathauwer, 2012),  $\hat{\mathbf{X}}_r = \mathbf{a}_r^{(1)} \circ \mathbf{a}_r^{(2)} \circ \dots \circ \mathbf{a}_r^{(M)}$  ( $r = 1, 2, \dots, R$ ) is considered as the rank-one tensor;  $\hat{\mathbf{X}}$  is used to estimate the original tensor  $\mathbf{X}$ ;  $\mathbf{A}^{(m)} = [\mathbf{a}_1^{(m)}, \mathbf{a}_2^{(m)}, \dots, \mathbf{a}_R^{(m)}] \in \Re^{I_m \times R}$  is regarded as the component matrix in  $m^{th}$  mode.

Herein, two-component CPD of the third-order tensor, which contains time ( $\mathbf{a}^{(t)}$ ), frequency ( $\mathbf{a}^{(s)}$ ), and space ( $\mathbf{a}^{(c)}$ ), is used as an example to clarify the interactions among the three modes and the relations between two components. When the third-order tensor is decomposed into two components by CPD, the

related decomposition can be expressed (Cong et al., 2015a):

$$\mathbf{X} \approx \mathbf{a}_1^{(t)} \circ \mathbf{a}_1^{(s)} \circ \mathbf{a}_1^{(c)} + \mathbf{a}_2^{(t)} \circ \mathbf{a}_2^{(s)} \circ \mathbf{a}_2^{(c)} = \hat{\mathbf{X}}_1 + \hat{\mathbf{X}}_2, \quad (22)$$

where,  $\mathbf{a}_1^{(t)}$ ,  $\mathbf{a}_1^{(s)}$ , and  $\mathbf{a}_1^{(c)}$  are characteristics of the first components in the temporal, spectral, and spatial modes, respectively. The three subcomponents of the first components are related to each other and their outer product is the rank-one tensor  $\hat{\mathbf{X}}_1$ . Likewise, for the second components  $\hat{\mathbf{X}}_2$ , its temporal  $\mathbf{a}_2^{(t)}$ , spectral  $\mathbf{a}_2^{(s)}$ , and spatial  $\mathbf{a}_2^{(c)}$  subcomponents are also associated with each other. However, all the subcomponents for the second component are not related to the first component in three modes (i.e.,  $\mathbf{a}_1^{(t)}$ ,  $\mathbf{a}_1^{(s)}$ , and  $\mathbf{a}_1^{(c)}$ ) (Cong et al., 2015a).

For Eq. 21, in the tensor-matrix product form, it can be converted as below:

$$\hat{\mathbf{X}} = \underline{\mathbf{I}} \times_1 \mathbf{A}^{(1)} \times_2 \mathbf{A}^{(2)} \times_3 \cdots \times_M \mathbf{A}^{(M)} + \mathbf{E} = \hat{\mathbf{X}} + \mathbf{E}, \quad (23)$$

where  $\underline{\mathbf{I}}$  is an identity tensor and the values of all elements in its super-diagonal line are equal to 1.

In the tensor decomposition, according to the properties of different modes, different additional constraint methods can be applied to some or all modes. For example, after the time-domain ERP signals are converted to time-frequency signals, the absolute or square of convolutions are calculated to obtain evoked or all brain activities (see Eqs. 14 and 15). Consequently, the values of all elements in different frequency bins and time points are non-negative, and thus, the non-negative constraint can be added to all modes.

### 2.3.1.2 The definition of Tucker decomposition

Regarding the application of Tucker decomposition on the  $M$ th-order tensor  $\mathbf{X} \in \Re^{I_1 \times I_2 \times \cdots \times I_M}$ , the related decomposition can be described as below (Cong et al., 2015a, 2013b):

$$\begin{aligned} \mathbf{X} &= \sum_{r_1=1}^{R_1} \sum_{r_2=1}^{R_2} \cdots \sum_{r_M=1}^{R_M} g_{r_1 r_2 \dots r_M} \mathbf{u}_{r_1}^{(1)} \circ \mathbf{u}_{r_2}^{(2)} \circ \cdots \circ \mathbf{u}_{r_M}^{(M)} + \mathbf{E} \\ &= \sum_{r_1=1}^{R_1} \sum_{r_2=1}^{R_2} \cdots \sum_{r_M=1}^{R_M} g_{r_1 r_2 \dots r_M} \hat{\mathbf{X}}_{r_1 r_2 \dots r_M} + \mathbf{E}, \end{aligned} \quad (24)$$

here,  $\mathbf{u}$  is used to represent the component of each mode in the Tucker decomposition rather than  $\mathbf{a}$  used in the CPD for avoiding confusion;  $\hat{\mathbf{X}}_{r_1 r_2 \dots r_M} = \mathbf{u}_{r_1}^{(1)} \circ \mathbf{u}_{r_2}^{(2)} \circ \cdots \circ \mathbf{u}_{r_M}^{(M)}$  is the outer product of  $M$  subcomponents from  $M$  component matrices in  $M$  modes and it is also a rank-one tensor;  $g_{r_1 r_2 \dots r_M}$  is considered as the core tensor  $\underline{\mathbf{G}} \in \Re^{R_1 \times R_2 \times \cdots \times R_M}$ . The values of  $R_1, R_2, \dots, R_{M-1}$ , and  $R_M$  can be variant when  $M$  is more than 3.

In terms of Tucker decomposition, Eq. 24 can also be expressed in the form of tensor-matrix as below:

$$\mathbf{X} = \underline{\mathbf{G}} \times_1 \mathbf{U}^{(1)} \times_2 \mathbf{U}^{(2)} \times_3 \cdots \times_M \mathbf{U}^{(M)} + \mathbf{E} = \hat{\mathbf{X}} + \mathbf{E}, \quad (25)$$

where  $\mathbf{U}^{(m)} = [\mathbf{u}_1^{(m)}, \mathbf{u}_2^{(m)}, \dots, \mathbf{u}_R^{(m)}] \in \Re^{I_m \times R_m}$  is used to denote the component matrix in  $m^{th}$  mode.

### 2.3.1.3 The differences between CPD and Tucker decomposition

As described in (Cong et al., 2015a), the key difference between CPD and Tucker decomposition is whether different components are allowed to be related or not. In detail, in the CPD, the sequences of the subcomponents from component matrix  $\mathbf{A}_r^{(m)}$  in different modes (e.g., temporal component, spatial component, spectral components, and so forth) are the same. For instance, as described in Eq. 22, the first component matrix  $\mathbf{A}$  must be constituted by the first temporal  $\mathbf{a}_1^{(t)}$ , spectral  $\mathbf{a}_1^{(s)}$ , and spatial  $\mathbf{a}_1^{(c)}$  components that are first component of  $\mathbf{A}^{(1)}$ ,  $\mathbf{A}^{(2)}$ , and  $\mathbf{A}^{(3)}$  respectively. However, for Tucker decomposition, there is no requirement that the sequences of the subcomponents for different modes in the same component matrix should be the same. This means that the orders of the selected component in different modes from the component matrices  $\mathbf{A}_{r_m}^{(m)}$  are allowed to be variant. That is,  $r_1, r_2, \dots, r_{M-1}$ , and  $r_M$  can be different.

There are also some other differences between CPD and Tucker decomposition. For example, the numbers of the reserved components for different modes are the same in the CPD but the numbers of components in different modes can be variant for Tucker decomposition. Moreover, the core tensor is the identify tensor in the CPD, and any tensor with compatible sizes can be used as the core tensor in Tucker decomposition. Furthermore, the yields obtained by CPD can be unique under mild additional assumptions, while the results for Tucker decomposition can not be unique without applying any additional constraints (Cong et al., 2015a; Zhou and Cichocki, 2012).

### 2.3.2 Applications of tensor decomposition on ERP datasets

Tensor decomposition aims to obtain the multi-domain features of event-related brain activities and use the interacted signatures of subjects under different experimental conditions to explore the differences in their cognitive processes. Condition, subject, and group modes are often merged as one mode in the last dimension of the formed tensor (Cong et al., 2015a).

For both CPD and Tucker decomposition, four steps are mainly involved in the extraction of event-related activities, namely, component number identification, component extraction, component selection, and component analysis (the last three steps are introduced simultaneously in one subsection for the applications CPD and Tucker decomposition, separately). Notation of sample is used to represent the combinations of subject, condition, and group in the following contents.

### 2.3.2.1 Determining the number of extracted components for tensor decomposition

Similar to the applications of PCA and ICA, when applying either CPD or Tucker decomposition, which are also seen as the BSS algorithms, on the tensor of TFRs of EEG/ERP data, the number of sources should be estimated. Specifically, regarding CPD, one parameter needs to determine for different modes since the extracted component numbers in different modes are invariant. However, the numbers of the parameters are same to the number of modes for Tucker decomposition.

To estimate the numbers of sources in different modes for tensor decomposition, several existing techniques can be used to determine these parameters, for example, the cross-validation of component models (Bro and Kiers, 2003; Bro et al., 2008), model order selection (He et al., 2010), and the difference of fit (DIFFIT) (Timmerman and Kiers, 2000; Mørup and Hansen, 2009). Compared with other techniques, DIFFIT has been widely used in the applications of tensor decomposition on EEG/ERP signals (Cong et al., 2013b, 2012; Zhang et al., 2020b; Wang et al., 2018; Yu et al., 2020; Wang et al., 2020).

DIFFIT is the trend of the fit with the increase of the estimated component number under either the canonical polyadic model or Tucker model (Timmerman and Kiers, 2000). Herein, the estimation of source number by means of DIFFIT under CP model is taken as an example. The fit under canonical polyadic model is implemented:

$$fit(k) = 1 - \frac{\|\mathbf{X} - \hat{\mathbf{X}}_k\|_F}{\|\mathbf{X}\|_F}, \quad (26)$$

where,  $\hat{\mathbf{X}}_k$  roughly represents the original tensor  $\mathbf{X}$  ( $k$  plays the same role as  $r$  in Eq. 21),  $k = 1, \dots, K$ ;  $\|\cdot\|_F$  denotes the Frobenius norm.

In practice, DIFFIT is to calculate the ratio between the adjacent difference fits, which is described as below:

$$DIFFIT(k) = \frac{DIF(k)}{DIF(k+1)}, \quad (27)$$

where  $k = 2, \dots, K-1$ . Usually, the number  $r$  with the largest DIFFIT value will be used as the estimation of source number. To gain a more accurate results, the same data are often decomposed many times by CPD (e.g.,  $L = 100$  times) for each  $k$ , and thus, the averaged fit value of  $L$  times  $\overline{fit(k)} = \frac{1}{L} \sum_{l=1}^L fit(k)$  to compute the difference fit of the adjacent fits (Cong et al., 2015a; Wang et al., 2018):

$$DIF(k) = \overline{fit(k)} - \overline{fit(k-1)}, \quad (28)$$

where  $k = 2, \dots, K$ .

### 2.3.2.2 Canonical polyadic decomposition of tensor of ERP datasets

For the TFRs of multi-subject and multi-condition EEG/ERP data, besides sample mode, the other modes are also included, such as temporal mode, spatial

mode, spectral mode, etc. Thus, the problem needs to solve that how to organize those modes to form a tensor. Generally, the samples are arranged into the last dimension of tensor and the other modes are organized into other dimensions. Consequently, the  $M$ th-order tensor  $\mathbf{X} \in \Re^{I_1 \times I_2 \times \dots \times I_M}$  ( $I_M$  is equal to the size of samples) can be expressed as below when using CPD (Cong et al., 2015a):

$$\begin{aligned}\mathbf{X} &= \sum_{r=1}^R \mathbf{a}_r^{(1)} \circ \mathbf{a}_r^{(2)} \circ \dots \circ \mathbf{a}_r^{(M-1)} \circ \mathbf{f}_r + \mathbf{E} \\ &= \mathbf{I} \times_1 \mathbf{A}^{(1)} \times_2 \mathbf{A}^{(2)} \times_3 \dots \times_{M-1} \mathbf{A}^{(M-1)} \times_M \mathbf{F}^{(M)} + \mathbf{E},\end{aligned}\quad (29)$$

where  $\mathbf{a}_r^{(m)} \in \Re^{I_m \times 1}$  denotes the  $k^{th}$  component for  $m^{th}$  mode ( $\|\mathbf{a}_r^{(m)}\|_2 = 1$ ); the component  $\mathbf{f}_r$  in the last mode represents the signatures of samples and it is named as feature component. Statistical analysis methods can be performed on the signatures of samples for the selected components to obtain the differences between/among different conditions. Following the line with the underlying idea in Eq. 29, many investigations have done to study the multi-domain characteristics of EROs of interest using tensor decomposition (Cong et al., 2014, 2013b, 2012; Zhang et al., 2020b; Wang et al., 2018; Yu et al., 2020).

According to different study purposes, different types of tensor with different modes from the TFRs of the ERP datasets can be formed. For example, a fourth-order tensor can be formed to study the interactions among time, frequency, and space modes. The related decomposition of the fourth-order tensor by using CPD is defined as (Cong et al., 2015a):

$$\mathbf{X} \approx \mathbf{I} \times_1 \mathbf{A}^{(t)} \times_2 \mathbf{A}^{(s)} \times_3 \mathbf{A}^{(c)} \times_4 \mathbf{F} = \sum_{r=1}^R \mathbf{a}_r^{(t)} \circ \mathbf{a}_r^{(s)} \circ \mathbf{a}_r^{(c)} \circ \mathbf{f}_r, \quad (30)$$

where  $\mathbf{A}^{(t)} = [\mathbf{a}_1^{(t)}, \mathbf{a}_2^{(t)}, \dots, \mathbf{a}_R^{(t)}] \in \Re^{I_t \times R}$  is seen as temporal component matrix and it contains the waveforms in time domain for different components;  $\mathbf{A}^{(s)} = [\mathbf{a}_1^{(s)}, \mathbf{a}_2^{(s)}, \dots, \mathbf{a}_R^{(s)}] \in \Re^{I_s \times R}$  is considered as the spectral component matrix and the spectrums in frequency domain for different components; Likewise,  $\mathbf{A}^{(c)} = [\mathbf{u}_1^{(c)}, \mathbf{a}_2^{(c)}, \dots, \mathbf{a}_R^{(c)}] \in \Re^{I_c \times R}$  is the spatial component matrix and it is topography for each extracted components;  $\mathbf{F} = [\mathbf{f}_1, \mathbf{f}_2, \dots, \mathbf{f}_R] \in \Re^{I \times R}$  is the multi-domain feature component matrix and includes the features of samples for each component (Cong et al., 2015a). Note that all the elements in the above equation are non-negative since  $\mathbf{X}$  is obtained by calculating the square of time-frequency results.

Although the SNR of interesting ERPs can be significantly increased during the preprocessing procedure, for the decomposed components obtained by tensor decomposition, four different types of signals are contained, namely, components of interest, components of non-interest, spontaneous brain activities, and noise activities. Therefore, those components of interest need to be identified from a number of the decomposed components. Usually, the extracted components of interest are identified based on prior knowledge. That is to say, when the

temporal, spectral, and spatial characteristics of the extracted components are in accordance with these of ERPs of interest, and then they are selected for the next step (Cong et al., 2015a).

For instance, a fourth-order tensor (i.e., time samples  $\times$  frequency bins  $\times$  channel  $\times$  (groups  $\times$  subjects):  $60 \times 71 \times 9 \times (2 \times 21)$ ) is first organized from the TFRs for the ERP datasets of two groups (21 subjects for each group) to investigate the discriminations between children with reading disability (RD) and children with attention deficit (AD) based on the multi-domain features of mismatch negativity (MMN) (Cong et al., 2012). Secondly, based on the DIFFIT in Eq. 27, the 36 components are obtained in all modes separately. Thirdly, the multi-domain features of the 12<sup>th</sup> component are identified for the next procedure (as shown in *Figure 14*) since the peak latency occurs within the time window of 100-160 ms, the maximum amplitude of the spectral component is below 5 Hz, and the amplitudes in the left hemisphere for the spatial component are larger than those in the right hemisphere. In other words, the temporal, spectral, and spatial properties of the 12<sup>th</sup> component are satisfied with those of MMN. Finally, statistical analysis methods can be performed, for example, the paired t-test, on the signatures of all subjects for the 12<sup>th</sup> component in the last mode to test the difference between two groups. Noticeably, in NCPD, all subjects share the same temporal, spectral, and spatial components, but the differences among subjects can be founded in the signatures of 42 children (i.e., multi-domain features of the last mode of 12<sup>th</sup> component).

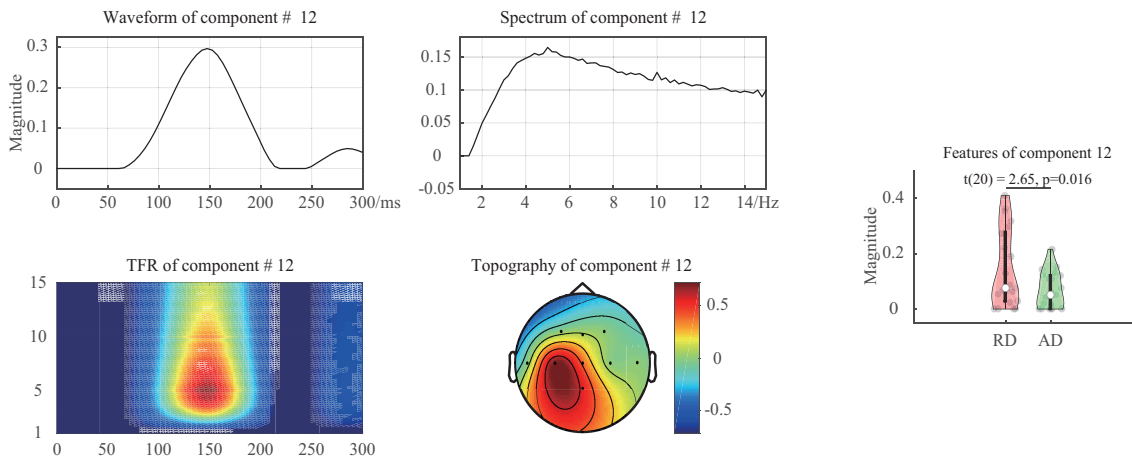


**FIGURE 14** An example of NCPD for a fourth-order tensor of ERP data (Adapted from (Cong et al., 2015a)). The waveform in temporal domain, spectrum in spectral domain, and topography in spatial domain for MMN are included. The features of MMN for different subjects are in last column and TFR is the outer product of temporal and spectral components .

### 2.3.2.3 Tucker decomposition of tensor of ERP datasets

When forming a tensor for Tucker decomposition, the samples of conditions and subjects are also put in the last dimension, and other modes are assigned to the other dimensions of the  $M$ th-order tensor  $\underline{\mathbf{X}} \in \Re^{I_1 \times I_2 \times \dots \times I_M}$ . Noted that the features of samples are expressed in core tensor  $\underline{\mathbf{G}} \in \Re^{R_1 \times R_2 \times \dots \times R_M}$  or in the last mode (Cong et al., 2013b, 2012).

Similar to the application of NCPD on ERP data analysis, the same procedures, i.e., component number identification, component extraction, component selection, and component analysis, are also involved in Tucker decomposition.

When using Tucker decomposition to decompose the fourth-order tensor (i.e.,  $60 \times 71 \times 9 \times (2 \times 21)$ ) (Cong et al., 2012) (see in the last paragraph of Subsection 2.3.2.2), the related temporal, spectral, and spatial component matrices can be obtained as below:

$$\underline{\mathbf{X}} \approx \underline{\mathbf{G}} \times_1 \mathbf{U}^{(t)} \times_2 \mathbf{U}^{(s)} \times_3 \mathbf{U}^{(c)}. \quad (31)$$

For  $r_t^{th}$  temporal component  $\mathbf{u}_{r_t}^{(t)}$ ,  $r_s^{th}$  spectral component  $\mathbf{u}_{r_s}^{(s)}$ , and  $r_c^{th}$  spatial component  $\mathbf{u}_{r_c}^{(c)}$ , the related multi-domain features of samples are expressed as  $\mathbf{f} = \underline{\mathbf{G}}(r_t, r_s, r_c, :)$ .  $r_t$ ,  $r_s$ , and  $r_c$  are allowed to be different.

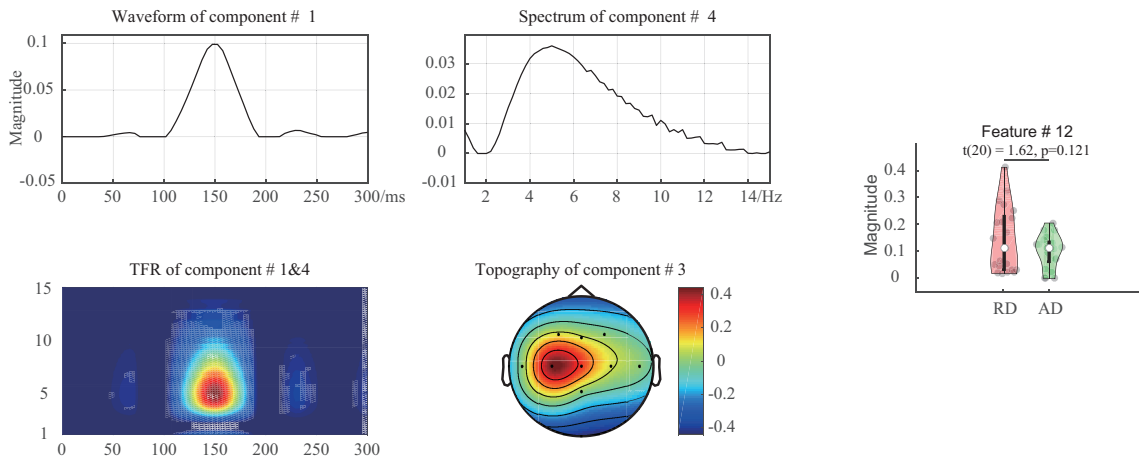


FIGURE 15 An example of Tucker decomposition with nonnegative constraint for a fourth-order tensor of ERP data (Adapted from (Cong et al., 2015a)). The waveform in temporal domain, spectrum in spectral domain, and topography in spatial domain for MMN are included. The features of MMN for different subjects are in last column and TFR is the outer product of temporal and spectral components

Based on Eq. 31, the temporal component number, the spectral component number, and the spatial component number are estimated to be 8, 4, and 6, respectively, and the core tensor  $\mathbf{F} = \underline{\mathbf{G}} \in \Re^{8 \times 4 \times 6 \times 42}$  shows the features of all subjects for the 192 extracted components ( $8 \times 4 \times 6$ ) (Cong et al., 2012). As shown in Figure 15, the 1<sup>st</sup> temporal, the 4<sup>th</sup> spectral, and the 3<sup>rd</sup> spatial components are

selected because they are satisfied with the properties of MMN in those modes. Finally, the paired t-test is performed on the features of MMN for all samples  $\mathbf{f}_{1,4,3} = \underline{\mathbf{G}}(1, 4, 3, :)$  to find the distinctions between RD and AD groups (see *Figure 15*).

### **3 SUMMARIES OF STUDIES AND AUTHOR CONTRIBUTIONS**

This chapter presents the overview of each study, including the motivation, methods, main results, and discussion. The author's contributions to the attached articles are also clarified.

#### **3.1 Study 1: Measuring temporal and spatial properties of the desired ERPs from individual subject's data by temporal-PCA**

**Publication I:** *Guanghui Zhang, Xueyan Li, Yingzhi Lu, Timo Tiihonen, Zheng Chang, and Fengyu Cong. Single-trial-based Temporal Principal Component Analysis on Extracting Event-related Potentials of Interest for an Individual Subject.* To be submitted.

##### **3.1.1 Motivation**

As a BSS algorithm, temporal-PCA has been widely used to perform on the spatial-stacked matrix (see *Figure 3 (b)*) obtained from the multiple subjects' ERP data to explore the properties of ERPs at the group level. The group temporal-PCA analysis assumes that there are no differences among the waveforms (i.e., time courses of PCA-extracted components) of ERPs of interest for all subjects (Dien, 2012). However, the waveforms of ERPs of interest for different subjects' data are always varied in phases, peak latencies, etc.

It should also be noted that several PCA-extracted components derived from the same ERP data cannot be analyzed simultaneously since the polarities and amplitudes of these PCA-extracted components are indeterminate. Such a problem also exists in other BSS algorithm named ICA (Makeig et al., 1997, 1999; Cong et al., 2011c,a). In order to tackle the problem, back-projection theory was conducted to the applications of ICA to EEG (Makeig et al., 1997, 1999) so that scales (i.e., polarity and amplitude) of ICA-extracted components could be cor-

rected, and these ICA-extracted components were analyzed at the microvolt level.

To address both defects in the previous group PCA analysis, PCA is performed on the spatial-stacked matrix generated from the EEG data of an individual subject to extract temporal and spatial properties of ERPs of interest. By applying back-projection theory, several PCA-extracted components can be analyzed simultaneously.

### 3.1.2 Methods

We use EEG data with two factors: Valence [Extreme vs. Moderate vs. Neutral]  $\times$  Negative-category [Disgusting vs. Fearful] collected from a within-subject designed emotional experiment (Lu et al., 2016) to evaluate the performances of the proposed technique and the three alternative techniques.

More specifically, for the proposed technique (individual-subject PCA), the components associated with ERP of interest (herein, N2) are first obtained by performing PCA on the spatial-concatenation matrix derived from the preprocessed single-trial EEG data of individual subject separately. Afterwards, we project the identified PCA-extracted components back to the electrode fields for correcting their indeterminateness in polarity and amplitude, and the waveforms of N2 are then reconstructed. Similarly, the waveforms of N2 at all electrodes are reconstructed by performing PCA on the matrices formed from the trial-averaged ERP data and the single-trial EEG data of all subjects separately. The former PCA category is named averaged group PCA, and the latter one is single-trial group PCA.

Afterwards, the mean and peak amplitudes of N2 for the reconstructed signals obtained by three different PCA categories and the original preprocessed ERP data are separately measured within the time window from 190 to 290 ms at electrodes FC3, FCz, FC4, C3, Cz, and C4.

Finally, we examine the effects of valence and negative-category using two-way rm-ANOVA based on the measured amplitudes of N2 for the four techniques separately. Moreover, the similarities of N2's topographies between any two different subjects (i.e., spatial similarities) are also computed to assess the performances of the four used techniques.

### 3.1.3 Results

When using mean measurement, the statistical analysis results indicate that there are no differences among the four used techniques. In detail, both the main effect of valence and the interaction effect between valence and negative category are significant for all the used techniques. Whereas the main effect of negative category do not reach a significant level. Regarding peak measurement, we observe a significant interaction effect between the two factors for the proposed technique but not for the other three techniques.

With respect to the spatial similarities, we observe that the mean values of the spatial similarities under different experimental conditions for the proposed

technique are significantly higher than those of the other techniques. Meanwhile, the standard deviations of the spatial similarities for the proposed technique are lower than those of the other ones. Both trends demonstrated that, for the proposed techniques, the spatial topographies of the estimated N2 for different subjects are more similar across different conditions, and their reliability is higher than for the other alternative methods.

### 3.1.4 Conclusion and discussion

In this study, a new approach is presented based on the PCA and Promax rotation plus back-projection theory to extract the properties of the interesting ERPs in temporal and spatial domains from the single-trial EEG data of an individual subject. Compared with the other techniques, when using the proposed technique, the statistical results of the mean and peak amplitudes for N2 could be more expected because the previous study also revealed similar statistical results (Lu et al., 2017).

We strongly expect that ERPs of interest could be elicited from each subject. In other words, similar topographies of a desired ERP for different subjects could be observed, which means that a high correlation coefficient between topographies of any two subjects could be obtained. Therefore, we use the similarities of topographies between any two different subjects to evaluate the performance of different techniques. Indeed, the similarities for the proposed technique supported that the proposed technique is an efficient way to extract ERP of interest from each subject's EEG data compared with the other group analysis techniques.

### 3.1.5 Author contributions

**Guanghui Zhang:** Conceptualization; Data Curation; Methodology; Software; Visualization; Writing-original draft. **Xueyan Li:** Visualization; Writing-original draft. **Yingzhi Lu:** Data Curation; Data preprocessing; Writing-original draft. **Timo Tiihonen:** Supervision; Writing original-draft. **Zheng Chang:** Supervision; Writing-original draft. **Fengyu Cong:** Conceptualization; Project administration; Supervision; Writing original-draft.

## 3.2 Study 2: Objectively measuring temporal and spectral properties of evoked ERPs via temporal-PCA and TFA

**Publication II:** **Guanghui Zhang**, Lili Tian, Huaming Chen, Peng Li, Tapani Ristaniemi, Huili Wang, Hong Li, Hongjun Chen, and Fengyu Cong (2018). Effect of parametric variation of center frequency and bandwidth of morlet wavelet transform on time-frequency analysis of event-related potentials. Proceedings of 2017 Chinese Intelligent Systems Conference. CISC 2017. Lecture Notes in Electrical Engineering, vol 459. Springer, Singapore. DOI: 10.1007/978-981-10-6496-8\_63

**Publication III:** **Guanghui Zhang**, Xueyan Li, and Fengyu Cong (2020). Objective Extraction of Evoked Event-Related Oscillation from Time-Frequency Representation of Event-Related Potentials, *Neural Plasticity*, vol. 2020, Article ID 8841354, 20 pages. DOI: 10.1155/2020/8841354

### 3.2.1 Motivation

Traditionally, evoked EROs are obtained from TFRs of the trial-averaged ERP data using some TFA algorithms (Tallon-Baudry and Bertrand, 1999; Herrmann et al., 2014; Makeig et al., 2004). Evoked EROs are often mixed with other oscillations of non-interest so that we may fail to accurately explain the related cognitive function. Moreover, the power of evoked EROs of interest is usually calculated within a predefined time window and a frequency range (i.e., rectangle method), which tends to be subjective. Although Bernat et al. (2005, 2007) had attempted to apply PCA to extract EROs of interest from TFRs (i.e., TFA-PCA), the core idea is to calculate the weightings between the extracted components and the original TFRs so that the yields obtained by TFA-PCA might be still mixtures. We have used the simulated ERP signals to demonstrated that the yields of TFA-PCA are still mixtures that come from different EROs (Zhang et al., 2020a).

These limitations give us motivation to propose a novel technique, which contains the following steps. Firstly, we extract ERPs of interest in the temporal and spatial domains by using temporal-PCA and Promax rotation. Afterwards, we compute TFRs of the extracted components based on the CMCWT (an optimal set of bandwidth and center frequency is set to define the mother wavelet, which was based on the work in Publication II). The edge detection algorithm is finally used to identify the regions of EROs. Please refer to Publications II and III for the details.

### 3.2.2 Methods

As shown in Publication III, the simulated data are used to demonstrate that the proposed technique can objectively obtain EROs (corresponding to different ERPs) from the preprocessed mixed-ERP signals. Meanwhile, an actual ERP data with two-factor (Waiting time [*Short* × *Long*] vs. Feedback [*Loss* × *Gain*]) are used to validate the performance of the proposed technique. Moreover, the yields of the proposed technique are also compared with the other two comparable techniques (i.e., conventional TFA and TFA-PCA).

For the simulated datasets, the 65 subjects' datasets are firstly generated by *Besa Simulator*<sup>1</sup>, which differ from each other in the amplitudes and latencies of N2/P3. Secondly, the SNR of the simulated signals is set to 20dB, 10dB, 5dB, and 1dB separately. The noise-contaminated datasets are subsequently filtered by wavelet filter with suggested parameters (Cong et al., 2015b). Finally, the performances of the three applied techniques are examined by calculating the correlation coefficients between waveforms/topographies/TFRs of any two signals

---

<sup>1</sup> <https://www.besa.de/updates/tools>

from source/mixed/extracted signals separately.

Regarding the preprocessed actual ERP data, the proposed technique, conventional TFA, and TFA-PCA are applied to extract P3-delta and N2-theta oscillations. The details of experimental materials and paradigm can be found in (Wang et al., 2014). The regions of evoked EROs corresponding to N2 and P3 are identified by the rectangle method and the edge detection algorithm, separately. For the measured energies of N2-theta and P3-delta oscillations, we use within-subject two-factor rm-ANOVA to examine the effects of the waiting-time and the feedback.

### 3.2.3 Results

For the simulated ERP datasets, the results reveal that all the correlation coefficients between the waveforms/topographies/TFRs of the source signals (i.e., the sources for N2 and P3) and those of the extracted signals by the proposed technique are approximately equal to 1. However, the correlation coefficients between TFRs of the source signals and those TFRs obtained by TFA-PCA are 0.79/0.59 and 0.51/0.57. Additionally, only one ERO is found in the TFRs for the conventional TFA, whereas two ERPs of interest are analyzed in the time-domain.

Regarding the actual ERP datasets, the statistical results indicated that N2-theta oscillation shows a significant difference between the long and short waiting-time conditions when using conventional TFA and the proposed technique, but not for TFA-PCA. In terms of P3-delta oscillation obtained by the proposed technique, the power of the loss condition is smaller than that of the gain condition associated with previous studies (Paul et al., 2020; Zhang et al., 2018b; Wu and Zhou, 2009) and the main effect of the waiting-time factor is significant. Likewise, the interaction effect between the waiting-time and the feedback factors reaches a significant level similar to the previous report (Höltje and Mecklinger, 2020).

### 3.2.4 Conclusion and discussion

Typically, two or more cognitive processes are involved in an ERP experiment reflected by different ERPs/EROs. These ERPs/EROs are often mixed with each other in temporal, spatial, and spectral domains. As a result, the related information cannot be thoroughly studied. To address this, a PCA-TFA-based framework is introduced to extract evoked EROs that correspond to different ERPs of interest. Through the yields of simulated datasets, we obtain that the temporal and spectral characteristics of evoked EROs could be extracted entirely from the mixed signals but not for the previously used techniques, such as conventional TFA and TFA-PCA. And then, the proposed technique is performed on an actual ERP data, which successfully extracted the information of P3-delta oscillation. In conclusion, the proposed technique provides new insight into exploring the temporal and spectral properties of evoked EROs and enables us to understand brain mechanisms in each cognitive stage better.

### 3.2.5 Author contributions

**Publication II, Guanghui Zhang:** Conceptualization; Data Curation; Methodology; Software; Visualization; Writing-original draft; Writing-review & Edit. **Lili Tian:** Writing-original draft; Writing-review & Edit. **Huaming Chen:** Methodology; Visualization. **Peng Li:** Writing-original draft; Discussion. **Tapani Ristaniemi:** Writing-original draft. **Huili Wang:** Writing-original draft. **Hong Li:** Writing-original draft; Discussion. **Hongjun Chen:** Supervision; Writing original-draft. **Fengyu Cong:** Conceptualization; Project administration; Supervision; Writing original-draft.

**Publication III, Guanghui Zhang:** Conceptualization; Data Curation; Methodology; Software; Visualization; Writing-original draft; Writing-review & Edit. **Xueyan Li:** Visualization; Writing-original draft; Writing-review & Edit. **Fengyu Cong:** Conceptualization; Project administration; Supervision; Writing original-draft; Writing-review & Edit.

## 3.3 Study 3: Measuring multi-domain properties of induced EROs using tensor decomposition

**Publication IV: Guanghui Zhang,** Chi Zhang, Shuo Cao, Xue Xia, Xin Tan, Lichengxi Si, Chenxin Wang, Xiaochun Wang, Chenglin Zhou, Tapani Ristaniemi, and Fengyu Cong (2020). Multi-domain Features of the Non-phase-locked Component of Interest Extracted from ERP Data by Tensor Decomposition. *Brain Topography*, 33(1), 37-47. DOI: 10.1007/s10548-019-00750-8

**Publication V: Guanghui Zhang,** Xueyan Li, Xiulin Wang, Wenya Liu, Yongjie Zhu, Xiaoshuang Wang, Reza Mahini, Rao Fu, Zheng Chang, Timo Tiihonen, and Fengyu Cong. Signal Processing Techniques for Event-related Potentials: from Single-way to Multi-way Component Analysis. To be submitted.

### 3.3.1 Motivation

There are two methods to obtain TFRs from the preprocessed ERP/EEG signals, namely, evoked and induced methods (Herrmann et al., 2014; Roach and Mathalon, 2008; Tallon-Baudry and Bertrand, 1999). For the former method, we usually use some TFA algorithms to calculate the TFRs of the trial-averaged ERP data and evoked oscillations can be obtained, which are phase-locked to the stimulus onset. For the latter one, the TFRs of single-trial EEG are first computed, and then the average procedure is conducted to the TFRs over trials result in both evoked and induced oscillations are included. Generally, induced EROs are studied using TFA, but the interactions of induced EROs among different modes are ignored. Furthermore, evoked EROs have been widely studied based on tensor decomposition algorithms (Wang et al., 2018; Cong et al., 2013b, 2014; Yu et al., 2020), but induced EROs are poorly explored. In this study, we attempt to study

induced EROs for the EEG data in a go/no-go task (experimental materials and paradigm refer to (Xia et al., 2018)).

### 3.3.2 Methods

The induced oscillation is explored from EEG data for no/nogo tasks of emotional picture selection paradigm (Zhang et al., 2020b). In detail, the time-domain signals of single-trial EEG are firstly converted into TFRs based on the CMCWT (the mother wavelet is defined with an optimal set of bandwidth and center frequency based on the work in Publication II). Secondly, TFRs are averaged across trials and the averaged TFRs are then arranged into a fourth-order tensor with temporal, spectral, spatial, and subject-condition modes. Next, multi-domain features of induced ERO are obtained from the fourth-order tensor by using NCPD. Finally, two-way rm-ANOVA is employed to examine the differences among different conditions. Meanwhile, the energies of induced oscillation under different experimental conditions are also measured within the predefined time window and frequency range from the TFRs of the conventional TFA.

### 3.3.3 Results

For the conventional TFA, we observe a theta oscillation emerged in frontal-central region about 400 ms stimulus onset which is considered as induced oscillation. The results reveal that the no-go task elicits more larger power than that of the go task. Although the power of the anger condition is also larger than that of the neural condition, there is no significant difference between them. It should be noted that the statistical results are influenced by the defined time window and frequency range.

Regarding the tensor decomposition, an interacted factor is in accordance with the properties of the induced oscillation of interest in temporal, spectral, spatial domains. By statistically analyzing the signatures of the related subject-condition mode, the yields reveal that the power of the anger condition is significantly larger than that of the neural condition and a significant difference is obtained between go and nogo tasks which are consistent with the previous findings (Benvenuti et al., 2017).

### 3.3.4 Conclusion and discussion

In this study, the multi-domain features of induced oscillation are investigated using tensor decomposition. Tensor decomposition allows to study the interactive properties of induced oscillation in multiple modes. By contrast, the widely used TFA only enables researchers to investigate the temporal and spectral properties of the interesting EROs. We validate both techniques in a go/nogo task under different emotional conditions and we successfully obtain a non-phase-locked oscillation by the tensor decomposition. It should be noted that we need to define a region (determined by a time window and a frequency range) and select some

electrodes based on the previous studies before calculating the energies of EROs of interest, which is a subjective method. Conversely, for tensor decomposition, the statistical analysis results are not influenced by both the experimenter-defined region and the selected electrodes.

### 3.3.5 Author contributions

**Publication IV, Guanghui Zhang:** Conceptualization; Data Curation; Methodology; Software; Visualization; Writing-original draft; Writing-review & Edit. **Chi Zhang:** Writing-original draft; Writing-review & Edit; Discussion. **Shuo Cao:** Writing-original draft; Writing-review & Edit; Discussion. **Xue Xia:** Data Curation; Data Preprocessing; **Xin Tan:** Visualization; Writing-original draft. **Lichengxi Si:** Visualization; Writing-original draft. **Chenxin Wang:** Visualization; Writing-original draft. **Xiaochun Wang:** Data Curation; Discussion. **Chenglin Zhou:** Data Curation; Discussion. **Tapani Ristaniemi:** Supervision; Writing original-draft. **Fengyu Cong:** Conceptualization; Project administration; Supervision; Writing original-draft.

**Publication V, Guanghui Zhang:** Conceptualization; Software; Visualization; Writing-original draft. **Xueyan Li:** Writing-original draft; Software; Visualization. **Xiulin Wang:** Concluded 'coupled tensor decomposition' section. **Wenya Liu:** Concluded the 'brain functional connectivity' section. **Yongjie Zhu:** Concluded 'brain connectivity based on tensor decomposition analysis'. **Xiaoshuang Wang:** Concluded 'EEG/ERP source localization' section. **Reza Mahini:** Concluded 'cluster analysis' section. **Rao Fu:** Concluded the preprocessing procedure section. **Zheng Chang:** Supervision; Writing original-draft; Discussion. **Timo Tiihonen:** Supervision; Writing original-draft; Discussion. **Fengyu Cong:** Conceptualization; Project administration; Supervision; Writing original-draft; Discussion.

## 4 CONCLUSION AND DISCUSSION

This chapter firstly presents the overview of this thesis. Afterwards, the limitations in all studies are also discussed. Finally, some potential directions for future work are described.

### 4.1 Overview

In this dissertation, three studies are used to tackle the problems in the current applications of PCA, TFA, and tensor decomposition separately for studying characteristics of event-related brain activities.

Specifically, in *study 1*, a developed PCA algorithm and a novel framework are introduced to address two problems in the existing PCA algorithms, e.g., PCA toolkit (Dien, 2010a) and Kayser's erpPCA (Kayser and Tenke, 2003). For the first problem, in the previous studies of group PCA analysis, it is impossible to analyze several PCA-extracted components simultaneously since their scales (i.e., amplitudes and polarities) may differ. For the other one, temporal-PCA analysis unreasonably supposes that the waveforms of one desired ERP for all subjects are constant. To solve both problems, the back-projection theory is used and ERPs of interest are extracted from EEG data of an individual subject. The results in *publication I* reveal that the proposed technique can yield better overall results than the other three commonly used techniques.

In *study 2*, we propose a novel framework to solve the limitations of extracting evoked EROs when using CMCWT. The first limitation is that how to select an optimal complex Morlet wavelet is poorly studied. The second one is that evoked EROs are usually mixed with others so that some cognitive functions cannot be accurately explained. These limitations are investigated separately in the following articles. Specifically, for the first problem, as shown in *publication II*, the CMCWT with 80 sets of center frequency and bandwidth (which are used to define the mother wavelet) are used to calculate the TFRs of the same ERP data with two factors. The results indicate that different variations of center frequency

and bandwidth might significantly effect on the time-frequency results, which is consistent with other report (Roach and Mathalon, 2008).

For the second drawback, in *publication III*, synthetic datasets of 68 subjects generated by using *Besa Simulator* are firstly used to validate the proposed approach could efficiently obtain the delta and theta EROs corresponding to the ERPs (i.e., P3 and N2) in time domain, respectively. The results indicate that the delta and theta EROs obtained by the proposed technique can be extracted efficiently but not with the other techniques. It should be noted that the center frequency and bandwidth were selected based on the work in *publication II*. Meanwhile, EEG data collected from a revised simple gambling task are also analyzed to study the evoked delta and theta EROs corresponding to P3 and N2, respectively. Delta oscillation for the reconstructed waveforms of P3 (obtained by using temporal-PCA) reveal that the power of the long waiting-time condition is larger than that of the short waiting-time condition. The gain condition elicits a larger delta oscillation than the loss condition. Both mentioned results are in accordance with the findings for P3 amplitude in previous studies (Zhang et al., 2018b; Paul et al., 2020; Höltje and Mecklinger, 2020). However, these trends are not observed in the delta oscillation obtained by conventional TFA and TFA-PCA.

In *study 3*, we investigate the multi-domain features of induced EROs from a go/nogo task EEG data with two factors using tensor decomposition. Traditionally, the power of induced EROs is studied from the TFRs computed by averaging TFRs of single-trial EEG data, but some potential interactions of induced EROs among different modes inevitably vanish in such an underlying idea. The yields of induced EROs in *publication IV* are more discriminative between different tasks than the conventional TFA. This trend seems to support that tensor decomposition can dig out some potential interactions of non-phase locked oscillations.

Overall, we employ the back-projection theory to the applications of PCA for extracting temporal and spatial properties of ERPs of interest in *study 1*. As a result, we have access to the synchronous analysis of several components derived from the same ERP or different ERPs of either individual subject's EEG data or all subjects' EEG/ERP data. Moreover, with the recommendations in *study 2*, the characteristics of EROs in temporal and spectral domains corresponding to different ERPs can be objectively explored, which enables us to efficiently and accurately investigate the cognitive functions in different cognitive process stages. Furthermore, tensor decomposition allows us to study potential interactions of induced EROs among different modes simultaneously as described in *study 3*.

## 4.2 Research limitations

Although the proposed techniques in these three studies are well conducted and the yields of the proposed techniques are also compared with other alternative techniques, it still exists some shortcomings in each study.

Specifically, in *study 1*, the selecting of PCA-extracted components associated with one ERP of interest is based on the prior knowledge and the correlation coefficients between the templated topographies and PCA-extracted spatial components. In other words, the experimenters decide how many PCA-extracted components to be used for the subsequent procedure.

In *study 2*, aiming at accurately obtaining the energies of EROs relative to different ERPs, two main steps are involved. The first step is to extract the ERPs of interest from the matrix formed by ERP datasets of all subjects by using temporal-PCA. The fundamental assumptions of this group PCA analysis are that the ERPs of interest can be extracted from all subjects' data and the source numbers and source sequences are also the same. However, those assumptions are not valid for actual EEG datasets as the cognitive processes of different subjects for the same task are different (different waveforms, reaction times). In the second step, the regions (determined by a time window and frequency range) of EROs are identified based on the grand averaged TFRs over all subjects. That is to say, the same region is used for EROs of all subjects' TFRs under the same experimental condition. However, the regions of EROs for different subjects are variant.

In *study 3*, the fourth-order tensor (time samples  $\times$  frequency bins  $\times$  channels  $\times$  subjects-conditions) is organized from the TFRs, which are obtained by averaging single-trial TFRs of all subjects under different experimental conditions. The induced EROs are then extracted from the formed fourth-order tensor using tensor decomposition. The underlying idea is that the EROs can be extracted from the TFRs of all subjects' data. For each decomposed component, the waveform in the temporal domain, spectrum in the spectral domain, and topographical distribution in the spatial domain for different subjects under different conditions are the same, and differences of different conditions are expressed in the signatures of subject-condition mode. These mean that we cannot investigate the differences of peak latencies for the desired EROs in either temporal or spectral domains, and we also fail to study the distinctions of desired EROs among different trials under the same condition.

It should also be noted that all three studies stay at the sensor level and due to the limited amount of sensors we can not explore the event related activities at the source level. Moreover, all the proposed techniques are merely applied to EEG data and are not employed to the other types of brain signals, for example, magnetoencephalography (MEG). Besides, in both study *study 2* and *study 3*, the phase property of EROs is not taken into consideration, while the phase information of oscillations is also essential to investigate the related cognitive mechanisms.

### 4.3 Future directions

This dissertation develops some advanced signal processing techniques and introduces some novel frameworks to study the characteristics of ERPs/EROs from

the different forms of representatives of EEG/ERP data at the sensor level. We can extend the techniques and frameworks to analyze MEG data (da Silva, 2013; Hansen et al., 2010) and examine the brain activities response to events at both sensor and source levels.

To overcome the drawbacks in the determination of PCA-extracted components (in *study 1*), two potential directions will be discussed below. In the first direction, for all PCA-extracted components from individual subjects' EEG data, we can use clustering algorithms, such as K-means, to classify the PCA-extracted components into several clusters based on the similarities of their topographies, spectrums, and dipoles as the application of ICA on individual subject's data (Rissling et al., 2014). Afterwards, we select the desired cluster for further analysis. For the other direction, we can also classify all PCA-extracted components into several classifications by using machine learning methods (Hosseini et al., 2020), and then select the desired classification.

Moreover, to fill the gap in the determination of regions for EROs (in *study 2*), we can determine the regions of the same analyzed EROs based on the specific distributions of EROs in the TFRs of individual subjects' EEG data instead of the same region which is used for TFRs of all subjects' data under the same condition.

Furthermore, in order to study the variations of desired ERPs among trials, TFRs of single-trial EEG for an individual subject can be formed into a tensor including time, frequency, channel, trial, and condition. Afterwards, we can perform tensor decomposition on the formed tensor from the individual subject to explore the variations of EROs among trials. For the unreasonable assumption in conventional tensor decomposition, that is, the extracted components in multiple modes exist in data of all subjects, and another alternative approach called linked component analysis is available to solve such problems (Zhou et al., 2015, 2016). The linked component analysis can extract shared features of desired ERPs and individual features from multiple blocks (e.g., the tensors for TFRs of different subjects' data).

To study both energy and phase of EROs, we can feed the complex values of time-frequency results instead of the absolute values into some complex-valued algorithms (e.g., PCA (Bazin et al., 2019), ICA (Qiu et al., 2019), and tensor (Trouillon et al., 2017)) to extract the meaningful information of interest.

## YHTEENVETO (SUMMARY IN FINNISH)

Tässä työssä tarkasteltiin aivotoiminnan aiheuttamien heräte-vaste-signaalien analysointiin kehitettyjä menetelmiä ja erityisesti vakiintuneisiin menetelmiin, kuten pääkomponenttianalyysi (principal component analysis, PCA), aika-taajuusanalyysi (time-frequency analysis, TFA) ja tensorihajotelmat, liittyviä haasteita ja rajoitteita. Näihin rajoitteisiin haettiin ratkaisuja kolmella eri tavalla.

Ensimmäisessä osatutkimuksessa tarkasteltiin PCA algoritmin käyttöä tilanteessa, jossa on tarve analysoida useita pääkomponentteja samanaikaisesti ja jossa vasteiden ajallinen käyttäytyminen on yksilöllistä. Perinteisten PCA menetelmien tuottamien pääkomponenttien amplitudeja ja polariteetteja ei voida hallita, jolloin usean pääkomponentin yhtäaikainen analysointi on mahdotonta. Vastaavasti perinteinen tapa keskiarvoistaan pääkomponentteja samaan ryhmään kuuluvien yksilöiden yli hävittää yksilölliset vaihtelut. Näiden puutteiden korjaamiseksi työssä esitettiin PCA menetelmä, jossa pääkomponentit määritellään yksilöllisesti ja valittujen pääkomponenttien joukko projisoidaan takaisin signaalialvaruuteen. Julkaisun I tulokset osoittavat, että esitetty menetelmä antaa tarkempia tuloksia, kuin tutkitut kolme verrokkimenetelmää.

Toisessa osatutkimuksessa keskityttiin herätteen synnyttämien oskillaatioiden analyysiin. Nämä oskillaatiot sekoittuvat käytännössä muiden kognitiivisten toimintojen aiheuttamiin samanaikaisiin oskillaatioihin, eikä niitä voida luotettavasti analysoida perinteisellä aika-taajuusanalyysillä, joka käytännössä olettaa, että tarkasteltavassa aika-taajuusikkunassa esiintyy vain tutkittava vaste. Työssä kehitettiin uusi lähestymistapa aika-taajuusanalyysiin. Julkaisussa III osoitettiin synteettisen datan avulla, että uusi menetelmä pystyi tehokkaasti tunnistamaan tunnettuihin herätevasteisiin (ns. P3 ja N2) liittyviä delta ja theta oskillaatioita. Erottelutarkkuus oli selvästi parempi kuin verrokkimenetelmillä. Työssä käytetty aika-taajuusikkuna pohjautui julkaisun II tuloksiin. Menetelmää testattiin myös yksinkertaisesta pelilanteesta mitattuihin EEG-signaaleihin. Näistä analysoitiin vastaavia theta ja delta oskillaatioita P3 ja N2 vasteisiin liittyen. Uusi menetelmä tunnisti odotetun delta oskillaation, toisin kuin verrokkeina käytetyt perinteisemmät TFA ja TFA-PCA menetelmät.

Kolmannessa osatutkimuksessa keskityimme herätevasteen indusoimien väärähtelyjen moniulotteiseen analyysiin. Aineistona oli yksinkertainen go/nogo tehtävä, jossa oli kaksi taustamuuttujaa (faktoria). Tarkastelemalla signaaleja tensorina ja soveltamalla tensorihajotelmia, pystytiin tunnistamaan eri faktorien välisiä vuorovaikutuksia, jotka eivät tulleet näkyviin perinteisillä aika-taajuusanalyyseillä. Julkaisun IV keskeinen tulos onkin, että käytetyn tensorihajotelman avulla voidaan tunnistaa menetelmiä tarkempi erottelukyky indusoitujen vasteiden analysoinnissa. Yhteenvedona voidaan todeta, että työssä kehitetyt kolme menetelmää parantavat kykyä analysoida herätevasteita. Uusien menetelmien avulla voidaan tutkia entistä paremmin kognitiivisia toimintoja ja niiden aiheuttamia herätevasteita erilaissa neuropsykiatrisissa tilanteissa.

## REFERENCES

- Abdi, H. and Williams, L. J. (2010). Principal component analysis. *Wiley Interdisciplinary Reviews: Computational Statistics*, 2(4):433–459.
- Alday, P. M. (2019). How much baseline correction do we need in ERP research? Extended GLM model can replace baseline correction while lifting its limits. *Psychophysiology*, 56(12):e13451.
- Barry, R. J. and De Blasio, F. M. (2018). EEG frequency PCA in EEG-ERP dynamics. *Psychophysiology*, 55(5):e13042.
- Barry, R. J., Steiner, G. Z., De Blasio, F. M., Fogarty, J. S., Karamacoska, D., and MacDonald, B. (2020). Components in the P300: Don't forget the Novelty P3! *Psychophysiology*, 57(7):e13371.
- Başar, E. (2013). Brain oscillations in neuropsychiatric disease. *Dialogues in Clinical Neuroscience*, 15(3):291.
- Başar, E., Başar-Eroglu, C., Karakaş, S., and Schürmann, M. (2001). Gamma, alpha, delta, and theta oscillations govern cognitive processes. *International Journal of Psychophysiology*, 39(2-3):241–248.
- Başar, E., Gölbaşı, B. T., Tülay, E., Aydin, S., and Başar-Eroğlu, C. (2016a). Best method for analysis of brain oscillations in healthy subjects and neuropsychiatric diseases. *International Journal of Psychophysiology*, 103:22–42.
- Başar, E. and Güntekin, B. (2008). A review of brain oscillations in cognitive disorders and the role of neurotransmitters. *Brain Research*, 1235:172–193.
- Başar, E., Schmiedt-Fehr, C., Mathes, B., Femir, B., Emek-Savaş, D. D., Tülay, E., Tan, D., Düzgün, A., Güntekin, B., Özerdem, A., et al. (2016b). What does the broken brain say to the neuroscientist? Oscillations and connectivity in schizophrenia, Alzheimer's disease, and bipolar disorder. *International Journal of Psychophysiology*, 103:135–148.
- Bazin, P.-L., Alkemade, A., Van Der Zwaag, W., Caan, M., Mulder, M., and Forstmann, B. U. (2019). Denoising high-field multi-dimensional MRI with local complex PCA. *Frontiers in Neuroscience*, 13:1066.
- Benvenuti, S. M., Buodo, G., and Palomba, D. (2017). Appetitive and aversive motivation in dysphoria: a time-domain and time-frequency study of response inhibition. *Biological Psychology*, 125:12–27.
- Bernat, E. M., Malone, S. M., Williams, W. J., Patrick, C. J., and Iacono, W. G. (2007). Decomposing delta, theta, and alpha time-frequency ERP activity from a visual oddball task using PCA. *International Journal of Psychophysiology*, 64(1):62–74.

- Bernat, E. M., Williams, W. J., and Gehring, W. J. (2005). Decomposing ERP time-frequency energy using PCA. *Clinical Neurophysiology*, 116(6):1314–1334.
- Bonmassar, C., Widmann, A., and Wetzel, N. (2020). The impact of novelty and emotion on attention-related neuronal and pupil responses in children. *Developmental Cognitive Neuroscience*, 42:100766.
- Bowers, M., Buzzell, G., Bernat, E., Fox, N., and Barker, T. (2018). Time-frequency approaches to investigating changes in feedback processing during childhood and adolescence. *Psychophysiology*, 55(10):e13208.
- Bro, R. and Kiers, H. A. (2003). A new efficient method for determining the number of components in parafac models. *Journal of Chemometrics: A Journal of the Chemometrics Society*, 17(5):274–286.
- Bro, R., Kjeldahl, K., Smilde, A. K., and Kiers, H. (2008). Cross-validation of component models: a critical look at current methods. *Analytical and Bioanalytical Chemistry*, 390(5):1241–1251.
- Bruns, A. (2004). Fourier-, Hilbert-and wavelet-based signal analysis: are they really different approaches? *Journal of Neuroscience Methods*, 137(2):321–332.
- Cao, S., Wang, Y., Wang, H., Chen, H., Zhang, G., and Kritikos, A. (2020). A facilitatory effect of perceptual incongruity on target-source matching in pictorial metaphors of chinese advertising: EEG evidence. *Advances in Cognitive Psychology*, 16(1):1.
- Cichocki, A., Mandic, D., De Lathauwer, L., Zhou, G., Zhao, Q., Caiafa, C., and Phan, H. A. (2015). Tensor decompositions for signal processing applications: From two-way to multiway component analysis. *IEEE Signal Processing Magazine*, 32(2):145–163.
- Cichocki, A., Zdunek, R., Phan, A. H., and Amari, S.-i. (2009). *Nonnegative matrix and tensor factorizations: applications to exploratory multi-way data analysis and blind source separation*. John Wiley & Sons.
- Cohen, M. X. (2014). *Analyzing neural time series data: theory and practice*. MIT press.
- Cohen, M. X. (2019). A better way to define and describe Morlet wavelets for time-frequency analysis. *NeuroImage*, 199:81–86.
- Comon, P. and Jutten, C. (2010). *Handbook of Blind Source Separation: Independent component analysis and applications*. Academic press.
- Cong, F., He, Z., Hämäläinen, J., Leppänen, P. H., Lyytinen, H., Cichocki, A., and Ristaniemi, T. (2013a). Validating rationale of group-level component analysis based on estimating number of sources in EEG through model order selection. *Journal of Neuroscience Methods*, 212(1):165–172.

- Cong, F., Kalyakin, I., Chang, Z., and Ristaniemi, T. (2011a). Analysis on subtracting projection of extracted independent components from EEG recordings. *Biomedical Engineering/Biomedizinische Technik*, 56(4):223–234.
- Cong, F., Kalyakin, I., Huttunen-Scott, T., Li, H., Lyytinen, H., and Ristaniemi, T. (2010). Single-trial based independent component analysis on mismatch negativity in children. *International journal of neural systems*, 20(04):279–292.
- Cong, F., Kalyakin, I., Li, H., Huttunen-Scott, T., Huang, Y., Lyytinen, H., and Ristaniemi, T. (2011b). Answering six questions in extracting children’s mismatch negativity through combining wavelet decomposition and independent component analysis. *Cognitive Neurodynamics*, 5(4):343.
- Cong, F., Kalyakin, I., and Ristaniemi, T. (2011c). Can back-projection fully resolve polarity indeterminacy of independent component analysis in study of event-related potential? *Biomedical Signal Processing and Control*, 6(4):422–426.
- Cong, F., Lin, Q.-H., Kuang, L.-D., Gong, X.-F., Astikainen, P., and Ristaniemi, T. (2015a). Tensor decomposition of EEG signals: a brief review. *Journal of Neuroscience Methods*, 248:59–69.
- Cong, F., Phan, A.-H., Astikainen, P., Zhao, Q., Wu, Q., Hietanen, J. K., Ristaniemi, T., and Cichocki, A. (2013b). Multi-domain feature extraction for small event-related potentials through nonnegative multi-way array decomposition from low dense array EEG. *International Journal of Neural Systems*, 23(02):1350006.
- Cong, F., Phan, A. H., Zhao, Q., Huttunen-Scott, T., Kaartinen, J., Ristaniemi, T., Lyytinen, H., and Cichocki, A. (2012). Benefits of multi-domain feature of mismatch negativity extracted by non-negative tensor factorization from EEG collected by low-density array. *International Journal of Neural Systems*, 22(06):1250025.
- Cong, F., Ristaniemi, T., and Lyytinen, H. (2015b). Wavelet filter design based on frequency responses for filtering ERP data with duration of one epoch. In *Advanced Signal Processing on Brain Event-Related Potentials*, pages 15–49. World Scientific.
- Cong, F., Zhou, G., Astikainen, P., Zhao, Q., Wu, Q., Nandi, A. K., Hietanen, J. K., Ristaniemi, T., and Cichocki, A. (2014). Low-rank approximation based non-negative multi-way array decomposition on event-related potentials. *International Journal of Neural Systems*, 24(08):1440005.
- da Silva, F. L. (2013). EEG and MEG: relevance to neuroscience. *Neuron*, 80(5):1112–1128.
- de Cheveigné, A. (2020). Zapline: A simple and effective method to remove power line artifacts. *NeuroImage*, 207:116356.
- de Cheveigné, A. and Nelken, I. (2019). Filters: when, why, and how (not) to use them. *Neuron*, 102(2):280–293.

- De Lathauwer, L. (2012). Block component analysis, a new concept for blind source separation. In *International Conference on Latent Variable Analysis and Signal Separation*, pages 1–8. Springer.
- Delorme, A. and Makeig, S. (2004). EEGLAB: an open source toolbox for analysis of single-trial EEG dynamics including independent component analysis. *Journal of Neuroscience Methods*, 134(1):9–21.
- Delplanque, S., Silvert, L., Hot, P., and Sequeira, H. (2005). Event-related P3a and P3b in response to unpredictable emotional stimuli. *Biological Psychology*, 68(2):107–120.
- Dien, J. (1998). Addressing misallocation of variance in principal components analysis of event-related potentials. *Brain Topography*, 11(1):43–55.
- Dien, J. (2010a). The ERP PCA toolkit: An open source program for advanced statistical analysis of event-related potential data. *Journal of Neuroscience Methods*, 187(1):138–145.
- Dien, J. (2010b). Evaluating two-step PCA of ERP data with geomin, infomax, oblimin, promax, and varimax rotations. *Psychophysiology*, 47(1):170–183.
- Dien, J. (2012). Applying principal components analysis to event-related potentials: a tutorial. *Developmental Neuropsychology*, 37(6):497–517.
- Dien, J., Beal, D. J., and Berg, P. (2005). Optimizing principal components analysis of event-related potentials: matrix type, factor loading weighting, extraction, and rotations. *Clinical Neurophysiology*, 116(8):1808–1825.
- Dien, J., Khoe, W., and Mangun, G. R. (2007). Evaluation of PCA and ICA of simulated ERPs: Promax vs. Infomax rotations. *Human Brain Mapping*, 28(8):742–763.
- Dimigen, O. (2020). Optimizing the ICA-based removal of ocular EEG artifacts from free viewing experiments. *NeuroImage*, 207:116117.
- Eichele, T., Rachakonda, S., Brakedal, B., Eikeland, R., and Calhoun, V. D. (2011). EEGIFT: group independent component analysis for event-related EEG data. *Computational Intelligence and Neuroscience*, 2011.
- Folstein, J. R. and Van Petten, C. (2008). Influence of cognitive control and mismatch on the N2 component of the ERP: a review. *Psychophysiology*, 45(1):152–170.
- Gentsch, K., Grandjean, D., and Scherer, K. R. (2013). Temporal dynamics of event-related potentials related to goal conduciveness and power appraisals. *Psychophysiology*, 50(10):1010–1022.
- Grandchamp, R. and Delorme, A. (2011). Single-trial normalization for event-related spectral decomposition reduces sensitivity to noisy trials. *Frontiers in Psychology*, 2:236.

- Gross, J. (2014). Analytical methods and experimental approaches for electrophysiological studies of brain oscillations. *Journal of Neuroscience Methods*, 228:57–66.
- Güntekin, B. and Başar, E. (2016). Review of evoked and event-related delta responses in the human brain. *International Journal of Psychophysiology*, 103:43–52.
- Handy, T. C. (2005). *Event-related potentials: A methods handbook*. MIT press.
- Hansen, P., Kringelbach, M., and Salmelin, R. (2010). *MEG: An introduction to methods*. Oxford university press.
- Harper, J., Malone, S. M., and Bernat, E. M. (2014). Theta and delta band activity explain N2 and P3 ERP component activity in a go/no-go task. *Clinical Neurophysiology*, 125(1):124–132.
- He, Z., Cichocki, A., Xie, S., and Choi, K. (2010). Detecting the number of clusters in n-way probabilistic clustering. *IEEE Transactions on Pattern Analysis and Machine Intelligence*, 32(11):2006–2021.
- Herrmann, C. S., Grigutsch, M., and Busch, N. A. (2005). EEG oscillations and wavelet analysis. *Event-related potentials: A methods handbook*, page 229.
- Herrmann, C. S., Rach, S., Vosskuhl, J., and Strüber, D. (2014). Time–frequency analysis of event-related potentials: a brief tutorial. *Brain Topography*, 27(4):438–450.
- Hitchcock, F. L. (1927). The expression of a tensor or a polyadic as a sum of products. *Journal of Mathematics and Physics*, 6(1-4):164–189.
- Höltje, G. and Mecklinger, A. (2020). Feedback timing modulates interactions between feedback processing and memory encoding: Evidence from event-related potentials. *Cognitive, Affective, & Behavioral Neuroscience*, pages 1–15.
- Horn, J. L. (1965). A rationale and test for the number of factors in factor analysis. *Psychometrika*, 30(2):179–185.
- Hosseini, M.-P., Hosseini, A., and Ahi, K. (2020). A review on machine learning for EEG signal processing in bioengineering. *IEEE reviews in biomedical engineering*.
- Hsu, Y.-F., Hamalainen, J., and Waszak, F. (2014). Both attention and prediction are necessary for adaptive neuronal tuning in sensory processing. *Frontiers in Human Neuroscience*, 8:152.
- Hu, L., Xiao, P., Zhang, Z., Mouraux, A., and Iannetti, G. D. (2014). Single-trial time–frequency analysis of electrocortical signals: Baseline correction and beyond. *NeuroImage*, 84:876–887.

- Hu, L., Zhang, Z., Mouraux, A., and Iannetti, G. D. (2015). Multiple linear regression to estimate time-frequency electrophysiological responses in single trials. *NeuroImage*, 111:442–453.
- Hu, S., Yao, D., Bringas-Vega, M. L., Qin, Y., and Valdes-Sosa, P. A. (2019). The statistics of EEG unipolar references: derivations and properties. *Brain Topography*, 32(4):696–703.
- Hughes, M. E., Fulham, W. R., Johnston, P. J., and Michie, P. T. (2012). Stop-signal response inhibition in schizophrenia: behavioural, event-related potential and functional neuroimaging data. *Biological Psychology*, 89(1):220–231.
- Huster, R. J., Messel, M. S., Thunberg, C., and Raud, L. (2020). The P300 as marker of inhibitory control—fact or fiction? *Cortex*, 132:334–348.
- Huster, R. J. and Raud, L. (2018). A tutorial review on multi-subject decomposition of EEG. *Brain Topography*, 31(1):3–16.
- Hyvärinen, A. (1999). Fast and robust fixed-point algorithms for independent component analysis. *IEEE transactions on Neural Networks*, 10(3):626–634.
- Hyvärinen, A. and Oja, E. (2000). Independent component analysis: algorithms and applications. *Neural networks*, 13(4-5):411–430.
- Jia, H., Peng, W., and Hu, L. (2015). A novel approach to identify time-frequency oscillatory features in electrocortical signals. *Journal of Neuroscience Methods*, 253:18–27.
- Jung, T.-P., Makeig, S., Westerfield, M., Townsend, J., Courchesne, E., and Sejnowski, T. J. (2000). Removal of eye activity artifacts from visual event-related potentials in normal and clinical subjects. *Clinical Neurophysiology*, 111(10):1745–1758.
- Kamp, S.-M. (2020). Preceding stimulus sequence effects on the oddball-P300 in young and healthy older adults. *Psychophysiology*, 57(7):e13593.
- KarakAŞ, S., Erzengin, Ö. U., and Başar, E. (2000). A new strategy involving multiple cognitive paradigms demonstrates that ERP components are determined by the superposition of oscillatory responses. *Clinical Neurophysiology*, 111(10):1719–1732.
- Karamacoska, D., Barry, R. J., De Blasio, F. M., and Steiner, G. Z. (2019). EEG-ERP dynamics in a visual continuous performance test. *International Journal of Psychophysiology*, 146:249–260.
- Kayser, J. and Tenke, C. E. (2003). Optimizing PCA methodology for ERP component identification and measurement: theoretical rationale and empirical evaluation. *Clinical Neurophysiology*, 114(12):2307–2325.

- Lachaux, J.-P., Rodriguez, E., Martinerie, J., and Varela, F. J. (1999). Measuring phase synchrony in brain signals. *Human Brain Mapping*, 8(4):194–208.
- Leue, A., Chavanon, M.-L., Wacker, J., and Stemmler, G. (2009). On the differentiation of N2 components in an appetitive choice task: Evidence for the revised reinforcement sensitivity theory. *Psychophysiology*, 46(6):1244–1257.
- Li, P., Baker, T. E., Warren, C., and Li, H. (2016). Oscillatory profiles of positive, negative and neutral feedback stimuli during adaptive decision making. *International Journal of Psychophysiology*, 107:37–43.
- Li, P., Peng, W., Li, H., and Holroyd, C. B. (2018). Electrophysiological measures reveal the role of anterior cingulate cortex in learning from unreliable feedback. *Cognitive, Affective, & Behavioral Neuroscience*, 18(5):949–963.
- Li, X., Zhang, G., Zhou, C., and Wang, X. (2019). Negative emotional state slows down movement speed: behavioral and neural evidence. *PeerJ*, 7:e7591.
- Lu, Y., Jaquess, K. J., Hatfield, B. D., Zhou, C., and Li, H. (2017). Valence and arousal of emotional stimuli impact cognitive-motor performance in an oddball task. *Biological Psychology*, 125:105–114.
- Lu, Y., Luo, Y., Lei, Y., Jaquess, K. J., Zhou, C., and Li, H. (2016). Decomposing valence intensity effects in disgusting and fearful stimuli: an event-related potential study. *Social Neuroscience*, 11(6):618–626.
- Luck, S. J. (2014). *An introduction to the event-related potential technique*. MIT press.
- MacDonald, B. and Barry, R. J. (2017). Significance and novelty effects in single-trial ERP components and autonomic responses. *International Journal of Psychophysiology*, 117:48–64.
- MacDonald, B. and Barry, R. J. (2020). Integration of three investigations of novelty, intensity, and significance in dishabituation paradigms: A study of the phasic orienting reflex. *International Journal of Psychophysiology*, 147:113–127.
- MacDonald, B., Barry, R. J., and Bonfield, R. C. (2015). Trials and intensity effects in single-trial ERP components and autonomic responses in a dishabituation paradigm with very long ISIs. *International Journal of Psychophysiology*, 98(3):394–412.
- Mahini, R., Li, Y., Ding, W., Fu, R., Ristaniemi, T., Nandi, A. K., Chen, G., and Cong, F. (2020). Determination of the time window of event-related potential using multiple-set consensus clustering. *Frontiers in Neuroscience*, 14:1047.
- Makeig, S., Debener, S., Onton, J., and Delorme, A. (2004). Mining event-related brain dynamics. *Trends in Cognitive Sciences*, 8(5):204–210.
- Makeig, S., Jung, T.-P., Bell, A. J., Ghahremani, D., and Sejnowski, T. J. (1997). Blind separation of auditory event-related brain responses into independent components. *Proceedings of the National Academy of Sciences*, 94(20):10979–10984.

- Makeig, S., Westerfield, M., Jung, T.-P., Covington, J., Townsend, J., Sejnowski, T. J., and Courchesne, E. (1999). Functionally independent components of the late positive event-related potential during visual spatial attention. *Journal of Neuroscience*, 19(7):2665–2680.
- Makeig, S., Westerfield, M., Jung, T.-P., Enghoff, S., Townsend, J., Courchesne, E., and Sejnowski, T. J. (2002). Dynamic brain sources of visual evoked responses. *Science*, 295(5555):690–694.
- Male, A. G. and Gouldthorp, B. (2020). Hemispheric differences in perceptual integration during language comprehension: An ERP study. *Neuropsychologia*, 139:107353.
- Michel, C. M. and Koenig, T. (2018). EEG microstates as a tool for studying the temporal dynamics of whole-brain neuronal networks: a review. *NeuroImage*, 180:577–593.
- Mognon, A., Jovicich, J., Bruzzone, L., and Buiatti, M. (2011). ADJUST: An automatic EEG artifact detector based on the joint use of spatial and temporal features. *Psychophysiology*, 48(2):229–240.
- Mørup, M. and Hansen, L. K. (2009). Automatic relevance determination for multi-way models. *Journal of Chemometrics: A Journal of the Chemometrics Society*, 23(7-8):352–363.
- Mørup, M., Hansen, L. K., and Arnfred, S. M. (2007). ERPWAVELAB: A toolbox for multi-channel analysis of time–frequency transformed event related potentials. *Journal of Neuroscience Methods*, 161(2):361–368.
- Mørup, M., Hansen, L. K., Herrmann, C. S., Parnas, J., and Arnfred, S. M. (2006). Parallel factor analysis as an exploratory tool for wavelet transformed event-related EEG. *NeuroImage*, 29(3):938–947.
- Murray, M. M., Brunet, D., and Michel, C. M. (2008). Topographic ERP analyses: a step-by-step tutorial review. *Brain Topography*, 20(4):249–264.
- Musacchia, G., Ortiz-Mantilla, S., Choudhury, N., Realpe-Bonilla, T., Roesler, C., and Benasich, A. A. (2017). Active auditory experience in infancy promotes brain plasticity in theta and gamma oscillations. *Developmental Cognitive Neuroscience*, 26:9–19.
- Näätänen, R. and Picton, T. (1987). The N1 wave of the human electric and magnetic response to sound: a review and an analysis of the component structure. *Psychophysiology*, 24(4):375–425.
- Onton, J., Westerfield, M., Townsend, J., and Makeig, S. (2006). Imaging human EEG dynamics using independent component analysis. *Neuroscience & Biobehavioral Reviews*, 30(6):808–822.

- Patel, S. H. and Azzam, P. N. (2005). Characterization of N200 and P300: selected studies of the event-related potential. *International Journal of Medical Sciences*, 2(4):147.
- Paul, M., Bellebaum, C., Ghio, M., Suchan, B., and Wolf, O. T. (2020). Stress effects on learning and feedback-related neural activity depend on feedback delay. *Psychophysiology*, 57(2):e13471.
- Pfurtscheller, G. and Da Silva, F. L. (1999). Event-related EEG/MEG synchronization and desynchronization: basic principles. *Clinical Neurophysiology*, 110(11):1842–1857.
- Polich, J. (2007). Updating P300: an integrative theory of P3a and P3b. *Clinical Neurophysiology*, 118(10):2128–2148.
- Qiu, Y., Lin, Q.-H., Kuang, L.-D., Gong, X.-F., Cong, F., Wang, Y.-P., and Calhoun, V. D. (2019). Spatial source phase: A new feature for identifying spatial differences based on complex-valued resting-state fMRI data. *Human Brain Mapping*, 40(9):2662–2676.
- Richman, M. B. (1986). Rotation of principal components. *Journal of Climatology*, 6(3):293–335.
- Rissling, A. J., Miyakoshi, M., Sugar, C. A., Braff, D. L., Makeig, S., and Light, G. A. (2014). Cortical substrates and functional correlates of auditory deviance processing deficits in schizophrenia. *NeuroImage: Clinical*, 6:424–437.
- Roach, B. J., Ford, J. M., Loewy, R. L., Stuart, B. K., and Mathalon, D. H. (2021). Theta phase synchrony is sensitive to corollary discharge abnormalities in early illness schizophrenia but not in the psychosis risk syndrome. *Schizophrenia Bulletin*, 47(2):415–423.
- Roach, B. J. and Mathalon, D. H. (2008). Event-related EEG time-frequency analysis: an overview of measures and an analysis of early gamma band phase locking in schizophrenia. *Schizophrenia Bulletin*, 34(5):907–926.
- Rogenmoser, L., Zollinger, N., Elmer, S., and Jäncke, L. (2016). Independent component processes underlying emotions during natural music listening. *Social Cognitive and Affective Neuroscience*, 11(9):1428–1439.
- Rosburg, T., Boutros, N. N., and Ford, J. M. (2008). Reduced auditory evoked potential component N100 in schizophrenia—a critical review. *Psychiatry Research*, 161(3):259–274.
- Rushby, J. A. and Barry, R. J. (2009). Single-trial event-related potentials to significant stimuli. *International Journal of Psychophysiology*, 74(2):120–131.
- Rushby, J. A., Barry, R. J., and Doherty, R. J. (2005). Separation of the components of the late positive complex in an ERP dishabituation paradigm. *Clinical Neurophysiology*, 116(10):2363–2380.

- Severo, M. C., Paul, K., Walentowska, W., Moors, A., and Pourtois, G. (2020). Neurophysiological evidence for evaluative feedback processing depending on goal relevance. *NeuroImage*, 215:116857.
- Spencer, K. M., Dien, J., and Donchin, E. (2001). Spatiotemporal analysis of the late ERP responses to deviant stimuli. *Psychophysiology*, 38(2):343–358.
- Stam, C. J., Nolte, G., and Daffertshofer, A. (2007). Phase lag index: assessment of functional connectivity from multi channel EEG and MEG with diminished bias from common sources. *Human Brain Mapping*, 28(11):1178–1193.
- Steele, V. R., Anderson, N. E., Claus, E. D., Bernat, E. M., Rao, V., Assaf, M., Pearson, G. D., Calhoun, V. D., and Kiehl, K. A. (2016). Neuroimaging measures of error-processing: Extracting reliable signals from event-related potentials and functional magnetic resonance imaging. *NeuroImage*, 132:247–260.
- Tadel, F., Baillet, S., Mosher, J. C., Pantazis, D., and Leahy, R. M. (2011). Brainstorm: a user-friendly application for MEG/EEG analysis. *Computational Intelligence and Neuroscience*, 2011.
- Tallon-Baudry, C. and Bertrand, O. (1999). Oscillatory gamma activity in humans and its role in object representation. *Trends in Cognitive Sciences*, 3(4):151–162.
- Tallon-Baudry, C., Bertrand, O., Delpuech, C., and Pernier, J. (1996). Stimulus specificity of phase-locked and non-phase-locked 40 Hz visual responses in human. *Journal of Neuroscience*, 16(13):4240–4249.
- Timmerman, M. E. and Kiers, H. A. (2000). Three-mode principal components analysis: Choosing the numbers of components and sensitivity to local optima. *British Journal of Mathematical and Statistical Psychology*, 53(1):1–16.
- Trouillon, T., Dance, C., Gaussier, E., Welbl, J., Riedel, S., and Bouchard, G. (2017). Knowledge graph completion via complex tensor factorization. *Journal of Machine Learning Research*, 18(130):1–38.
- Tucker, L. R. (1966). Some mathematical notes on three-mode factor analysis. *Psychometrika*, 31(3):279–311.
- van den Broeke, E. N., De Vries, B., Lambert, J., Torta, D. M., and Mouraux, A. (2017). Phase-locked and non-phase-locked EEG responses to pinprick stimulation before and after experimentally-induced secondary hyperalgesia. *Clinical Neurophysiology*, 128(8):1445–1456.
- van Dinteren, R., Arns, M., Jongsma, M. L., and Kessels, R. P. (2014). P300 development across the lifespan: a systematic review and meta-analysis. *Plos One*, 9(2):e87347.
- Van Dinteren, R., Huster, R., Jongsma, M., Kessels, R., and Arns, M. (2018). Differences in cortical sources of the event-related P3 potential between young and old participants indicate frontal compensation. *Brain Topography*, 31(1):35–46.

- Villena-González, M., Palacios-García, I., Rodríguez, E., and López, V. (2018). Beta oscillations distinguish between two forms of mental imagery while gamma and theta activity reflects auditory attention. *Frontiers in Human Neuroscience*, 12:389.
- Vogel, E. K. and Luck, S. J. (2000). The visual N1 component as an index of a discrimination process. *Psychophysiology*, 37(2):190–203.
- Wacker, M. and Witte, H. (2013). Time-frequency techniques in biomedical signal analysis. *Methods of Information in Medicine*, 52(04):279–296.
- Wang, D., Zhu, Y., Ristaniemi, T., and Cong, F. (2018). Extracting multi-mode ERP features using fifth-order nonnegative tensor decomposition. *Journal of Neuroscience Methods*, 308:240–247.
- Wang, J., Chen, J., Lei, Y., and Li, P. (2014). P300, not feedback error-related negativity, manifests the waiting cost of receiving reward information. *Neuroreport*, 25(13):1044–1048.
- Wang, X., Liu, W., Toivainen, P., Ristaniemi, T., and Cong, F. (2020). Group analysis of ongoing EEG data based on fast double-coupled nonnegative tensor decomposition. *Journal of Neuroscience Methods*, 330:108502.
- Widmann, A., Schröger, E., and Maess, B. (2015). Digital filter design for electrophysiological data—a practical approach. *Journal of Neuroscience Methods*, 250:34–46.
- Widmann, A., Schröger, E., and Wetzel, N. (2018). Emotion lies in the eye of the listener: Emotional arousal to novel sounds is reflected in the sympathetic contribution to the pupil dilation response and the P3. *Biological Psychology*, 133:10–17.
- Winkler, I., Haufe, S., and Tangermann, M. (2011). Automatic classification of artifactual ICA-components for artifact removal in EEG signals. *Behavioral and Brain Functions*, 7(1):1–15.
- Wu, Y. and Zhou, X. (2009). The P300 and reward valence, magnitude, and expectancy in outcome evaluation. *Brain Research*, 1286:114–122.
- Xia, X., Zhang, G., and Wang, X. (2018). Anger weakens behavioral inhibition selectively in contact athletes. *Frontiers in Human Neuroscience*, 12:463.
- Yao, D., Qin, Y., Hu, S., Dong, L., Vega, M. L. B., and Sosa, P. A. V. (2019). Which reference should we use for EEG and ERP practice? *Brain Topography*, 32(4):530–549.
- Yu, J., Wang, Y., Yu, J., Zhang, G., and Cong, F. (2020). Nudge for justice: An ERP investigation of default effects on trade-offs between equity and efficiency. *Neuropsychologia*, 149:107663.

- Zhang, G., Li, X., and Cong, F. (2020a). Objective extraction of evoked event-related oscillation from time-frequency representation of event-related potentials. *Neural Plasticity*, 2020.
- Zhang, G., Li, X., Lu, Y., Tiihonen, T., Chang, Z., and Cong, F. (2021). Single-trial-based temporal principal component analysis on extracting event-related potentials of interest for an individual subject. *bioRxiv*.
- Zhang, G., Tian, L., Chen, H., Li, P., Ristaniemi, T., Wang, H., Li, H., Chen, H., and Cong, F. (2018a). Effect of parametric variation of center frequency and bandwidth of Morlet wavelet transform on time-frequency analysis of event-related potentials. In *In: Jia Y., Du J., Zhang W. (eds) Proceedings of 2017 Chinese Intelligent Systems Conference. CISC 2017. Lecture Notes in Electrical Engineering, vol 459.*, pages 693–702. Springer,Singapore.
- Zhang, G., Zhang, C., Cao, S., Xia, X., Tan, X., Si, L., Wang, C., Wang, X., Zhou, C., Ristaniemi, T., et al. (2020b). Multi-domain features of the non-phase-locked component of interest extracted from ERP data by tensor decomposition. *Brain Topography*, 33(1):37–47.
- Zhang, X., Lei, Y., Yin, H., Li, P., and Li, H. (2018b). Slow is also fast: feedback delay affects anxiety and outcome evaluation. *Frontiers in Human Neuroscience*, 12:20.
- Zhou, G. and Cichocki, A. (2012). Fast and unique tucker decompositions via multiway blind source separation. *Bulletin of the Polish Academy of Sciences. Technical Sciences*, 60(3):389–405.
- Zhou, G., Cichocki, A., Zhang, Y., and Mandic, D. P. (2015). Group component analysis for multiblock data: Common and individual feature extraction. *IEEE Transactions on Neural Networks and Learning Systems*, 27(11):2426–2439.
- Zhou, G., Zhao, Q., Zhang, Y., Adali, T., Xie, S., and Cichocki, A. (2016). Linked component analysis from matrices to high-order tensors: Applications to biomedical data. *Proceedings of the IEEE*, 104(2):310–331.
- Zhu, Y., Zhang, C., Poikonen, H., Toivainen, P., Huotilainen, M., Mathiak, K., Ristaniemi, T., and Cong, F. (2020). Exploring frequency-dependent brain networks from ongoing EEG using spatial ICA during music listening. *Brain Topography*, 33(3):289–302.



## **ORIGINAL PAPERS**

**PI**

### **SINGLE-TRIAL-BASED TEMPORAL PRINCIPAL COMPONENT ANALYSIS ON EXTRACTING EVENT-RELATED POTENTIALS OF INTEREST FOR AN INDIVIDUAL SUBJECT**

by

Guanghui Zhang, Xueyan Li, Yingzhi Lu, Timo Tiihonen, Zheng Chang, and Fengyu Cong 2021

To be submitted

Reproduced with kind permission of Authors.



## **PII**

# **EFFECT OF PARAMETRIC VARIATION OF CENTER FREQUENCY AND BANDWIDTH OF MORLET WAVELET TRANSFORM ON TIME-FREQUENCY ANALYSIS OF EVENT-RELATED POTENTIALS**

by

Guanghui Zhang, Lili Tian, Huaming Chen, Peng Li, Tapani Ristaniemi, Huili Wang, Hong Li, Hongjun Chen, and Fengyu Cong 2018

In: Jia Y., Du J., Zhang W. (eds) Proceedings of 2017 Chinese Intelligent Systems Conference. CISC 2017. Lecture Notes in Electrical Engineering, vol 459, pp. 693–702, [https://doi.org/10.1007/978-981-10-6496-8\\_63](https://doi.org/10.1007/978-981-10-6496-8_63)

Reproduced with kind permission of Springer, Singapore.



# **Effect of Parametric Variation of Center Frequency and Bandwidth of Morlet Wavelet Transform on Time-frequency Analysis of Event-related Potentials**

**Guanghui Zhang<sup>1,2</sup>, Lili Tian<sup>3</sup>, Huaming Chen<sup>1</sup>, Peng Li<sup>4</sup>, Tapani Ristaniemi<sup>2</sup>,  
Huili Wang<sup>3</sup>, Hong Li<sup>4</sup>, Hongjun Chen<sup>3</sup>, Fengyu Cong<sup>1,2</sup>**

**Abstract.** Time-frequency (TF) analysis of event-related potentials (ERPs) using Complex Morlet Wavelet Transform has been widely applied in cognitive neuroscience research. It has been widely suggested that the center frequency ( $f_c$ ) and bandwidth ( $\sigma$ ) should be considered in defining the mother wavelet. However, the issue how parametric variation of  $f_c$  and  $\sigma$  of Morlet wavelet transform exerts influence on ERPs time-frequency results has not been extensively discussed in previous research. The current study, through adopting the method of Complex Morlet Continuous Wavelet Transform (CMCWT), aims to investigate whether time-frequency results vary with different parametric settings of  $f_c$  and  $\sigma$ . Besides, the nonnegative canonical polyadic decomposition (NCPD) is used to further confirm the differences manifested in time-frequency results. Results showed that different parametric settings may result in divergent time-frequency results, including the corresponding time-frequency representation (TFR) and topographical distribution. Furthermore, no similar components of interest were obtained from different TFR results by NCPD. The current research, through highlighting the importance of parametric setting in time-frequency analysis of ERP data, suggests that different parameters should be attempted in order to get optimal time-frequency results.

**Keywords:** Complex Morlet Wavelet Transform, event-related potentials, center frequency, bandwidth, time-frequency representation.

---

Guanghui Zhang, Lili Tian, Huaming Chen, Peng Li, Tapani Ristaniemi, Huili Wang, Hong Li, Hongjun Chen (✉), Fengyu Cong (✉)

1. Department of Biomedical Engineering, Faculty of Electronic Information and Electrical Engineering, Dalian University of Technology, 116024, Dalian, China.  
E-mail: cong@dlut.edu.cn
2. Department of Mathematical Information Technology, University of Jyväskylä, 40014, Jyväskylä, Finland
3. School of Foreign Languages, Dalian University of Technology, 116024, Dalian, China  
E-mail: chenhj@dlut.edu.cn
4. College of Psychology and Sociology, Shenzhen University, 518060, Shenzhen, China

## 1 Introduction

Electroencephalogram (EEG) has been extensively applied in cognitive neuroscience research. EEG, according to different experimental paradigms and external stimuli, can be divided into three categories: spontaneous EEG [1], event-related potentials (ERP) [2], and ongoing EEG [3]. The main methods employed in ERP data processing are as the following: 1) Time-domain analysis, 2) Frequency-domain analysis and 3) Time-frequency analysis [4-8]. As ERP signals are non-stationary and time-varying, neither the time-domain nor the frequency-domain analysis can be used to effectively reveal the time-frequency information of ERP data. Time-frequency analysis, by focusing on the time-varying features of ERP components, is conducted to transform a one-dimensional time signal into a two-dimensional time-frequency density function, which aims to reveal the number of frequency components and how each component varies over time.

In 1996, Tallon-Baudry *et al.* introduced the Morlet wavelet for time-frequency analysis of ERP data [9]. Since then, the Morlet wavelet has been widely applied by researchers in conducting time-frequency analysis, with its citations over 1100 times (From the Google scholar). However, a synthesis of previous research showed that in most cases the value of  $K$  is fixed (e.g.,  $K = 7$ ) [9-12], therefore leaving the issue whether parametric variation of  $f_c$  and  $\sigma$  has an impact on time-frequency results unresolved. This study is devoted to investigation of the issue.

## 2 Method

### 2.1 Data Description

The data was collected to investigate whether a short delay in presenting an outcome affects brain activity. For the detailed information of experimental procedure, readers can refer to Wang *et al.* research [13]. Twenty-two undergraduates and graduate students participated in the experiment as volunteers. All the participants, aged from 18 to 24, were right-handed with normal or corrected-to-normal vision and no one was reported to have neurological or psychological disorders. EEG was recorded using a 64-channel system (Brain Products GmbH, Gilching, Germany) with reference on the left mastoid. The vertical and horizontal electrooculogram (EOG) was recorded from electrodes placed above and below the right eye and on the outer canthi of the left and right eyes respectively. Electrode impedance was maintained below 10k Ohm. The EEG and EOG were sampled continuously at 500Hz with 0.01-100Hz bandpass filtering.

### 2.2 Complex Morlet Wavelet Transform

The CMCWT method, based on the Complex Morlet Wavelets, was adopted for time-frequency analysis in the present study.

If  $x(t)$  is a discrete sequence of length  $T$ , the definition of the Continuous Wavelet Transform (CWT) can be expressed as follows:

$$X(a, b) = \frac{1}{\sqrt{|a|}} \sum_{t=0}^{T-1} x(t) \Phi\left(\frac{t-b}{a}\right). \quad (1)$$

In the above formula,  $x(t)$  represents the signal to be transformed;  $a$  refers to the scaling and  $b$  the time location or shifting parameters;  $\Phi(t)$  stands for the mother wavelet. In this study, the Complex Morlet Wavelets is defined as the mother wavelet [9-12]:

$$\Phi(t, f_c) = \frac{1}{\sqrt{\pi\sigma^2}} e^{i2\pi t f_c} e^{\frac{-t^2}{2\sigma^2}}. \quad (2)$$

According to the above formula, a Gaussian shape respectively in the time and frequency domain around its  $f_c$  can be obtained.

A wavelet family is characterized by a constant ratio:

$$K = \frac{f_c}{\sigma_f} = 2\pi\sigma f_c. \quad (3)$$

In this formula,  $\sigma_f = 1/(2\pi\sigma)$ ,  $K$  should be greater than 5 [9].

Taken together, this method (CMCWT) can be described as below:

$$\text{CMCWT}(t, f) = |\Phi(t, f) * x(t)|^2. \quad (4)$$

In the above formula, ‘\*’ refers to convolution.

### 2.3 Nonnegative Canonical Polyadic Decomposition

Nonnegative Canonical Polyadic Decomposition (NCPD) has been widely applied to study time-frequency representation (TFR) of EEG [14, 15]. For example, given a third-order tensor including the modes of time, frequency and space,  $\underline{X} \in \mathcal{R}^{I_1 \times I_2 \times I_3}$ , the NCPD can be defined:

$$\underline{X} = \sum_{r=1}^R t_r \circ f_r \circ s_r + \underline{E} = \sum_{r=1}^R \underline{X}_r + \underline{E} = \widehat{\underline{X}} + \underline{E} \approx \widehat{\underline{X}}. \quad (5)$$

In this formula, the symbol ‘◦’ denotes the outer product of vectors. The  $t_r$ ,  $f_r$ , and  $s_r$  correspond to the temporal component #  $r$ , the spectral component #  $r$ , and the spatial component #  $r$ , and the three components reveal the properties of the multi-domain properties of an ERP in the time, frequency and space domains [14].

For the same multi-channel EEG data, different parameters of CMCWT may produce different TFR (indeed, third-order tensors in this study) in terms of visual inspection. Then, the application of NCPD on those tensors can assist to investigate whether the similar components of interest can be extracted from different tensors resulting different TFR parameters of the same EEG data. For the detailed

information of the number of extracted components for each mode, and the criteria of selecting multi-domain features, readers can refer to Cong *et al.* research [15].

### 3 Data Processing and Analysis

The ERP data were pre-processed in MATLAB and EEGLAB [16], including the following steps: a 50Hz notch filter to remove line noise, a low-pass filtering of 100Hz, segmentation of the filtered continuous EEG into single trials (each trial was extracted offline from 200ms pre-stimulus onset to 1000ms post-stimulus onset), baseline correction, artifact rejection and averaging.

In CMCWT analysis, the frequency range was set from 1 to 30Hz, respectively in 0.1 Hz step ( $fc = 9, 10$ , respectively), in 0.2Hz step ( $fc = 5, 6, 7, 8, 9, 10$ , respectively), in 0.3Hz step ( $fc = 3, 4, 5, 6, 7, 8, 9, 10$ , respectively), in 0.4Hz step ( $fc = 3, 4, 5, 6, 7, 8, 9, 10$ , respectively), in 0.5Hz step ( $fc = 2, 3, 4, 5, 6, 7, 8, 9, 10$ , respectively), in 0.6Hz step ( $fc = 2, 3, 4, 5, 6, 7, 8, 9, 10$ , respectively), in 0.7Hz ( $fc = 2, 3, 4, 5, 6, 7, 8, 9, 10$ , respectively), in 0.8Hz step ( $fc = 2, 3, 4, 5, 6, 7, 8, 9, 10$ , respectively), in 0.9Hz step ( $fc = 1, 2, 3, 4, 5, 6, 7, 8, 9, 10$ , respectively) and in 1Hz step ( $fc = 1, 2, 3, 4, 5, 6, 7, 8, 9, 10$ , respectively). All the above parametric settings met the requirement of constant ratio (greater than 5).

To further investigate whether parametric variation of  $fc$  and  $\sigma$  has an impact on time-frequency results, four steps are carried out in the following sequence:

(1) Select a typical topographical distribution of TFR results as the template. When  $\sigma_0 = 1$ , the value of  $fc$  can be respectively set as 1,2,3,4,5,6,7,8,9 and 10. The topographical distribution of  $fc_4 = 4$  is finally chosen as the template  $T_{template}(\sigma_0, fc_4)$  in terms of the prior knowledge of the ERP of interest.

(2) Define a  $fc_n$ , calculate the Correlation Coefficients (CCs) between the template ( $T_{template}$ ) and each spatial component  $s_r(\sigma_0, fc_n)$  obtained by NCPD (R components were extracted in each mode), which can be described as:

$$Y(\sigma_0, fc_n, r) = \rho(s_r(\sigma_0, fc_n), T_{template}(\sigma_0, fc_4)). \quad (6)$$

In the above formula,  $r = 1, 2, \dots, 21$ ,  $n = 1, 2, \dots, 10$ . Subsequently, the maximal CC is chosen as:

$$q(\sigma_0, fc_n) = \max(Y(\sigma_0, fc_n, 1), Y(\sigma_0, fc_n, 2), \dots, Y(\sigma_0, fc_n, R)). \quad (7)$$

Then, the corresponding  $r^{\text{th}}$  components with the maximum CC were obtained.

(3) Based on the obtained components of each dimension and their corresponding TFR results, we need to judge whether the TFR results of different parameters are similar or not. The TFR results are different when the  $fc$  is respectively set as 1 and 9. Besides, the corresponding 16<sup>th</sup> components of  $fc_1 = 1$  and 1<sup>th</sup> components of  $fc_9 = 9$  are similar in the spacial dimension, but not the temporal and spectral dimension (as shown in the first and third row of Figure 4).

(4) With the same procedure mentioned above, we can analyze the results of other  $\sigma$  and  $fc$  parameters to explore potential differences in the time-frequency results.

## 4 Results

Results showed that parametric variations of  $\sigma$  and  $fc$  lead to different time-frequency representation and topographical distribution. The data results shown in Figure 1, Figure 2, Figure 3, Figure 4 and Figure 5 are all from one subject in one condition (short-gain condition), and the data used for statistical analysis (Figure 6) are from 22 subjects in four conditions (waiting time (short, long)  $\times$  feedback valence (loss, gain)). Due to the space limitation, only the results of  $\sigma = 1$ ,  $fc = 1, 2, 3, 4, 5, 6, 7, 8, 9, 10$  are presented here.

Figure 1 shows the waveform at Cz electrode in the left panel and the waveform of all channels in the right. From the waveform, certain ERP components can be recognized. As shown in Figure 2, the comparison of the TFR results of  $fc = 1, 2, 3, 4, 5$  with other parameters ( $fc = 6, 7, 8, 9, 10$ ) shows differences in the time frequency resolution. In Figure 3, the topographical distributions are obtained by averaging the area of each rectangle. Within the time window of 100-400ms and frequency range of 7-10Hz, it can be observed that the topographical distributions are highly similar among each other when  $fc = 1, 2, 3, 4, 5, 6, 7, 8$ .

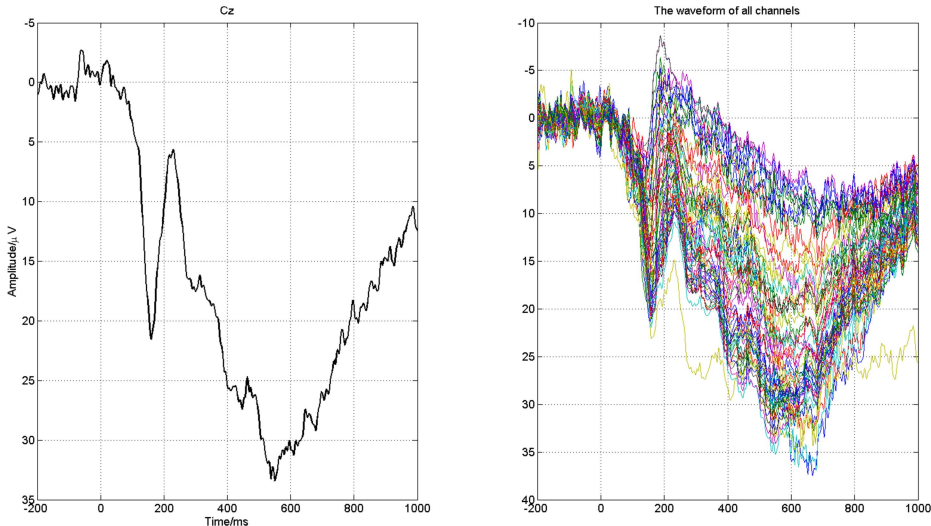


**Figure 1** Waveforms at Cz and all channels

As shown in Figure 4, the topographical distribution of  $fc = 4$  is selected as the template. The correlation coefficient values between the template and the three components of spatial dimension (the fourth column) are respectively 0.8495, 0.8947 and 0.8915. A comparison of the waveform, spectrum, TFR and topographical distribution in first row (or the second row) with those of the third row shows commonalities only in the topographical distribution, but not waveform, spectrum and TFR. As shown in Figure 5, the time window is from 100 to 400ms and the frequency from 7 to 10Hz. In Figure 5(a), different lines represent different  $\sigma$ ; in Figure 5(b),

different lines represent different  $fc$ . The topographical distribution of  $\sigma = 1, fc = 4$  is chosen as the template. Then, correlation analyses are conducted between the topographical distributions of each parameter and the template. When  $\sigma$  (or  $fc$ ) is fixed, the correlation coefficient shows a decreasing tendency with the increasement of  $fc$  (or  $\sigma$ ).

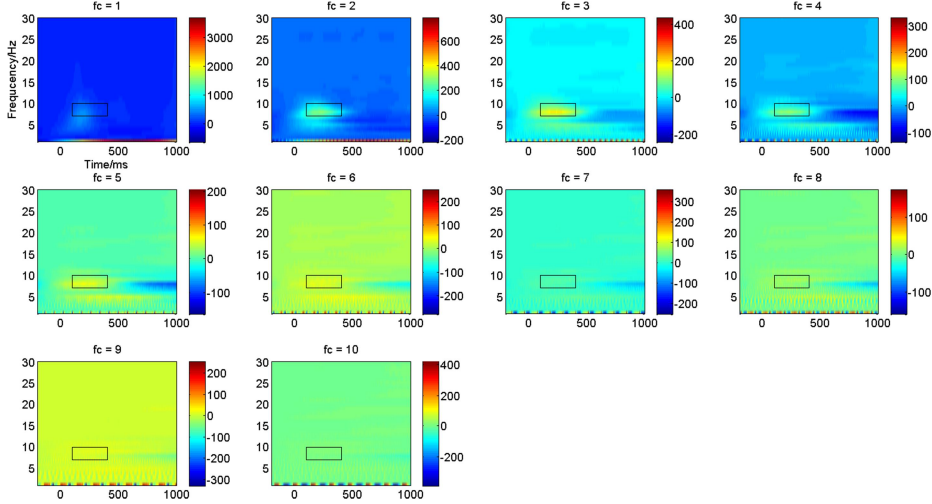


**Figure 2** TFR results with CMCWT method at Cz electrode.  $\sigma = 1$ , the time window of the rectangle area was from 100 to 400ms and its frequency range from 7 to 10Hz.

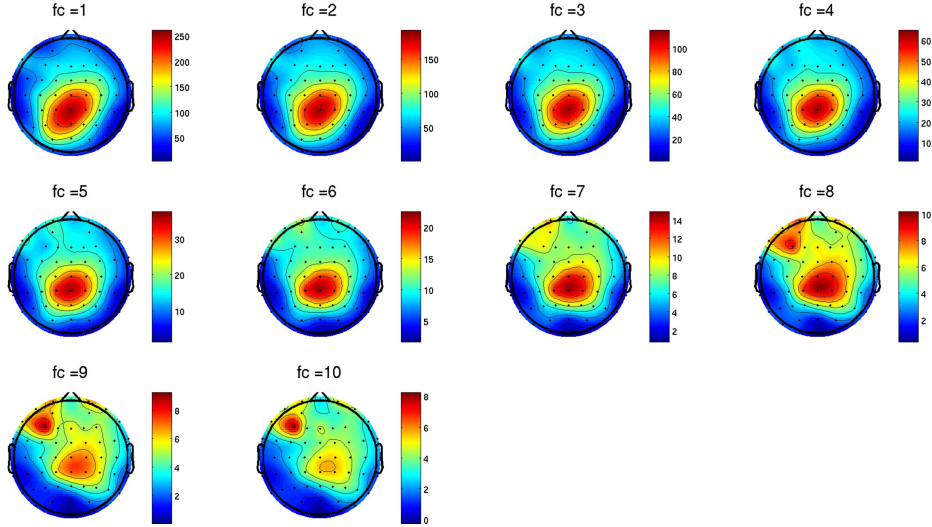


**Figure 3** The corresponding topographical distribution of rectangle areas in Figure 2

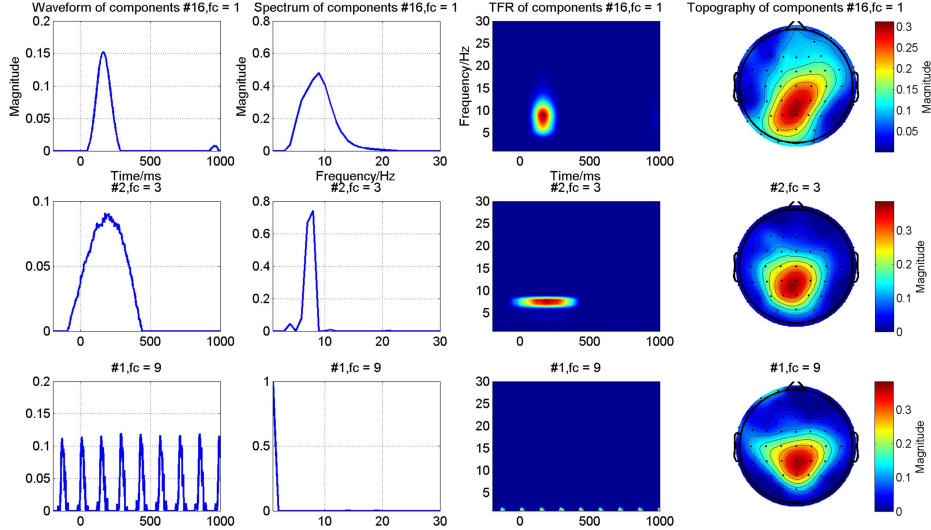


**Figure 4** The corresponding temporal, spectral, and spatial components of different parameters. The third-order ERP tensor of the TFR for NCPD includes frequency (30 frequency bins), time (600 samples), and feature modes (58 channels). 21 components were extracted from each mode for NCPD, the order and variance of each component for NCPD are not determined. The TFR is based on the outer product of the temporal and spectral components.

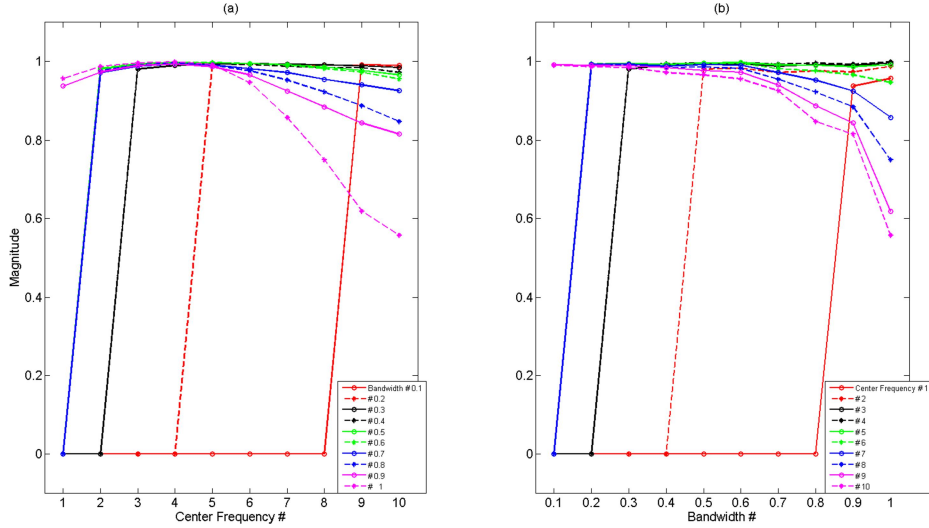


**Figure 5** The Correlation coefficients between topographical distributions of each parameter and the template ( $\sigma = 1, fc = 4$ )

In Figure 6, the power of the region of interest (time: 100-400ms, frequency: 7-10Hz) of Cz with different parametric settings of  $fc$  and  $\sigma$  is analyzed. The first/second/third row respectively shows the  $p$  value of the waiting time condition/feedback condition/interaction. The figure shows how the  $p$  value changes with  $fc$

(or  $\sigma$ ), when  $\sigma$  (or  $fc$ ) is a constant. When  $\sigma$  (or  $fc$ ) is fixed, the  $p$  value shows an increasing tendency with the increasement of  $fc$  (or  $\sigma$ ). The corresponding statistical analysis results may also differ with different settings of  $fc$  and  $\sigma$ .

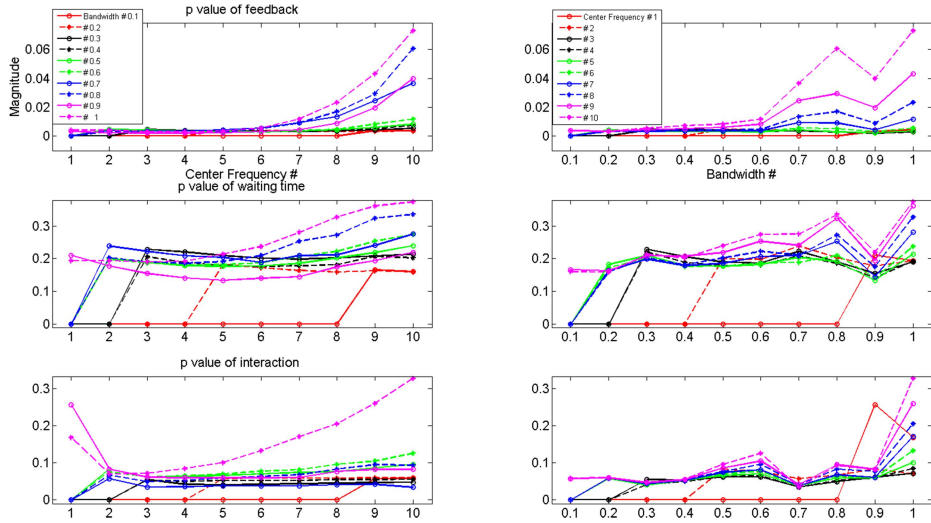


**Figure 6** Two-way repeated measurements ANOVA results of different  $fc$  and  $\sigma$  parameters. Two factors refer to waiting time (short, long) and feedback valence (loss, gain)

## 5 Conclusion

The current study, through employing the methods of CMCWT, explored the influence of  $fc$  and  $\sigma$  variation on the time-frequency and topographical results of ERP data. Besides, NCPD was used to further confirm the differences manifested in time-frequency results. Results showed that parametric variation of  $\sigma$  and  $fc$  had an effect on time-frequency results. Moreover, it was found that different components would be obtained from different TFR results by NCPD. The current study therefore suggests that different parameters should be examined in order to get optimal time-frequency results. Meanwhile, the NCPD method is highly encouraged to be applied for the further confirmation of differences in time-frequency results.

## 6 Acknowledgments

This work was supported by National Natural Science Foundation of China (Grant No. 81471742) and the Fundamental Research Funds for the Central Universities [DUT16JJ(G)03] in Dalian University of Technology in China.

## 7 References

1. Niedermeyer, E. and F.L. da Silva, *Electroencephalography: basic principles, clinical applications, and related fields*. 2005: Lippincott Williams & Wilkins.
2. Luck, S.J., *An Introduction to the Event-Related Potential Technique*. 2005. 66.
3. Cong, F., et al., Linking brain responses to naturalistic music through analysis of ongoing EEG and stimulus features. *IEEE Transactions on Multimedia*, 2013. 15(5): p. 1060-1069.
4. Herrmann, C.S., et al., Time-frequency analysis of event-related potentials: a brief tutorial. *Brain topography*, 2014. 27(4): p. 438-450.
5. Sánchezmácher, N., et al., Event-related brain responses as correlates of changes in predictive and affective values of conditioned stimuli. *Brain Research*, 2011. 1414(1): p. 77-84.
6. Sanchezalavez, M. and C.L. Ehlers, Event-related oscillations (ERO) during an active discrimination task: Effects of lesions of the nucleus basalis magnocellularis. *International Journal of Psychophysiology Official Journal of the International Organization of Psychophysiology*, 2016. 103: p. 53.
7. Mathes, B., et al., Maturation of the P3 and concurrent oscillatory processes during adolescence. *Clinical Neurophysiology Official Journal of the International Federation of Clinical Neurophysiology*, 2016. 127(7): p. 2599.
8. Ergen, M., et al., Time-frequency analysis of the event-related potentials associated with the Stroop test. *International Journal of Psychophysiology Official Journal of the International Organization of Psychophysiology*, 2014. 94(3): p. 463-72.
9. Tallon-Baudry, C., et al., Stimulus specificity of phase-locked and non-phase-locked 40 Hz visual responses in human. *The Journal of Neuroscience*, 1996. 16(13): p. 4240-4249.
10. Tallon-Baudry, C., et al., Induced  $\gamma$ -band activity during the delay of a visual short-term memory task in humans. *The Journal of neuroscience*, 1998. 18(11): p. 4244-4254.
11. Tallon-Baudry, C., et al., Oscillatory  $\gamma$ -band (30–70 Hz) activity induced by a visual search task in humans. *The Journal of neuroscience*, 1997. 17(2): p. 722-734.
12. Tallon-Baudry, C. and O. Bertrand, Oscillatory gamma activity in humans and its role in object representation. *Trends in cognitive sciences*, 1999. 3(4): p. 151-162.
13. Wang, J., et al., P300, not feedback error-related negativity, manifests the waiting cost of receiving reward information. *Neuroreport*, 2014. 25(13): p. 1044-8.
14. Cong, F., et al., Multi-domain feature extraction for small event-related potentials through nonnegative multi-way array decomposition from low dense array EEG. *International journal of neural systems*, 2013. 23(02): p. 1350006.
15. Cong, F., et al., Tensor decomposition of EEG signals: a brief review. *Journal of neuroscience methods*, 2015. 248: p. 59-69.
16. Delorme, A. and S. Makeig, EEGLAB: an open source toolbox for analysis of single-trial EEG dynamics including independent component analysis. *Journal of neuroscience methods*, 2004. 134(1): p. 9-21.



## **PIII**

### **OBJECTIVE EXTRACTION OF EVOKED EVENT-RELATED OSCILLATION FROM TIME-FREQUENCY REPRESENTATION OF EVENT-RELATED POTENTIALS**

by

Guanghui Zhang, Xueyan Li, and Fengyu Cong 2020

Neural Plasticity, vol. 2020, Article ID 8841354, 20 pages,  
<https://doi.org/10.1155/2020/8841354>

Reproduced with kind permission of Hindawi Limited.



## Research Article

# Objective Extraction of Evoked Event-Related Oscillation from Time-Frequency Representation of Event-Related Potentials

Guanghui Zhang ,<sup>1,2</sup> Xueyan Li,<sup>3</sup> and Fengyu Cong ,<sup>1,2,4,5</sup>

<sup>1</sup>School of Biomedical Engineering, Faculty of Electronic Information and Electrical Engineering, Dalian University of Technology, Dalian 116024, China

<sup>2</sup>Faculty of Information Technology, University of Jyväskylä, Jyväskylä 40014, Finland

<sup>3</sup>School of Foreign Languages, Dalian University of Technology, Dalian 116024, China

<sup>4</sup>School of Artificial Intelligence, Faculty of Electronic Information and Electrical Engineering, Dalian University of Technology, Dalian 116024, China

<sup>5</sup>Key Laboratory of Integrated Circuit and Biomedical Electronic System, Dalian University of Technology, Dalian 116024, China

Correspondence should be addressed to Guanghui Zhang; [guanghai.zhang@foxmail.com](mailto:guanghai.zhang@foxmail.com) and Fengyu Cong; [cong@dlut.edu.cn](mailto:cong@dlut.edu.cn)

Received 4 August 2020; Revised 8 September 2020; Accepted 28 October 2020; Published 21 December 2020

Academic Editor: Jian Ting Cao

Copyright © 2020 Guanghui Zhang et al. This is an open access article distributed under the Creative Commons Attribution License, which permits unrestricted use, distribution, and reproduction in any medium, provided the original work is properly cited.

Evoked event-related oscillations (EROs) have been widely used to explore the mechanisms of brain activities for both normal people and neuropsychiatric disease patients. In most previous studies, the calculation of the regions of evoked EROs of interest is commonly based on a predefined time window and a frequency range given by the experimenter, which tends to be subjective. Additionally, evoked EROs sometimes cannot be fully extracted using the conventional time-frequency analysis (TFA) because they may be overlapped with each other or with artifacts in time, frequency, and space domains. To further investigate the related neuronal processes, a novel approach was proposed including three steps: (1) extract the temporal and spatial components of interest simultaneously by temporal principal component analysis (PCA) and Promax rotation and project them to the electrode fields for correcting their variance and polarity indeterminacies, (2) calculate the time-frequency representations (TFRs) of the back-projected components, and (3) compute the regions of evoked EROs of interest on TFRs objectively using the edge detection algorithm. We performed this novel approach, conventional TFA, and TFA-PCA to analyse both the synthetic datasets with different levels of SNR and an actual ERP dataset in a two-factor paradigm of waiting time (short/long) and feedback (loss/gain) separately. Synthetic datasets results indicated that N2-theta and P3-delta oscillations can be stably detected from different SNR-simulated datasets using the proposed approach, but, by comparison, only one oscillation was obtained via the last two approaches. Furthermore, regarding the actual dataset, the statistical results for the proposed approach revealed that P3-delta was sensitive to the waiting time but not for that of the other approaches. This study manifested that the proposed approach could objectively extract evoked EROs of interest, which allows a better understanding of the modulations of the oscillatory responses.

## 1. Introduction

EEG has been widely used in neuroscience field to evaluate the temporal, spectral, and spatial dynamics of cognitive processes. One typical technique is event-related potential (ERP), which is obtained by averaging multitrial EEG data, and the other one is evoked event-related oscillation (ERO) in the time, frequency, or time-frequency domains based on

the ERPs [1]. Evoked EROs have been applied for investigating the distinctions of cognitive functions between normal and neuropsychiatric disordered people [2, 3], and different approaches can be employed to obtain evoked EROs, such as digital filtering (like 4–8 Hz for theta band), power spectral density-based spectral analysis, and time-frequency analysis (TFA) [4]. It should be noted that the underlying ideas of calculating evoked EROs by the first two approaches are similar,

and the amplitudes are measured either in the time or frequency domains. In terms of the digital filtering method, evoked EROs are obtained by filtering the ERP waveforms (i.e., the averaged EEG data over signal trials) with a band-pass filter, and then, the power of the filtered signals is analysed in the time domain. However, it is difficult to see how evoked EROs change with frequencies in each time point. The approach of TFA can overcome this obstacle, allowing the examination of evoked EROs both in time and frequency domains simultaneously.

Nevertheless, TFA also has its drawbacks in exploring evoked EROs of interest in multicondition ERP experiments. In most previous investigations, the power of evoked EROs was usually calculated in a predefined region with a particular time window and a frequency range. This predefined region was commonly settled down based on the visual inspection of grand averaged time-frequency representation (TFR) distributions in computing the related energies [5–11] and was conventionally computed in a rectangle region so that the method was named as “conventional rectangle method.” However, the shape of evoked EROs, in reality, was more like a waterdrop than a rectangle. If the predefined rectangle region was smaller than the real waterdrop shape of evoked EROs, some useful information would be neglected. Similarly, when the predefined region was larger than the real boundary of evoked EROs, unrelated information would be involved. As reported in these studies [5, 7, 12], the other drawback should also be considered that the number of the visible evoked EROs identified from the grand averaged TFR was smaller than the number of the practical analysed ERPs. Thus, it remains challenges that the expatiations of some stages of cognitive processes would not be present. Bernat et al. [13, 14] suggested that those EROs, which were overlapped in the time and frequency domains, could be effectively extracted by performing principal component analysis (PCA) and Varimax rotation on the matrix of TFRs (i.e., time and frequency domains were rearranged into columns, and the other variables, such as channels, conditions, and subjects, were integrated into rows) in a multicondition ERP experiment (we called this method as “TFA-PCA” here). One of his studies revealed that the decomposed delta and theta oscillations by TFA-PCA were greatly associated with the N2-P3 [15], whereas they merely explained the occurred time course of the selected theta or delta was closest to that of the N2-P3 complex and did not demonstrate which ERP made the most contributions to theta or delta oscillations. Importantly, the core idea of TFA-PCA was to weight the extracted components with the original TFRs, which would result in the decomposed EROs might be still mixtures.

To address these gaps, we proposed an approach to objectively extract evoked EROs of interest (the illustration of the proposed approach was displayed in Figure 1). More specifically, temporal PCA (t-PCA) and Promax rotation were conducted to extract the temporal and spatial components. Afterward, the components of interest were selected and projected to the electrode fields for correcting the variance and polarity indeterminacies. It was noted that the back-projection procedure was also used to tackle the problem that several components could not be analysed together

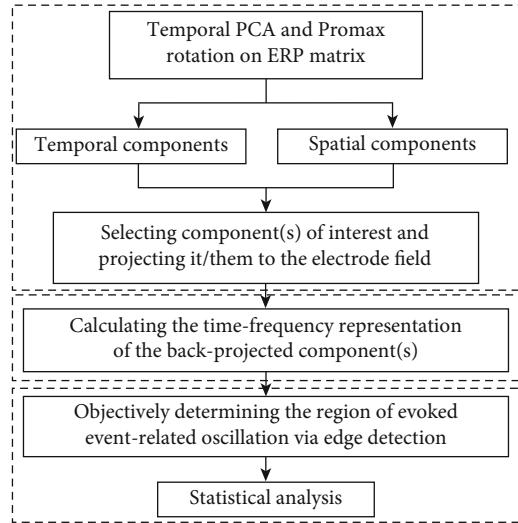


FIGURE 1: The diagram for extracting evoked event-related oscillations (EROs) from ERP datasets using the proposed method. First, exploring the temporal and spatial components of interest using temporal principal component analysis (t-PCA) and Promax rotation and projecting them to the electrode fields. Second, transforming the projection of the components of interest into time-frequency representations (TFRs) using complex morlet continuous wavelet transform. Third, determining the time and frequency positions of evoked event-related oscillation objectively using edge detection technique for statistical analysis.

in the previous PCA toolbox, like Dien’s PCA toolbox [16]. Next, a complex morlet continuous wavelet transform was applied to compute the TFRs of the back-projected component(s) in the electrode fields. Finally, an edge detection algorithm based on Canny detector was introduced to calculate the specific time and frequency positions of evoked EROs from the associated TFRs for further statistical analysis. In addition, correlation coefficients between the topographies of any two participants were calculated to evaluate the homogeneity of ERPs/components/evoked EROs.

In order to evaluate the results of the proposed approach and the other existing approaches, the proposed approach, the conventional TFA, and TFA-PCA were performed on the simulation datasets which were contaminated by different levels of noise (i.e., 20 dB, 10 dB, 5 dB, and 1 dB). As a result, we could obtain the stably results from those simulation datasets using our proposed approach. Meanwhile, the results for the datasets with different levels of SNR, all the extracted components in the time-space domain, and the associated TFRs of evoked EROs in the time-frequency domain were much closer to their sources. We demonstrated this supposition with two aspects as below. One aspect, for different levels of noise-contaminated simulation datasets, we separately calculated the correlation coefficients between any two of the waveforms/topographies/TFRs of the source, mixed, and extracted signals; We also computed the correlation coefficients between the TFRs of the source signal and weighted TFRs obtained by TFA-PCA. The other aspect was to illustrate TFRs obtained by the conventional TFA, the proposed approach,

and TFA-PCA. The waveforms/topographies of the source, mixed, and extracted signals were also displayed when SNR is equal to 10 dB. Meanwhile, we also, respectively, performed the proposed, TFA, and TFA-PCA approaches on a real ERP dataset to extract evoked EROs of interest.

In this study, we used the notation of “component(s)” to represent the results obtained by t-PCA and Promax rotation. Likewise, the results gained by the back-projection procedure were considered to be “projected N2/P3”; N2 and P3 were labelled as “ERP” in the original signals; the time-frequency results computed by the conventional TFA, the proposed approach, and TFA-PCA were, respectively, named as “TFR,” “extracted TFR,” and “weighted TFR.” The related codes for the proposed approach can be found from this link: <https://guanghuizhang0328.github.io/publications/>.

## 2. Data Collections and Methods

### 2.1. EEG and Synthetic Dataset Collection and Analysis

**2.1.1. Synthetic Dataset.** The synthetic signal was generated with “Dipole-Simulator” (BESA Tool version; it can be downloaded from: <http://www.besa.de/updates/tools>). The duration of the signal was 1000 ms (from -200 ms to 800 ms). The sampling rate was 150 Hz. There were four simulated ERPs (N1, P2, N2, and P3) whose maximum amplitudes were measured at electrodes Fz, CPz, FCz, and Cz, respectively. In this study, N2 and P3 were considered as the interested ERPs and others were deemed concomitant ones. The maximum negative peaks for N2 and P3 were located at 260–400 ms and 370–580 ms, separately. The details of their associated waveforms, topographic maps in the time domain, and TFR distributions could be found in Figure 2. Meanwhile, we also displayed correlation coefficients between any two of waveforms/topographic maps/TFRs of the four original sources and their mixture to show the degree of overlap and how much the four original sources contribute to the original mixed signal (see the last row in Figure 2). In order to simulate the signals as close to the actual ERP signals as possible, the variations were set in latency and amplitude of P3 and N2 of the original mixed signal (as illustrated in Figure 2), which was applied to simulate the single trial dataset [17]. Following this idea, the 68-set data were subsequently simulated. Different levels of white Gaussian noise were, respectively, added to the mixed 68-set signals (as shown in Figures 3 and 4; the filtered mixed signal plays the role of a real preprocessed ERP dataset), and the signal-noise-ratio (SNR) was set to 20 dB, 10 dB, 5 dB, and 1 dB separately.

**2.1.2. Actual Dataset.** Twenty-one undergraduate and graduate students were recruited to participate as paid volunteers in the collection of the actual dataset. Nine were females and twelve were males (mean age: 20.95 years old). All the subjects were right-handed, with normal or corrected to normal visual acuity, and they did not know or see the experimental paradigm before the experiment. The details of the experiment materials and the paradigm can be found in this research [18]. EEG recordings at 64 locations were collected according to the standard 10-20 system (Brain Products

GmbH, Gilching, Germany). The EEG data were referenced online against the left and right mastoids. Meanwhile, we also collected the vertical and horizontal electrooculogram (EOG) from four electrodes which were placed above and below the right eye and on the outer canthus of the right and left eyes, respectively. All impedances were less than 10 kΩ for each electrode. The EEG and EOG for each participant were recorded with a 500 Hz sampling rate, and the data were filtered between 0.01 and 100 Hz using a band-pass filter. The signals from six electrodes (i.e., “HEOL,” “VEOD,” “HEOR,” “VEOU,” “M1,” and “M2”) were not involved in further analysis.

### 2.1.3. Data Preprocessing and Analysis

**(1) Synthetic Dataset.** According to our previous study [19], as for the frequency band of the components of interest, the synthetic datasets with different levels of SNR were first filtered, respectively, using wavelet filter with the following parameters: the number of levels for decomposition was 8; the selected mother wavelet was “rbio6.8”; the detail coefficients of the number of levels at 4, 5, 6, 7, and 8 were chosen for signal reconstruction. Temporal PCA and Promax rotation were then employed to extract the components of interest and project them to the electrode fields for correcting their variance and polarity indeterminacies. Sequentially, TFRs were calculated by the wavelet transform for the source, mixed, and projected signals separately. During this step, aiming at obtaining better time resolution and frequency resolution of TFRs, the centre frequency and bandwidth were set as 1, respectively, to define a mother wavelet as applied in our previous study [20]. The frequency range of interest was defined from 1 to 15 Hz with 30 frequency bins in non-linear distribution. For each frequency layer, the power values were baseline corrected by subtracting the mean power of the baseline (200 ms before the stimulus onset) for each point using the subtraction approach [21–23].

We also examined the noise-contaminated simulation datasets by performing PCA on the matrix of TFRs of the mixed signal with 4420 cases (65 channels by 68 subjects) and 3600 variables (30 frequency bins by 120 time point, that is, frequencies ranging from 1 to 15 Hz and time ranging from 0 to 800 ms) using covariance matrix with Kaiser normalization and Varimax rotation [13, 14, 24]. Then, we selected the components of interest from the separated ones and weighted them with the original TFRs based on the main functions of the Bernat’s toolbox ([http://www.ccnlab.umd.edu/Psychophysiology\\_Toolbox](http://www.ccnlab.umd.edu/Psychophysiology_Toolbox)).

To verify that the proposed approach could efficiently extract the evoked EROs of interest from the noise contaminated with different SNR levels without changing their TFR properties, the correlation coefficients between any two of the waveforms/topographies/TFRs of the source, mixed, and extracted signals were separately computed as illustrated in Figures 5(a)–5(i). Likewise, the correlation coefficients between the weighted TFRs of early/late theta and source N2/P3 were also measured (see Figures 5(j) and 5(k)). Furthermore, the related waveforms/topographies in the time

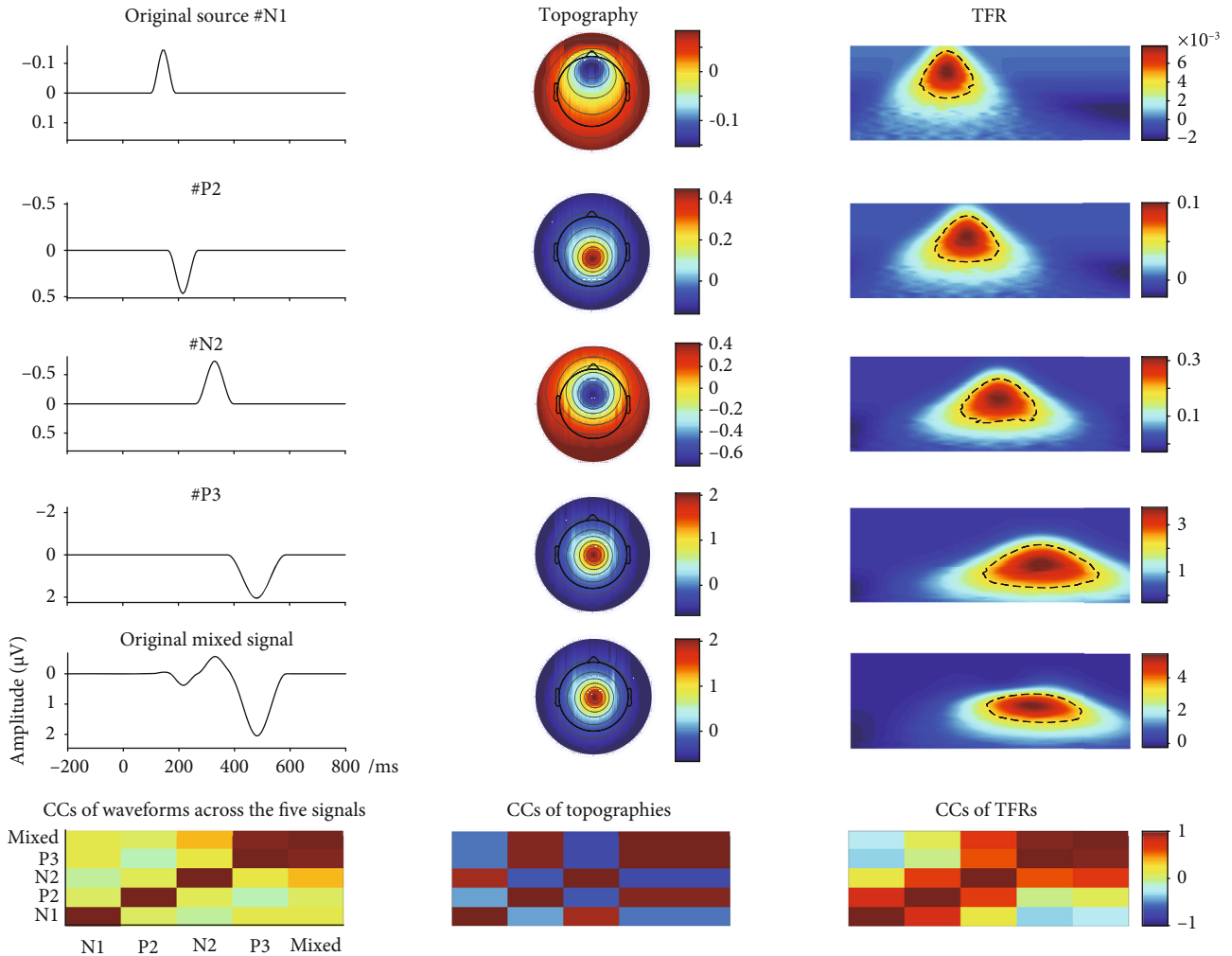


FIGURE 2: The waveforms, associated topographies, and time-frequency representations (TFRs) for single source N1 (Fz), P2 (CPz), N2 (FCz), P3 (Cz), and mixed signal (Cz), respectively (the first five rows). The last row represents the correlation coefficients (CCs) of waveforms/topographies/TFRs among all five signals. The 65 sets of simulation signals were generated from these sources based on setting the variations of amplitude and latency for N2/P3.

domain and TFRs were also plotted for the source and mixed signals (see Figures 3 and 4) when SNR was set to 10 dB.

(2) *Actual Dataset.* The actual datasets were first resampled to 128 Hz so that PCA and Varimax rotation could be performed on the TFRs of the averaged signal with the comparable sampling rate to the simulation datasets. The EEG signals were then filtered offline using a notch FIR filter with 45–55 Hz and a low pass FIR filter with 30 Hz. Sequentially, the filtered continuous recordings were segmented from 200 ms before the stimulus onset to 1000 ms after the stimulus onset. Epochs whose magnitude exceeded  $\pm 100 \mu\text{V}$  were excluded (6.93% epochs were rejected), and the remaining ones were baseline corrected. Next, the multitrial datasets were averaged across every condition of each participant, and the averaged datasets were then filtered by the wavelet filter as used above to improve the SNR.

In order to extract the evoked EROs by the proposed approach, temporal PCA and Promax rotation were per-

formed on the filtered signals to obtain the components related to N2/P3 and project them to all electrodes. To obtain the TFRs of the original averaged and projected signals separately, the frequency range of interest was then set from 0.5 to 14.5 Hz with 30 frequency bins. Additionally, the centre frequency and bandwidth were also set as 1, respectively, as used above for the noise-contaminated simulation datasets.

Another comparison method was also applied to extract the delta and theta oscillatory responses from the TFRs (obtained from the averaged ERP signals) with a frequency range of 0.5–14.5 Hz and time window of 0–1000 ms. Namely, PCA and Varimax rotation were first performed on the matrix formed by TFRs of the original filtered signal with 4872 cases (58 channels by 4 conditions by 21 subjects) and 3840 variables (30 frequency bins by 128 time points). Sequentially, the weighting procedure was separately achieved between the original TFR and the selected components.

The conventional rectangle method and edge detection algorithm were, respectively, conducted to obtain the region of ERO from the TFR of each condition for the conventional

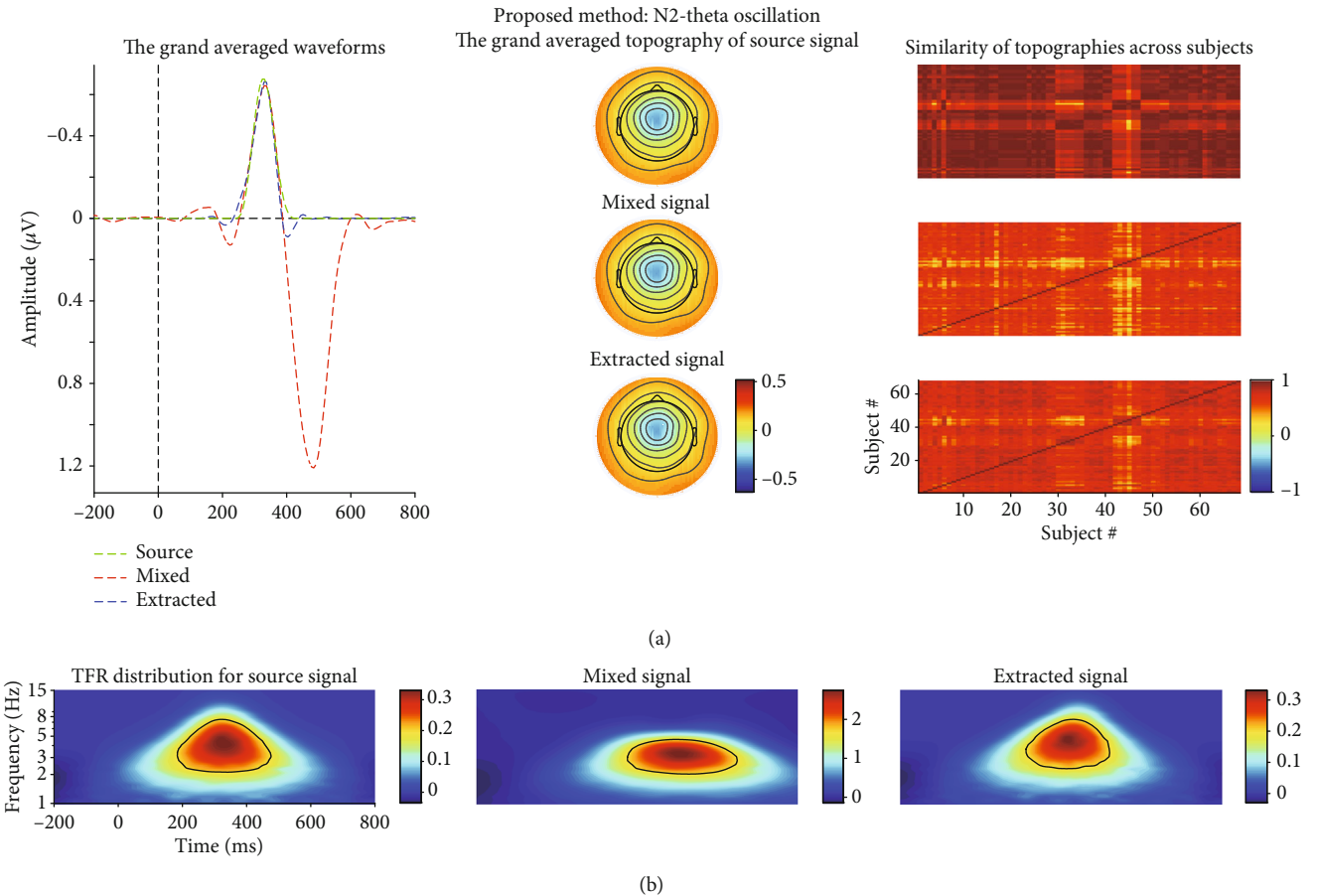


FIGURE 3: (a) The grand averaged waveform at FCz electrode, topography (the time window was from 300 to 400 ms), and similarity of topographies among subjects of the source/mixed/extracted N2 for the synthetic dataset when SNR is equal to 10 dB. (b) The associated grand averaged time-frequency representations (TFRs) at FCz of the source, mixed, and extracted (using the proposed approach) signals for N2-theta oscillation separately. The mixed signal plays the role of the preprocessed ERPs with the consideration of a real ERP dataset.

TFA (“M1”), the proposed approach (“M2”), and TFA-PCA (“M3”). The power of theta oscillation for each condition was measured in the averaged TFR at Fz, FCz, and Cz electrodes, and the delta oscillation energy was computed at five electrodes Fz, FCz, Cz, CPz, and Pz.

Briefly, with regard to the theta oscillation, when the conventional rectangle method was applied to determine the regions of the oscillatory responses, two regions were measured (“R1”: 100-300 ms and 3-7 Hz; “R2”: 200-400 ms and 3-7 Hz) from the grand averaged TFRs. We also, respectively, predefined “R3” (4-8 Hz and 150-300 ms) and “R5” (100-400 ms and 3-7 Hz) in the TFRs of the proposed approach and TFA-PCA to compute the related energies. In addition, the determined regions of the evoked EROs for the last two methods were named as “R4” and “R6” when using the edge detection algorithm. The statistical results were not computed for delta oscillation of the conventional TFA because we did not find the region using the edge detection algorithm.

In terms of delta oscillation, using conventional rectangle method, we also calculated two regions of every condition of TFR obtained by the conventional TFA (“R7”: 200-600 ms and 0.5-2 Hz; “R8”: 300-600 ms and 0.5-2 Hz). Likewise, we used “R10” (1-3 Hz and 200-600 ms) and “R12” (200-

600 ms and 0.5-2 Hz) to calculate the power of delta oscillation obtained by the proposed approach and TFA-PCA, respectively. The recognized regions of delta oscillations using the edge detection algorithm for the conventional TFA, the proposed approach, and TFA-PCA corresponded to “R9,” “R11,” and “R13,” respectively.

Finally, two-way repeated-measurement-ANOVA (rm-ANOVA) with waiting time (short/long) and feedback valence (loss/gain) as within-subject factors was used for analysing each determined region of delta and theta oscillations separately. The correction of the number of degrees of freedom would be carried out by the Greenhouse-Geisser method if necessary. All displayed topographic maps in the time domain for simulation and real datasets were obtained using the mean values of the predefined time window. Meanwhile, during PCA procedure, the singular value decomposition was used to decompose the original matrix formed by ERP signals into the sum of several principal components using Matlab function-pca with default parameters (version 2018b, the Mathworks, Inc., Natick, MA).

**2.2. Proposed Approach for Data Processing.** In order to overcome the challenges that evoked EROs could not be

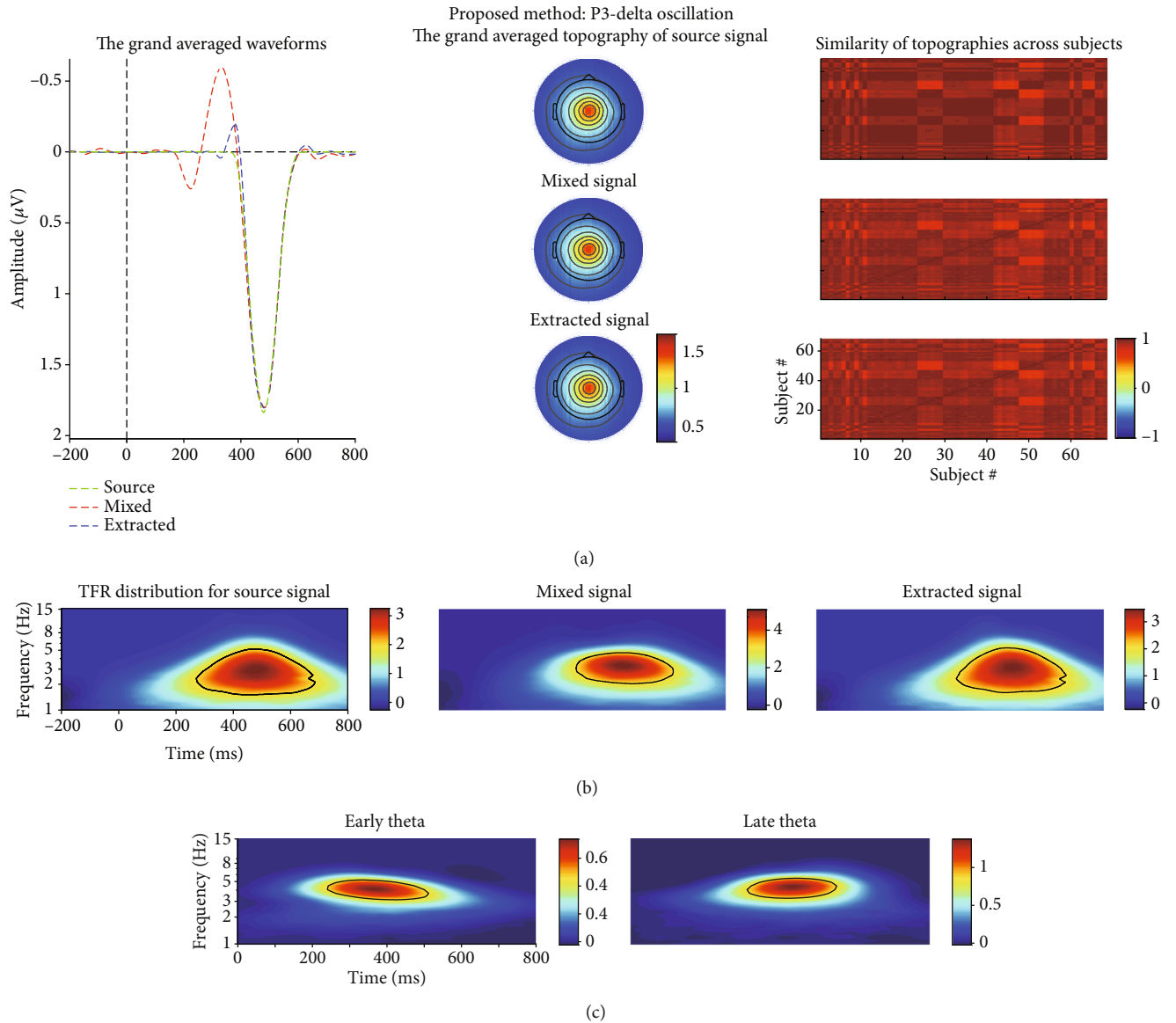


FIGURE 4: (a) The grand averaged waveform at Cz electrode, topography (the time window was from 400 to 550 ms), and similarity of topographies among subjects of the source/mixed/extracted P3 for the synthetic dataset when SNR is equal to 10 dB. (b) The associated grand averaged time-frequency representations (TFRs) at Cz of the source, mixed, and extracted (by the proposed approach) signals for P3-delta oscillation separately. The mixed signal plays the role of the preprocessed ERPs with the consideration of a real ERP dataset. (c) Weighted TFRs of early and late theta using TFA-PCA. The mixed signal plays the role of the preprocessed ERPs with the consideration of a real ERP dataset.

extracted completely by the conventional TFA or TFA-PCA approaches, we used the following steps to extract evoked EROs of interest. Firstly, a matrix  $\hat{\mathbf{Z}} = \mathbf{Z}^T \in \mathcal{R}^{N \times M}$

was separately formed from the synthetic datasets with different noise levels and real datasets separately to explore the component(s) of interest [25–28]. Herein, it should be noted that time samples were variables in columns of matrix  $\hat{\mathbf{Z}}$ , and the other factors, such as channels, conditions, and subjects, were integrated into rows that were labelled as observations. Then, t-PCA and Promax rotation were fulfilled to decompose this matrix into  $R$  components, and the components of interest were selected to

project to all of the scalp electrodes for correcting the variance and polarity indeterminacies. Subsequently, the calculation of the TFRs of the back-projected components was carried out at all electrodes. Finally, the determination of the regions of evoked EROs at the typical electrodes was worked out using the edge detection algorithm.

**2.2.1. Extracting the Components of Interest and Their Back-Projection.** The purpose of the t-PCA and Promax rotation was to use a smaller set of nonredundant descriptive variables (i.e., components) to represent the original ERP signal  $\hat{\mathbf{Z}}$  and then choose the interested components for back-projection

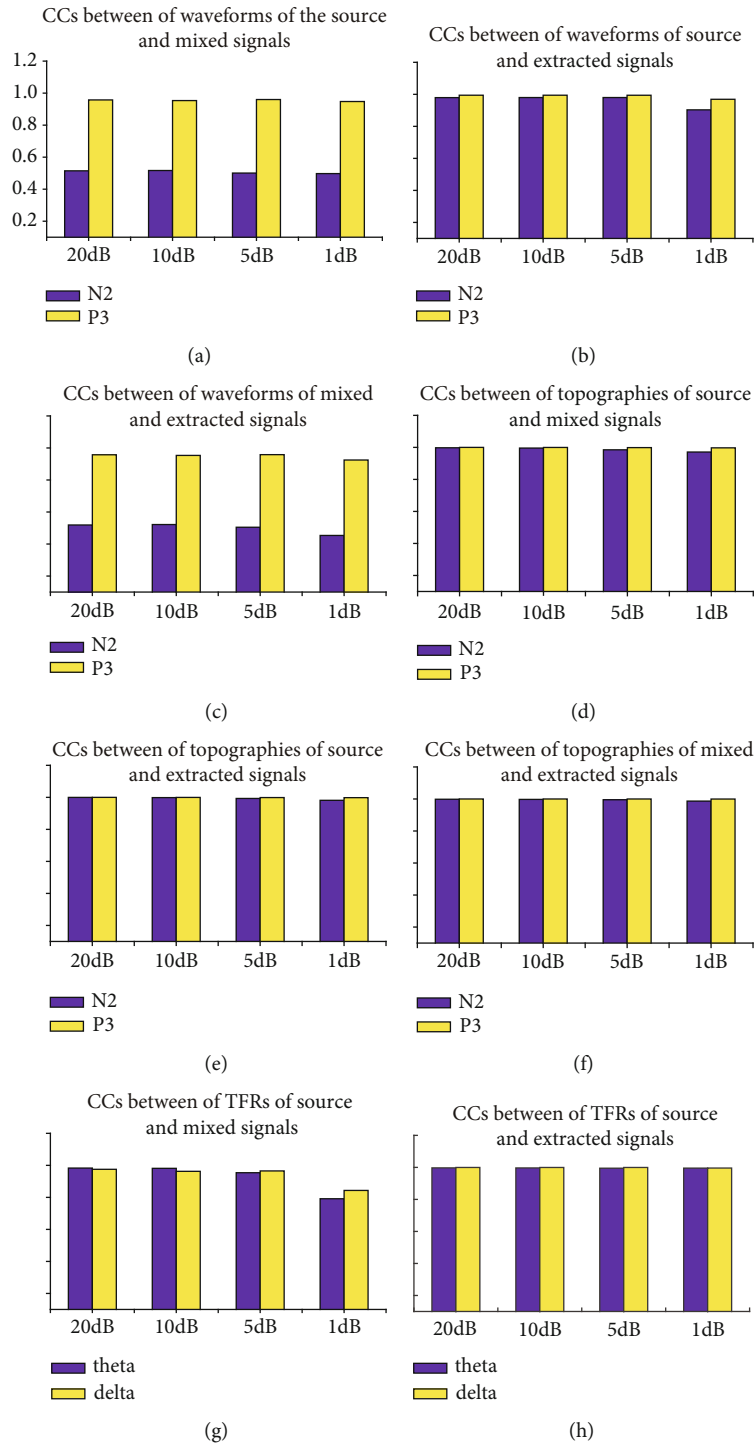


FIGURE 5: Continued.

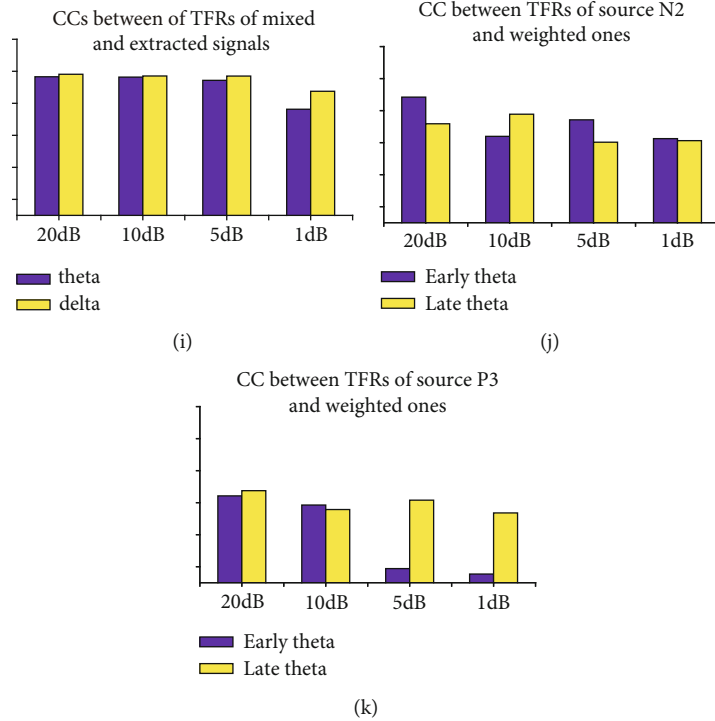


FIGURE 5: (a-i) The correlation coefficients (CCs) between any two waveforms/topographies/time-frequency representations (TFRs) of the source, mixed, and proposed method extracted N2 (theta)/P3 (delta) for the synthetic datasets with different levels of SNR (i.e., 20 dB, 10 dB, 5 dB, and 1 dB), respectively. (j, k) The CCs between the weighted TFR of source N2/P3 and early/late theta oscillations (using TFA-PCA method), respectively.

(see *Appendix A* and *Appendix B* for the details of the related theories). Importantly, four steps needed to be done during this procedure as below.

The first was about the determination of the number of the remained principal components (PCs). The number of the remained PCs was usually determined based on a predefined percentage ratio, such as 95% or 99%. Such a regulation has been widely applied in various fields. The calculation of this percentage ratio was achieved by the sum of a certain number of lambda values over the sum of all lambda values (i.e.,  $L = \sum_{r=1}^R \lambda_r / \sum_{m=1}^M \lambda_m$ , where  $R$  is the number of the retained PCs;  $M$  is the number of the columns of the matrix  $\hat{Z}$ ,  $M > R$ ; this percentage ratio was named as cumulative explained variance here) [29, 30].

The second was about the selection of the rotation method. Promax rotation could generate better results than Varimax rotation [31], and it was more efficient for t-PCA decomposition [32]. Hence, Promax rotation was also applied to the study.

The third was about the selection of the temporal and spatial components of interest. If the temporal and spatial properties of the extracted components were consistent with the interested ERPs and its correlation coefficients between any two spatial components of subjects were higher (for example, more than 0.4), the components were then considered for the next analysis. Overall, in terms of the following three aspects, the projected components for ERPs of interest were selected [25]: (a) the polarity and latency of temporal

component; (b) the polarity and location of the excitation region of spatial component; (c) the correlation coefficients between any two spatial components, herein spatial components were topographies, of every condition.

The fourth was about the back-projection ( $\underline{Z}$ )<sup>T</sup> of the selected components to the electrode fields. The components, derived from blind separation algorithm [33], herein t-PCA and Promax rotation, had the polarity and the variance indeterminacies, and the back-projection theory could be applied to correct them [34–37]. In practice, ERPs were often decomposed into several temporal and spatial components due to the fluctuation of the original waveforms of the interested ERPs over different subjects. Thus, all of them should be selected to project to the electrode fields for correcting their indeterminacies.

**2.2.2. Transforming the Back-Projected Components into Time-Frequency Representations.** For the back-projected components ( $\underline{Z}$ )<sup>T</sup> from the original signal  $\hat{Z}$ , we turned this time domain signal to time-frequency domain signal  $Z_{TF}$  using the complex morlet wavelet transform [20, 38–44]. Specifically, a mother wavelet was first defined using a set of bandwidth and centre frequency. Then, the frequency range of interest (e.g., 0.5–14.5 Hz) and frequency bins were set for calculation of TFR. Next, the baseline correction was finished using the values of each point in the time-frequency distribution subtracting the mean power of the baseline (for instance, 200 ms before the stimulus onset).

**2.2.3. Objectively Determining the Region of evoked EROs via Edge Detection Algorithm.** The conventional rectangle method was widely used to determine the regions of evoked EROs [5–10, 45]. As the demonstration in section 3.2.1, different statistical results could be displayed because the conventional rectangle method was a subjective method to calculate the region. To address this, an edge detection algorithm, Canny detector [46], was used to objectively distinguish the shape of evoked ERO for each condition from the TFR distribution, which can precisely and objectively mark the position of the oscillatory responses in the TFR based on their shapes (time and frequency positions) [47–49].

The displayed TFR was usually generated from  $Z_{TF}$  by calculating the mean values of the specific electrodes. In this study, we used the symbol  $\varphi_{f,t,c,s}$  to represent the value of any point in TFR distribution for  $s^{\text{th}}$  subject under  $c^{\text{th}}$  condition. As shown in Figures 6–9, the interested evoked ERO of each condition had a boundary that clearly distinguished evoked ERO from others in the TFR distribution. Following this context, we can use a typical approach, Canny detection algorithm, to determine the optimal boundary and then gain the associated region of evoked ERO.

The procedure of the original Canny algorithm for the determination of the boundary of a target can be approximately divided into the following steps [46, 50].

First, any noise was filtered out from the original image using Gaussian filter before trying to use this detector to detect any edges. Indeed, this step was to calculate the convolution between the raw image and the mask.

Second, aiming to find the edge strength, the gradient amplitude and direction at any pixel location were calculated. The gradient amplitude was determined as the square root of the sum of the square of the horizontal  $G_x(i, j)$  and vertical gradient  $G_y(i, j)$  amplitudes.

$$G(i, j) = \sqrt{G_x(i, j)^2 + G_y(i, j)^2}. \quad (1)$$

Then, the gradient direction at every pixel can be defined as follows:

$$\theta_G(i, j) = \arctan\left(\frac{G_y(i, j)}{G_x(i, j)}\right). \quad (2)$$

Third, the nonmaxima suppression was applied to the gradient amplitude to make the blurred edges sharper. In other words, the gradient direction at every pixel was computed to find the maximum magnitude. For one thing, when the gradient direction of this pixel was considered as one of 8 possible primary directions (i.e., 0 degree, 45 degrees, 90 degrees, 135 degrees, 180 degrees, 225 degrees, 270 degrees, and 315 degrees), the comparisons were made between the gradient magnitude of this pixel and its two neighbours along the gradient direction. If this value was the greatest one, it was then remained and otherwise, it would be set to zero. For another thing, if the gradient direction was not belonging to any of these possible directions, it would be finished to cal-

culate the neighbouring gradients based on interpolation theory [50].

Fourth, the edge map was determined via hysteresis thresholding. It needed two thresholds to better recognize the edges: a high threshold  $T_1$  and a low one  $T_2$ . If the value of any pixel was (i.e., the gradient amplitudes  $G(i, j)$ ) greater than  $T_1$ , it would be looked as strong edge and then recorded. Meanwhile, if the gradient amplitudes of the pixels were greater than  $T_2$  and connected to the strong edges, those pixels would be selected as strong edges. Otherwise, they were not included in the final edge image.

Practically, the region of interest needed to be determined based on the recognized boundary for further statistical analysis. Any position (it was determined by a frequency bin-  $f_1$  and a time point -  $t_1$ ) within the marked boundary was first calculated by performing on the frequency bins, time points, and the pixels of the boundary. Each value  $\psi_{f,t,c,s}$  of the point within the determined boundary was remained for every subject  $s$  under each condition  $c$  at electrodes of interest as below.

$$\psi_{f,t,c,s} = \begin{cases} \varphi_{f,t,c,s} & f = f_1, \quad t = t_1 \\ 0 & \text{otherwise} \end{cases}. \quad (3)$$

Last, the demanded value  $\bar{\psi}_{c,s}$  for each subject of each condition was gained by computing the mean value of the marked evoked ERO. Note that the parameters of  $T_1$  and  $T_2$  were set with the default values in the Matlab function (version 2018b, the Mathworks, Inc., Natick, MA).

### 3. Results

**3.1. Synthetic Dataset Results.** Figures 5(a)–5(i) show the correlation coefficients between any two waveforms/topographies/TFRs of source, mixed, and projected N2 (theta)/P3 (delta) for the synthetic datasets with different levels of noise, respectively. Meanwhile, Figures 5(j) and 5(k) show the correlation coefficients between the weighted TFR of source N2/P3 and early and late theta oscillations, respectively, for different noise-contaminated simulated datasets using TFA-PCA. Noticeably, all the correlation coefficients between the waveforms/topographies/TFRs of source and extracted N2/P3 for different noise-contaminated simulated datasets were almost equal to 1 (see Figures 5(b), 5(e), and 5(f)), whereas the unstable results were obtained when using TFA-PCA (see Figures 5(j) and 5(k)). Those indicated that evoked ERO for each ERP of interest could be stably and efficiently extracted from low to high SNR-simulated datasets by our proposed approach but not for TFA-PCA approach.

Afterward, we used the results of one simulated dataset (i.e., SNR is 10 dB) to explain the application and assess the performance of the proposed approach and TFA-PCA approach.

In the application of the proposed approach, 17 components were retained, which explained 99% of variance. According to the temporal and spatial properties of P3 and the similarity of the spatial components over all subjects (we used “spatial similarity” to represent it in the following parts), the 1st, 3rd, and 10th components were selected for

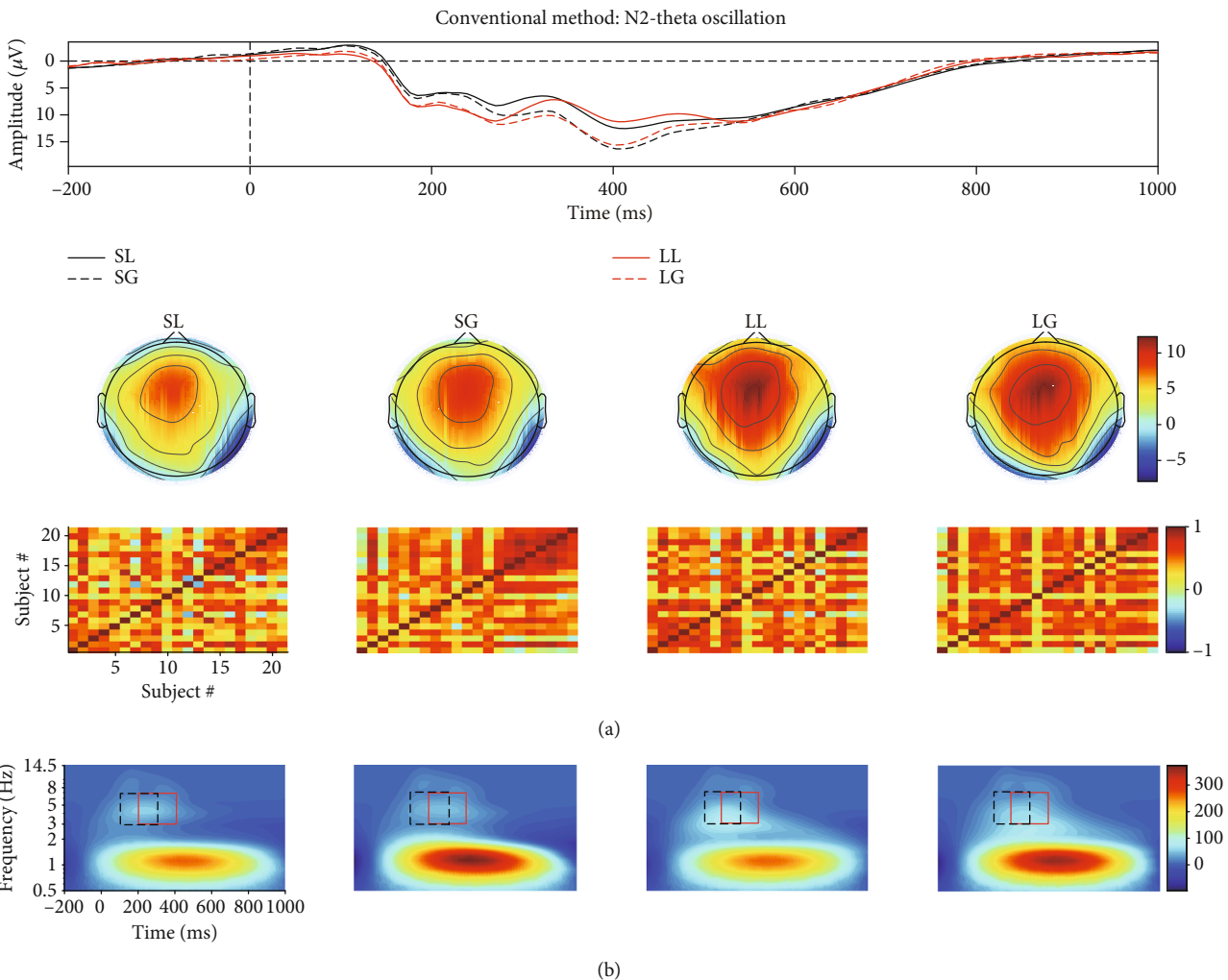


FIGURE 6: (a) The grand averaged waveform (at Fz, FCz, and Cz electrodes), topography (time window: 180-240 ms), and similarity of topographies across participants of each condition for the filtered real signal. (b) The associated grand averaged time-frequency representation (TFR) of every condition. The region of evoked ERO of each condition is determined by the edge detection algorithm and the conventional rectangle method (for the black dotted rectangle, the time window is 100-300 ms and frequency range is 3-7 Hz, “R1”; the red solid rectangle: 200-400 ms and 3-7 Hz, “R2”) separately. SL: loss condition under short waiting time; SG: gain condition under short waiting time; LL: loss of long waiting time; LG: gain of long waiting time.

P3 and they explained 68.02% (spatial similarity:  $0.89 \pm 0.07$ ), 3.86% (spatial similarity:  $0.87 \pm 0.07$ ), and 1.39% (spatial similarity:  $0.41 \pm 0.28$ ) of variance, respectively. Similarly, the 2nd and 5th components were chosen for N2, and they accounted for 6.60% (spatial similarity:  $0.73 \pm 0.10$ ) and 2.07% (spatial similarity:  $0.36 \pm 0.19$ ) of variance, respectively.

As shown in Figures 3(b) and 4(b), the power of source N2-theta oscillation (about  $0.3 \mu\text{V}^2/\text{Hz}$ ) was much smaller than that of source P3-theta oscillation (approximately  $3 \mu\text{V}^2/\text{Hz}$ ) so that the former easily disappeared in the TFR of the mixed signal. This was confirmed in the TFR of the mixed signal, and that is to say, only one oscillation was observed. This was also proved by the correlation coefficient method. Specifically, the correlation coefficient between the TFRs of the mixed and source/extracted N2-theta was roughly  $0.74/0.69$  while this value was approximately  $0.95/0.96$  for P3-delta (see Figures 5(g) and 5(i)).

The correlation coefficients between the waveforms of the mixed and source/projected N2/P3 were about  $0.52/0.95$  (see Figures 5(a) and 5(c)). This meant that P3 made the biggest contribution to the mixed signal that led to the abovementioned situation, and consequently, N2 accounted for a small part.

Two evoked EROs were obtained corresponding to N2 (see Figure 3(b)) and P3 (see Figure 4(b)), respectively, when using the proposed approach. What is more, the similarity of topographies across all subjects of the projected signal (especially for N2: from  $0.64 \pm 0.11$  to  $0.72 \pm 0.09$ ) was improved using the proposed approach when compared with the similarity of the mixed signal. Through the comparisons of the waveforms/topographies/TFRs of the source, mixed, and projected signals as shown in Figures 3 and 4, we could easily obtain that they were almost identical with each other, respectively. Regarding the correlation coefficients between the waveforms/topographies/TFRs of the source and

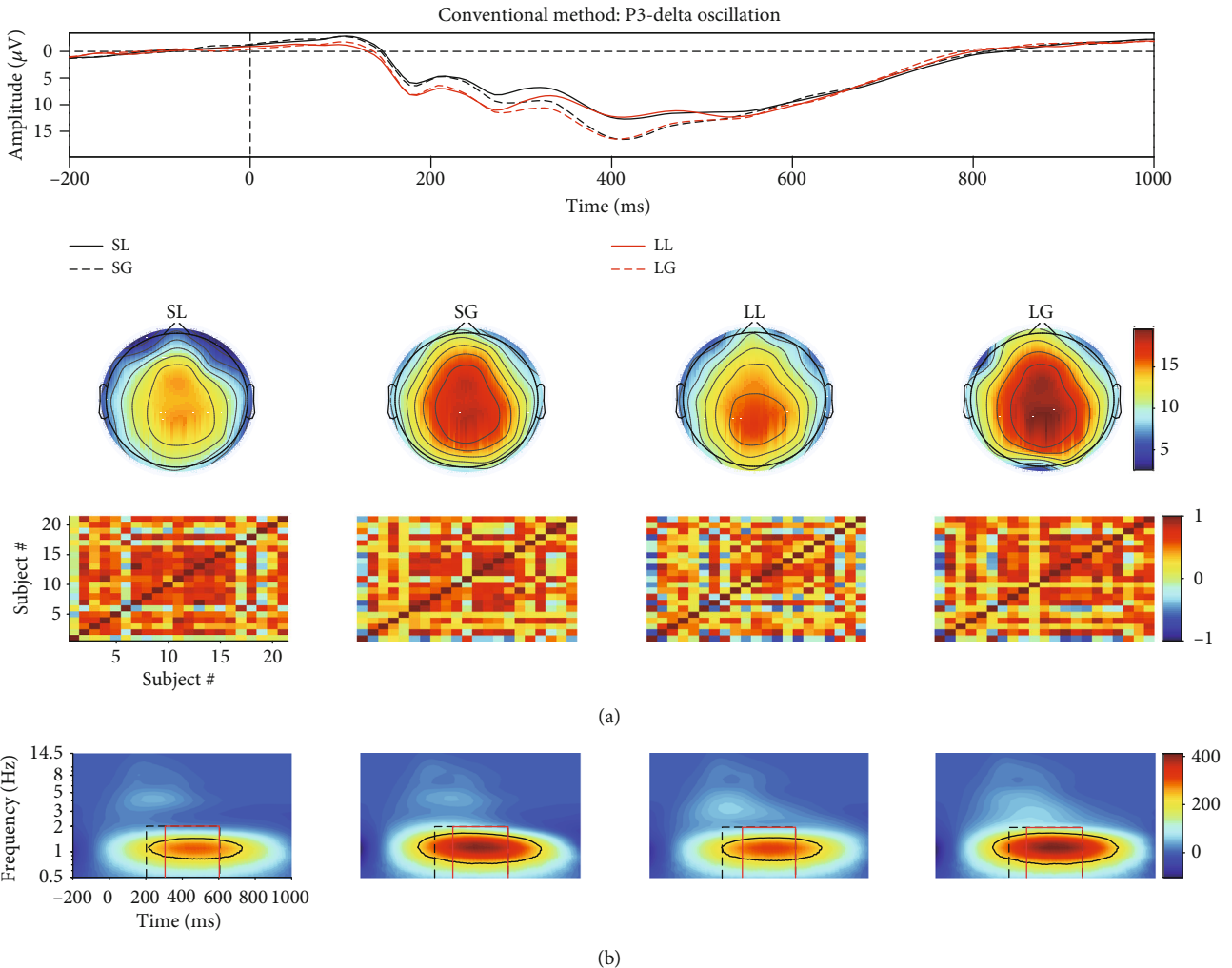


FIGURE 7: (a) The grand averaged waveform (at Fz, FCz, Cz, CPz, and Pz electrodes), topography (time window: 300–600 ms), and similarity of topographies across participants of each condition for the filtered real signal. (b) The associated grand averaged time-frequency representation (TFR) of every condition obtained by the conventional TFA. The region of evoked ERO of each condition was determined by the edge detection algorithm and the conventional rectangle method separately (for the black dotted rectangle, the time window was set from 200 to 600 ms and frequency range was defined from 0.5 to 2 Hz, “R7”; the red solid rectangle: 300–600 ms and 0.5–2 Hz, “R8”) separately.

projected signals for N2-theta/P3-delta, obviously, they were all roughly equal to 1.00 (see Figures 5(b), 5(e), and 5(h)). Hence, we concluded that the proposed approach can efficiently and objectively extract the ERPs of interest from the mixed signals.

With regard to the results of TFA-PCA, 7 components were retained, which was explained 99% of variance. Then, the 2nd and 3rd components were, respectively, weighted with the original TFRs and the weighted results, respectively, corresponded to late and early theta oscillations. They were just classified as one part of the theta oscillation of TFRs for the mixed signal (Figure 4(c)) due to their time window and frequency range were similar with the original theta oscillation. This was demonstrated by the correlation coefficients (0.79/0.59 and 0.51/0.57) between the TFRs of the weighted early/late theta oscillations and the source N2/P3 separately (see Figures 5(j) and 5(k)).

### 3.2. Actual ERP Dataset Results

**3.2.1. Conventional Time-Frequency Analysis Results.** For N2-theta oscillation in Figure 6(b), the statistical results of the two regions determined by the conventional rectangle method demonstrated that no significant differences were found for either the main effect of feedback or interaction effect as shown in “R1” and “R2” of Table 1, whereas the main effect of waiting time reached significant level. The related region for LL condition was not recognized when we used the edge detection algorithm, and thus, the statistical analysis was not further processed.

As for the P3-delta oscillation in Figure 7(b), the statistical results of the determined regions obtained by the conventional rectangle method indicated that the main effect of feedback was significant but not for the waiting time. In addition, the interaction effect between waiting time and feedback

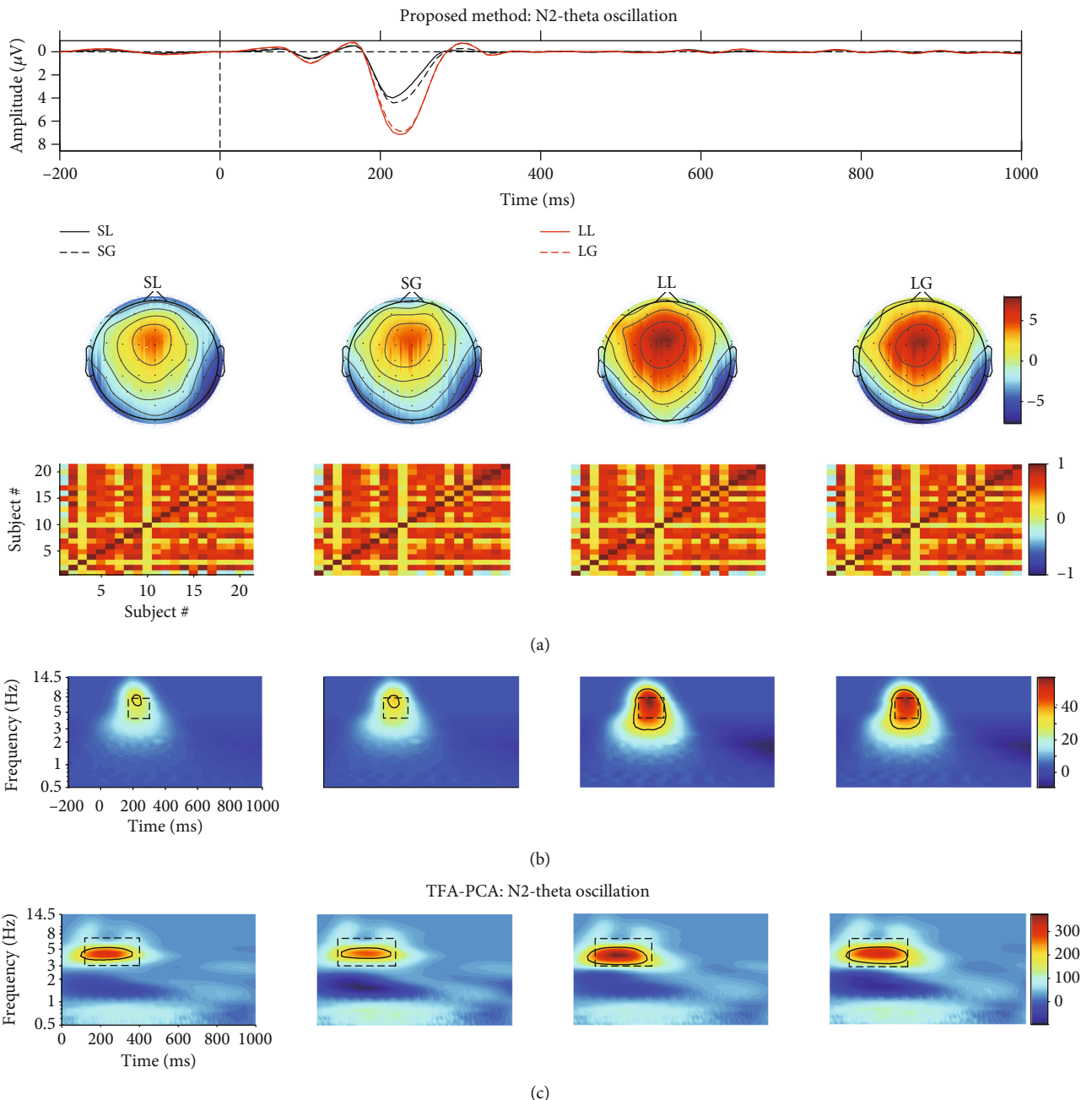


FIGURE 8: (a) The projected waveform (at Fz, FCz, and Cz electrodes), topography (180–240 ms), and similarity of topographies across participants of every condition for N2 which were extracted from the real mixed signal using t-PCA and Promax rotation. (b) The associated grand averaged time-frequency representation (TFR) of every condition for N2-theta oscillation using the proposed approach. The black dotted rectangle (the time window was defined as 150–300 ms, and the frequency range was set as 4–8 Hz, “R3”) for every condition was marked using the conventional rectangle method, and the other (“R4”) was gained by the edge detection algorithm. (c) The weighted N2-theta oscillation by TFA-PCA. The black dotted rectangle was 100–400 ms and 3–7 Hz (“R5”), and the other one (“R6”) was gained by edge detection algorithm.

was also insignificant (see Table 2, “R7” and “R8”). However, we did not find any significant main or interaction effects for the ANOVA results when using the edge detection algorithm (Table 2, “R9”).

**3.2.2. Proposed Approach Results.** Figures 8 and 9 depict the projected waveform at some typical electrodes, the topo-

graphic distribution in the time domain, associated similarity of topographies across all subjects, and TFR of every condition for N2-theta and P3-delta, respectively. 20 components were retained, and they accounted for 99% of the variance when applying t-PCA and Promax rotation.

The 9th and 18th components were finally selected for further analysis based on the properties of N2 in the temporal

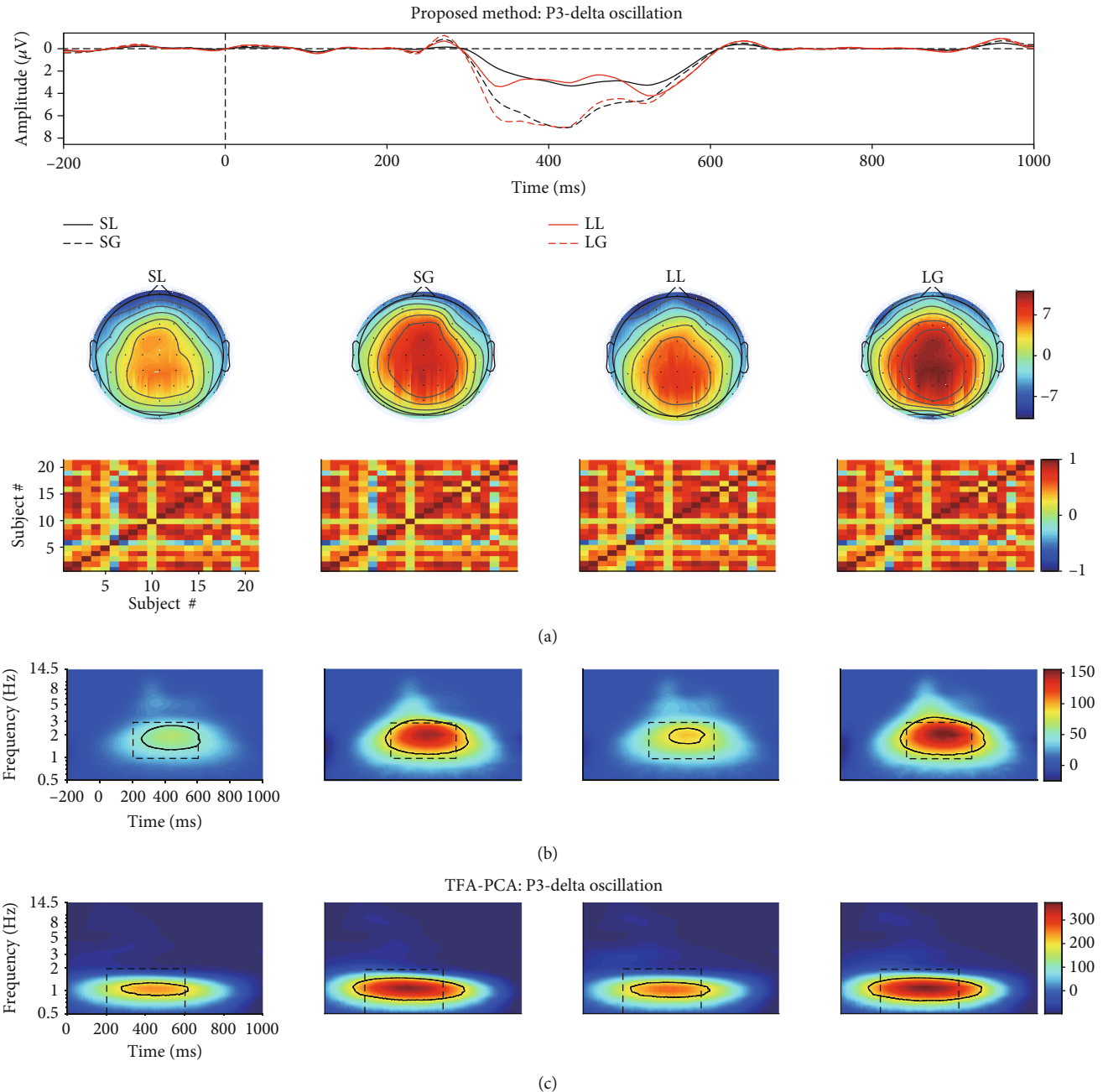


FIGURE 9: (a) The projected waveform (at Fz, FCz, Cz, CPz, and Pz electrodes), topography (300–600 ms), and similarity of topographies across participants of every condition for N2 which were extracted from the real mixed signal using proposed approach. (b) The associated grand averaged time-frequency representation (TFR) of every condition. The black dotted rectangle (the time window was 200–600 ms, and the frequency range was 1–3 Hz, “R10”) for every condition was marked using the conventional rectangle method, and the other (“R11”) was gained by the edge detection algorithm. (c) The weighted TFRs of P3-delta oscillation when using TFA-PCA. The black dotted rectangle was 200–600 ms and 0.5–2 Hz (“R12”), and the other one (“R13”) was gained by edge detection algorithm.

and spatial and the similarity of spatial components across all subjects (we used “spatial similarity” to represent it in the following parts), and they explained 0.91% (spatial similarity:  $0.44 \pm 0.30$ ) and 0.15% (spatial similarity:  $0.59 \pm 0.28$ ) of variance, respectively. The evolution and the tendency of the projected N2 waveform kept consistent with the conventional grand averaged waveform. For the recognized regions of the evoked theta for TFRs of the projected N2 by the edge

detection method (Table 1, “R4”), the related statistical results indicated that the main effect was insignificant for either waiting time ( $F_{(1,20)} = 3.122, p = 0.093$ , and  $\eta_p^2 = 0.135$ ) or feedback ( $F_{(1,20)} = 0.382, p = 0.543$ , and  $\eta_p^2 = 0.019$ ). Meanwhile, the interaction effect between waiting time and feedback was also not significant ( $F_{(1,20)} = 0.633, p = 0.436$ , and  $\eta_p^2 = 0.031$ ). These findings were consistent with the previous study

TABLE 1: The statistical results of N2-theta oscillation for the conventional time-frequency analysis (“M1”), the proposed approach (“M2”), and TFA-PCA (“M3”).

Method	ROI	WT			FB			WT * FB		
		F	$\eta_p^2$	p	F	$\eta_p^2$	p	F	$\eta_p^2$	p
M1	R1	6.067	0.233	0.023	0.72	0.035	0.406	0.206	0.01	0.655
	R2	4.853	0.195	0.039	0.042	0.002	0.84	0.038	0.002	0.848
M2	R3	8.492	0.298	0.009	0.052	0.003	0.821	0.569	0.028	0.46
	R4	3.122	0.135	0.093	0.382	0.019	0.543	0.633	0.031	0.436
M3	R5	3.255	0.14	0.086	0.084	0.004	0.775	0.006	<0.001	0.941
	R6	0.393	0.019	0.0538	0.411	0.02	0.529	0.015	0.001	0.903

R1: 100-300ms and 3-7 Hz; R2: 200-400 ms and 3-7 Hz; R3: 150-300 ms and 4-8 Hz; R4: EDM; R5: 100-400 ms and 3-7 Hz; R6: EDM. EDM: the edge detection method; WT: waiting time; FB: feedback; ROI: region of interest.

TABLE 2: The statistical results of P3-delta oscillation for the conventional time-frequency analysis (“M1”), the proposed approach (“M2”), and TFA-PCA (“M3”).

Method	ROI	WT			FB			WT * FB		
		F	$\eta_p^2$	p	F	$\eta_p^2$	p	F	$\eta_p^2$	p
M1	R7	0.997	0.048	0.33	13.236	0.398	0.002	0.25	0.012	0.622
	R8	1.027	0.049	0.323	12.653	0.387	0.002	0.167	0.008	0.688
M2	R9	0.064	0.003	0.802	2.634	0.116	0.12	0.004	<0.001	0.952
	R10	3.93	0.164	0.061	7.755	0.279	0.011	2.991	0.13	0.099
M3	R11	6.886	0.256	0.016	5.886	0.227	0.025	9.573	0.324	0.006
	R12	1.007	0.048	0.328	12.299	0.381	0.002	0.274	0.014	0.607
	R13	0.125	0.006	0.727	2.141	0.097	0.159	0.06	0.003	0.809

R7: 200-600ms and 0.5-2 Hz; R8: 300-600 ms and 0.5-2 Hz; R9: EMD; R10: 200-600 ms and 1-3 Hz; R11: EDM; R12: 200-600 ms and 0.5-2 Hz; R13: EDM. EDM: the edge detection method; WT: waiting time; FB: feedback; ROI: region of interest.

of the results for the time domain analysis [18]. Nevertheless, when the conventional rectangle method was performed to determine the region (“R3”: the time window is 150-300; the frequency range is 4-8 Hz) for TFR of each condition, we found a significant main effect of waiting time factor ( $F_{(1,20)} = 8.92$ ,  $p = 0.009$ , and  $\eta_p^2 = 0.298$ ), whereas the other main or interaction effect did not reach a significant level.

Similarly, with regard to P3, the 1st, 5th, 13th, 14th, 16th, and 17th components (they explained 52.7% (spatial similarity:  $0.66 \pm 0.20$ ), 3.82% (spatial similarity:  $0.46 \pm 0.33$ ), 0.31% (spatial similarity:  $0.58 \pm 0.25$ ), 0.27% (spatial similarity:  $0.66 \pm 0.20$ ), 0.19% (spatial similarity:  $0.70 \pm 0.17$ ), and 0.16% (spatial similarity:  $0.54 \pm 0.32$ ) of the variance, respectively) were selected and projected back to the electrode fields. We then computed the TFRs of the back-projection via wavelet transform. The results revealed that the long waiting time ( $96.583 \pm 21.773 \mu\text{V}^2/\text{Hz}$ ) elicited a larger power than short waiting time ( $76.251 \pm 18.461 \mu\text{V}^2/\text{Hz}$ ). A larger power was also observed upon gain condition ( $106.238 \pm 26.993 \mu\text{V}^2/\text{Hz}$ ) than lose condition ( $66.596 \pm 13.773 \mu\text{V}^2/\text{Hz}$ ), which was similar with the previous investigations [51–53]. The statistical results of the determined regions obtained by the edge detection algorithm (Table 2, “R11”) displayed that there was a significant interaction effect between waiting time and feedback ( $F_{(1,20)} = 9.573$ ,  $p = 0.006$ , and  $\eta_p^2 = 0.324$ ). However, this

significant interaction effect between them was not found in the previous study [18]. In addition, the main effects of both waiting time ( $F_{(1,20)} = 6.886$ ,  $p = 0.016$ , and  $\eta_p^2 = 0.256$ ) and feedback ( $F_{(1,20)} = 5.886$ ,  $p = 0.025$ , and  $\eta_p^2 = 0.227$ ) reached a significant level. Then, post hoc analysis was used for further investigation. The results demonstrated that a significant difference was found in the feedback factor under short waiting time condition ( $p = 0.007$ ). By contrast, there was an insignificant main effect of feedback under long waiting time condition ( $p = 0.172$ ). However, when the rectangle method was applied to determine the region (time window is from 200 to 600 ms, and the frequency range is 1-3 Hz), only the significant main effect was observed for feedback factor ( $F_{(1,20)} = 7.755$ ,  $p = 0.011$ , and  $\eta_p^2 = 0.279$ ).

**3.2.3. TFA-PCA Results.** Eight components were reserved when TFA-PCA was performed on the TFRs of the averaged ERP waveforms, which explained 99% of the total variances. The 1st (75.15%) and 4th (1.76%) were selected to weight with the original TFR, and the weighted TFRs were associated with delta and theta oscillation, respectively, as depicted in Figures 8(c) and 9(c). The statistical results of all determined delta/theta oscillation obtained by the conventional rectangle method and edge detection algorithm revealed that

either main or interaction effects did not reach a significant level (see the statistical results of "M3" in Tables 1 and 2).

#### 4. Conclusion and Discussion

We developed a novel approach to objectively explore evoked event-related oscillations (EROs) of interest mainly including three steps: (1) temporal principal component analysis (t-PCA) and Promax rotation were performed on the ERP waveform matrix to extract the temporal and spatial components of interest simultaneously and then the components of interest were projected to the electrode fields to correct their indeterminacies in the variance and the polarity. (2) The time-frequency representations (TFRs) of the back-projection waveforms were computed using the complex morlet continuous wavelet transform in the electrode fields. (3) The edge detection algorithm based on the Canny detector was applied on the TFRs to recognize the specific time and frequency positions of evoked EROs at some typical electrodes for the further statistical analysis.

As displayed in Figures 5(b), 5(e), and 5(f), all the correlation coefficients between the waveforms/topographies/TFRs of source and extracted N2/P3 for different noise-contaminated simulated datasets were roughly 1. However, the correlation coefficients between TFRs of weighted and source N2/P3 signals were easily influenced by noise using TFA-PCA (see Figures 5(j) and 5(k)). These mean that our proposed approach could efficiently extract evoked EROs of interest from a series of SNR signals but not for TFA-PCA approach. Hereafter, we use the results of one noise-polluted simulation data (i.e., 10 dB) to explain that the proposed approach outperformed t-PCA. Specifically, only one identifiable delta oscillation around 300–600 ms can be recognized from the TFR distribution for the mixed synthetic dataset by wavelet transform method as shown in the second row in Figures 3(b) and 4(b). In contrast, two oscillations were obtained by the proposed approach which corresponded to N2 and P3, respectively, as illustrated in Figures 3(b) and 4(b). Early and late theta oscillations were gained by TFA-PCA, but we categorized them as one part of the theta oscillation of the mixed signals. Likewise, the statistical results of the real dataset for the proposed approach were more satisfied with experimental purpose than TFA and TFA-PCA approaches as follows. P3-delta statistical results of the proposed approach revealed that the loss condition reflected smaller power than the gain did, which was similar to the results in the previous reports [51–54]. Besides, the interaction effect between the two factors was significant, which was consistent with the findings in the prior study [51]. However, when we applied the conventional TFA method to the signals, only the distinction between the two feedback conditions was found for delta oscillation. Meanwhile, we did not find any significant main or interaction effect when using the TFA-PCA approach.

The proposed approach is an efficient and objective method. Firstly, the results of three applied methods, which

were described in Tables 1 and 2, revealed that the statistical results achieved by the edge detection algorithm were more stable when compared with those of the conventional rectangle method [5–10, 55]. Secondly, the statistical results of P3-delta for the conventional TFA/TFA-PCA and the rectangle method did not reflect that the feedback was sensitive to the waiting time probably due to the following aspects. (a) The evoked P3-delta was overlapped with other EROs and artifacts to some degree in the temporal, spatial, and spectrum. (b) Information of each ERO for the projected signal cannot be completely included or some useless information was involved when using the rectangle method to determine the region of interest, such as the region was marked as shown in Figures 8(b) and 9(b). However, when using our approach, we found that the power values of feedback for the long and short waiting time were significantly different, which was consistent with the previous study [51].

Furthermore, Promax rotation is used to rearrange the initial principal components (PCs) such that PCs have a simple and more interpretable structure in the time domain. We expect that one PC can interpret one ERP but the generated PC will not have a simple relationship with ERP, for example, one PC might be a part of the P2 plus a part of N2 and plus a part of P3 and so forth. Several rotation approaches have been developed for this purpose, and the key difference between them is whether they are oblique or orthogonal, that is, whether the PCs are forced to be correlated or not. Varimax and Promax are the typical algorithms for orthogonal and oblique rotations, respectively, which the former forces the PCs to be uncorrelated while the latter allows the PCs to be related. The previous study revealed that Promax rotation can yield much better results than Varimax rotation both in real and simulated ERP datasets [31, 56–58], and Promax rotation can give the improved results for t-PCA [32, 56]. Therefore, we applied Promax rotation during t-PCA procedure to rotate the original extracted PCs in this study.

Moreover, the selection of the components in this study also depends on the similarity of the topographies of different subjects, and it is expected that different subjects' topographies are as homogeneous as possible. Regarding one component of the t-PCA plus Promax rotation, all subjects in one group have the same temporal course and variant spatial components (i.e., topographies here). This means that, for t-PCA and Promax rotation, given an estimated ERP component, the waveform is invariant for all subjects and its topography is variant across all subjects. However, it is strongly expected that the topographies across different subjects for an ERP can be as similar as possible since we expect a homogeneous ERP dataset for the repeatable and reliable data analysis. For the results of synthetic and real datasets, the similarities were improved for the projected components to some extent after the proposed method was used (especially for N2 of the extracted signal ( $0.72 \pm 0.09$ ) when compared with the mixed signal ( $0.64 \pm 0.11$ ) as illustrated in the last column the Figure 3(a)). This demonstrated that the homogeneity of the topographies of different subjects was better than before with the proposed approach.

Another technique can also be used to identify the region of evoked ERO of interest based on the subtle change for

their topographies as used in a previous study [59]. In order to identify the precise region (i.e., uniquely topographic was included in the identified region) for the ERO of interest, two main stages were involved as below [59]. First, TFRs were obtained from either averaged or sing-trial ERP signals. Second, all time-frequency points were divided into time-frequency features (i.e., regions) based on the correlation coefficients of topographies between the time-frequency points and templates using k-means cluster. Likewise, in this study, we used the following steps to gain the “pure” regions for evoked EROs of interest. The components of interest corresponded to the EROs of interest were first extracted from the averaged ERP dataset in the time domain using t-PCA and Promax rotation. Next, we calculated the TFRs of the extracted signals and identified the regions of evoked EROs of interest using the edge detection algorithm. Obviously, the former approach can be used to explore the EROs from both averaged and single-trial ERP datasets, but the proposed approach only extracts the ERO from the averaged ERP datasets. Furthermore, it should be noted that if the edge detection algorithm is directly used to recognize the regions of EROs from the TFRs of the original averaged ERP data, consequently, different spatially distinct oscillations may be involved in one region when those components are overlapped in time and frequency domains. By contrast, this situation will not happen for the results obtained by topographic segmentation analysis. That is, the spatial distributions of all points in the same region are highly similar to each other [59].

There are some potential drawbacks to the proposed approach. Firstly, only the time-locked and phase-locked information of the event-related responses can be explored due to we first performed our proposed approach on the averaged ERP datasets to extract components of interest and then calculated the related TFRs to find the time-frequency features. Secondly, the selection of the temporal and spatial components obtained by t-PCA and Promax rotation might be affected by the experimenters. Although we give a criterion that the extracted components are chosen for further analysis when the properties of components in the time and space domains are consistent with ERPs, the experimenters can still determine which component was involved in the next stage. Thirdly, we have to define a mother wavelet by a set of bandwidth and frequency centre (BWCF) before we used morlet wavelet transformation to transform the time-domain signals into time-frequency signals. According to our previous study [20], different sets of BWCF could lead to different time-frequency results; thus, the experimenters have to attempt the number of BWCF for TFA and then select an optimal one from them for the TFA of ERP signals.

Regarding the future investigations, it can be carried out from the following aspects. Firstly, we merely focused on the extraction of evoked oscillations from the averaged ERP as mentioned above in this study. It should be noted that some important information like induced oscillation was cancelled out by the averaging procedure over trials in the time domain [60, 61]. In addition, the induced oscillatory response was probably generated by nonlinear and possibly autonomous mechanisms, and it would belong to high-

order processes. Whereas evoked oscillation was related to stimulus-locked time [17]. In past decades, the induced oscillation had been widely used to investigate the neural mechanisms of attention modulation [62], the functions of the alcohol use disorder patients [63], and so on. Our proposed approach used for the single-trial level analysis will be helpful to explore the mechanisms of the induced oscillation in the mentioned fields. Secondly, regarding the selection of components of interest from the extracted ones obtained by t-PCA and Promax rotation, one strategy can be used based on the absolute of the correlation coefficients between any two extracted spatial components and the peak time points for the extracted component. For example, there are two extracted components, their spatial correlation coefficient is 0.9 and the peak time points are 190 ms and 220 ms. As a result, they are considered as one thing and are projected together onto electrode fields for further analysis. Thirdly, some TFA techniques with free parameter settings, like the combination of Wigner-Ville distribution and Gabor transform with the matching pursuit decomposition, can provide an appropriate time-frequency resolution in all frequencies [64], which can also be applied to the ERO analysis as the alternatives to the proposed approach in our study.

## Appendix

### A. The Explanation of Temporal PCA and Promax Rotation from the View of Blind Source Separation

When applying temporal PCA and Promax rotation [65] to decompose an ERP dataset  $\mathbf{Z}^T \in \mathcal{R}^{N \times M}$  ( $N$  and  $M$ , respectively, represent the number of sensors of all subjects under all conditions and the number of time points within one epoch), the related procedures can be interpreted via the linear model as below [34, 35].

$$\mathbf{Z} = \mathbf{HS}_1 + \mathbf{E} = \mathbf{H}(\mathbf{S}_1 + \mathbf{S}_2) = \mathbf{HS}, \quad (4)$$

where  $\mathbf{H}$  is the mixing matrix with full rank;  $\mathbf{S} = \mathbf{S}_1 + \mathbf{S}_2$  ( $\mathbf{S} \in \mathcal{R}^{R \times N}$ ),  $\mathbf{E} = \mathbf{HS}_2$ , and they are the unknown correlated source signals and the sensor noise, respectively.

As described in [34], the assumption of the model in Eq. (4) is overdetermined and it means that the number of the observed signals  $M$  is larger than that of the source signals  $R$ . Once the estimation of the number of the sources is done (the determination can be based on the model order selection algorithms, and here, it is the cumulative explained variance as mentioned in Section 2.2.1 in this study), the overdetermined model can be changed to the determined one as follows

$$\mathbf{X} = \mathbf{V}^T \mathbf{Z} = \mathbf{V}^T \mathbf{HS} = \mathbf{AS}, \quad (5)$$

where  $\mathbf{X} \in \mathcal{R}^{R \times N}$ ;  $\mathbf{V}^T \in \mathcal{R}^{R \times M}$  represents the dimension reduction matrix generated from performing PCA on  $\mathbf{Z}^T$ ,  $\mathbf{A} \in \mathcal{R}^{(R \times R)}$  is also named the mixing matrix.

Aiming to separate the mixture in Eq. (5), the blind source separation algorithm can be applied [33]. Here, Promax rotation [65] is used to obtain an unmixing matrix  $\mathbf{W}$  in this study. The algorithm of Promax rotation is described in *Appendix B* and the inverse matrix  $\mathbf{B} = \mathbf{W}^{-1}$  represents the estimation of  $\mathbf{A}$  [34].

And then we use this unmixing matrix  $\mathbf{W}$  to turn the mixture in Eq. (5) into a matrix of estimated components as below [34].

$$\mathbf{Y} = \mathbf{WX} = \mathbf{WAS} = \mathbf{CS}. \quad (6)$$

In the above formulation,  $\mathbf{Y}$  is the estimation of  $\mathbf{S}$  and its each row can be assembled to the topographic map of each source;  $\mathbf{C} = \mathbf{WA}$  is the global matrix.

Under this determined model condition in Eq. (5), aiming to solve the issue that different components, which are derived from the matrix  $\mathbf{X}$ , cannot be statistically further analysed together because their polarities and amplitudes are indeterminates [33], and we project the component(s) of interest back to the electrode fields in this study which is always used in many other blind source separation for EEG, for example, independent component analysis procedures [34–37]. The back-projection can be illustrated as [34–36].

$$\mathbf{Q}_r = \mathbf{b}_r \circ \mathbf{y}_r, \quad (7)$$

here,  $\mathbf{Q}_r \in \mathcal{R}^{R \times N}$  is the projection of  $r^{\text{th}}$  component at all virtue time points in this study;  $\mathbf{b}_r$  is the  $r^{\text{th}}$  column of the inverse matrix  $\mathbf{B}$ , and  $\mathbf{y}_r$  is the  $r^{\text{th}}$  row of the estimated matrix  $\mathbf{Y}$ ; “ $\circ$ ” denotes the outer product of vectors.

Under the global optimization, there exists only one non-zero element in each row and each column of  $\mathbf{C}$ . In other words, the  $r^{\text{th}}$  extracted component is unknown scaled version of the  $j^{\text{th}}$  source signal. Hence, the projection in Eq. (7) can be described as [34, 35].

$$\mathbf{Q}_r = \mathbf{b}_r \circ \mathbf{y}_r = \mathbf{a}_j \circ \mathbf{s}_j, \quad (8)$$

where  $\mathbf{a}_j$  is the  $j^{\text{th}}$  column of the mixing matrix  $\mathbf{A}$ , and  $\mathbf{s}_j$  is the  $j^{\text{th}}$  row of the source matrix  $\mathbf{S}$  in Eq. (5).

To the original overdetermined model in Eq. (4), the  $r^{\text{th}}$  component derived from the matrix  $\mathbf{Z}$  can be projected to the all electrodes as below

$$\begin{aligned} \underline{\mathbf{Z}}_r &= \mathbf{u}_r \circ \mathbf{y}_r, \\ \mathbf{U} &= \mathbf{VB}, \end{aligned} \quad (9)$$

where  $\mathbf{u}_r$  is the  $r^{\text{th}}$  column of  $\mathbf{U}$  and denotes the time course or waveform of multisubject of multicondition. We use combination of the inverse matrix  $\mathbf{B}$  and the dimension reduction matrix  $\mathbf{V}$  to represent  $\mathbf{U}$ , which is achieved to estimate the mixing matrix  $\mathbf{H}$  in Eq. (4) [34]. This has been illustrated by Figures 3 and 4.

In most cases, several components need to be projected back to electrodes simultaneously [35, 66]; hence, the

related projection of several components can be implemented as follows

$$\begin{aligned} \underline{\mathbf{Z}} &= \left[ \mathbf{u}_{k_1}, \dots, \mathbf{u}_{k_r} \right] \left[ \mathbf{y}_{k_1}, \dots, \mathbf{y}_{k_r} \right] \\ &= \mathbf{u}_{k_1} \circ \mathbf{y}_{k_1} + \dots + \mathbf{u}_{k_r} \circ \mathbf{y}_{k_r}, \end{aligned} \quad (10)$$

where  $k_1, \dots, k_r (1 \leq k_r < R)$  are the number of selected components; “ $\circ$ ” denotes the outer product of vectors. The size of each dimension of the matrix  $\underline{\mathbf{Z}}$  is the same with that of  $\mathbf{Z}$ . This has been illustrated by Figures 3, 4, 8, and 9.

## B. Oblique Procrustes Transformation

Mathematically, Procrustes equation can be defined as [65, 67].

$$\mathbf{P} = \mathbf{VW} + \underline{\mathbf{E}}, \quad (11)$$

where  $\mathbf{P}$  is called as the pattern matrix;  $\mathbf{W}$  is the transformation matrix;  $\underline{\mathbf{E}}$  is the residual matrix. The satisfactory result is that we can find a transformation matrix to make the value of  $\underline{\mathbf{E}}^T \underline{\mathbf{E}}$  as close zero as possible.

Specifically, the pattern matrix  $\mathbf{P}$  is first generated from the matrix of unrotated factor loadings  $\mathbf{V}$  by the target Procrustes transformation, and the determination of  $\mathbf{V}$  is based on PCA here, and it is used in the Eq. (5).

$$p(i, j) = \frac{|v(i, j)^{k+1}|}{|v(i, j)|}, \quad (12)$$

where  $k > 1$ . The matrix  $\mathbf{P}$  stands for the matrix  $\mathbf{V}$  raised to the  $k^{\text{th}}$  power, and its original sign is unchanged.

Next, the least squares method is performed to calculate the fit of the orthogonal matrix  $\mathbf{V}$  of the factor loadings to the pattern matrix so that  $\underline{\mathbf{E}}^T \underline{\mathbf{E}}$  is a minimum.

$$\mathbf{W} = (\mathbf{V}^T \mathbf{V})^{-1} \mathbf{V}^T \mathbf{P}, \quad (13)$$

where  $\mathbf{W}$  is called the transformation matrix in Promax rotation [67];  $\mathbf{V}^T$  is the transpose matrix of the orthogonal rotated matrix  $\mathbf{V}$ ;  $(\cdot)^{-1}$  is the inverse of a matrix.

## Data Availability

The datasets used for supporting the findings in this study are available from the corresponding author on reasonable request.

## Disclosure

The draft version of the manuscript has been submitted as a preprint according to the following link: <https://www.biorxiv.org/content/10.1101/2020.05.17.100511v1>.

## Conflicts of Interest

All authors declare no conflicts of interest.

## Authors' Contributions

GZ performed the experiments and wrote the article; XL wrote the article; FC proposed the idea, supervised the study, and wrote the article.

## Acknowledgments

This work was supported by the National Natural Science Foundation of China (Grant No. 91748105), the National Foundation in China (No. JCKY2019110B009 & 2020-JCJQ-JJ-252), the Fundamental Research Funds for the Central Universities (DUT2019, DUT20LAB303) in Dalian University of Technology in China, and the scholarships from China Scholarship Council (No. 201806060165). This study is to memorize Prof. Tapani Ristaniemi for his great help to the three authors, and Prof. Tapani Ristaniemi has supervised this study very much. The authors also would like to thank Professor Peng Li who works at Shenzhen University for sharing their ERP datasets with us and helping us in ERP study.

## References

- [1] E. Başar, M. Schürmann, T. Demiralp, C. Başar-Eroğlu, and A. Ademoglu, “Event-related oscillations are ‘real brain responses’—wavelet analysis and new strategies,” *International Journal of Psychophysiology*, vol. 39, no. 2-3, pp. 91–127, 2001.
- [2] E. Başar, “A review of gamma oscillations in healthy subjects and in cognitive impairment,” *International Journal of Psychophysiology*, vol. 90, no. 2, pp. 99–117, 2013.
- [3] E. Başar, B. T. Gölbasi, E. Tülay, S. Aydin, and C. Başar-Eroğlu, “Best method for analysis of brain oscillations in healthy subjects and neuropsychiatric diseases,” *International Journal of Psychophysiology*, vol. 103, pp. 22–42, 2016.
- [4] B. Güntekin and E. Başar, “Review of evoked and event-related delta responses in the human brain,” *International Journal of Psychophysiology*, vol. 103, pp. 43–52, 2016.
- [5] M. Ergen, S. Saban, E. Kirmizi-Alsan, A. Uslu, Y. Keskin-Ergen, and T. Demiralp, “Time-frequency analysis of the event-related potentials associated with the Stroop test,” *International Journal of Psychophysiology*, vol. 94, no. 3, pp. 463–472, 2014.
- [6] S. Her, K. S. Cha, J. W. Choi et al., “Impaired visuospatial attention revealed by theta- and beta-band cortical activities in idiopathic REM sleep behavior disorder patients,” *Clinical Neurophysiology*, vol. 130, no. 10, pp. 1962–1970, 2019.
- [7] K. A. Jones, B. Porjesz, D. Chorlian et al., “S-transform time-frequency analysis of P300 reveals deficits in individuals diagnosed with alcoholism,” *Clinical Neurophysiology*, vol. 117, no. 10, pp. 2128–2143, 2006.
- [8] N. Lally, P. G. Mullins, M. V. Roberts, D. Price, T. Gruber, and C. Haenschel, “Glutamatergic correlates of gamma-band oscillatory activity during cognition: a concurrent ER-MRS and EEG study,” *NeuroImage*, vol. 85, pp. 823–833, 2014.
- [9] A. Sandre and A. Weinberg, “Neither wrong nor right: theta and delta power increase during performance monitoring under conditions of uncertainty,” *International Journal of Psychophysiology*, vol. 146, pp. 225–239, 2019.
- [10] Z. Zhang, G. Guo, J. Zhang et al., “Do theta oscillations explain the somatosensory change detection mechanism?,” *Biological Psychology*, vol. 143, pp. 103–112, 2019.
- [11] E. Erdogdu, E. Kurt, A. D. Duru, A. Uslu, C. Başar-Eroğlu, and T. Demiralp, “Measurement of cognitive dynamics during video watching through event-related potentials (ERPs) and oscillations (EROs),” *Cognitive Neurodynamics*, vol. 13, no. 6, pp. 503–512, 2019.
- [12] R. J. Barry, “Evoked activity and EEG phase resetting in the genesis of auditory Go/NoGo ERPs,” *Biological Psychology*, vol. 80, no. 3, pp. 292–299, 2009.
- [13] E. M. Bernat, W. J. Williams, and W. J. Gehring, “Decomposing ERP time-frequency energy using PCA,” *Clinical Neurophysiology*, vol. 116, no. 6, pp. 1314–1334, 2005.
- [14] E. M. Bernat, S. M. Malone, W. J. Williams, C. J. Patrick, and W. G. Iacono, “Decomposing delta, theta, and alpha time-frequency ERP activity from a visual oddball task using PCA,” *International Journal of Psychophysiology*, vol. 64, no. 1, pp. 62–74, 2007.
- [15] J. Harper, S. M. Malone, and E. M. Bernat, “Theta and delta band activity explain N2 and P3 ERP component activity in a go/no-go task,” *Clinical Neurophysiology*, vol. 125, no. 1, pp. 124–132, 2014.
- [16] J. Dien, “The ERP PCA toolkit: an open source program for advanced statistical analysis of event-related potential data,” *Journal of Neuroscience Methods*, vol. 187, no. 1, pp. 138–145, 2010.
- [17] O. David, J. M. Kilner, and K. J. Friston, “Mechanisms of evoked and induced responses in MEG/EEG,” *NeuroImage*, vol. 31, no. 4, pp. 1580–1591, 2006.
- [18] J. Wang, J. Chen, Y. Lei, and P. Li, “P300, not feedback error-related negativity, manifests the waiting cost of receiving reward information,” *Neuroreport*, vol. 25, no. 13, pp. 1044–1048, 2014.
- [19] F. Cong, T. Ristaniemi, and H. Lyytinen, “Wavelet filter design based on frequency responses for filtering ERP data with duration of one epoch,” in *Advanced Signal Processing on Brain Event-Related Potentials*, 2015World Scientific.
- [20] G. Zhang, C. Zhang, S. Cao et al., “Multi-domain features of the non-phase-locked component of interest extracted from ERP data by tensor decomposition,” *Brain Topography*, vol. 33, no. 1, pp. 37–47, 2020.
- [21] S. M. Benvenuti, G. Buodo, and D. Palomba, “Appetitive and aversive motivation in dysphoria: a time-domain and time-frequency study of response inhibition,” *Biological Psychology*, vol. 125, pp. 12–27, 2017.
- [22] L. Hu, P. Xiao, Z. G. Zhang, A. Mouraux, and G. D. Iannetti, “Single-trial time-frequency analysis of electrocortical signals: baseline correction and beyond,” *NeuroImage*, vol. 84, pp. 876–887, 2014.
- [23] W. Peng, Z. Y. Tang, F. R. Zhang et al., “Neurobiological mechanisms of TENS-induced analgesia,” *NeuroImage*, vol. 195, pp. 396–408, 2019.
- [24] L. Hu, Z. G. Zhang, A. Mouraux, and G. D. Iannetti, “Multiple linear regression to estimate time-frequency electrophysiological responses in single trials,” *NeuroImage*, vol. 111, pp. 442–453, 2015.
- [25] R. J. Barry et al., “Components in the P300,” *Don't forget the Novelty P3!* *Psychophysiology*, Wiley Online Library. e13371, 2019.

- [26] J. F. Cavanagh, P. Kumar, A. A. Mueller, S. P. Richardson, and A. Mueen, "Diminished EEG habituation to novel events effectively classifies Parkinson's patients," *Clinical Neurophysiology*, vol. 129, no. 2, pp. 409–418, 2018.
- [27] J. Dien, "Applying principal components analysis to event-related potentials: a tutorial," *Developmental Neuropsychology*, vol. 37, no. 6, pp. 497–517, 2012.
- [28] J. S. Fogarty, R. J. Barry, and G. Z. Steiner, "Sequential processing in the classic oddball task: ERP components, probability, and behavior," *Psychophysiology*, vol. 56, no. 3, p. e13300, 2019.
- [29] F. Artoni, A. Delorme, and S. Makeig, "Applying dimension reduction to EEG data by principal component analysis reduces the quality of its subsequent independent component decomposition," *NeuroImage*, vol. 175, pp. 176–187, 2018.
- [30] R. J. Huster and L. Raud, "A tutorial review on multi-subject decomposition of EEG," *Brain Topography*, vol. 31, no. 1, pp. 3–16, 2018.
- [31] J. Dien, D. J. Beal, and P. Berg, "Optimizing principal components analysis of event-related potentials: matrix type, factor loading weighting, extraction, and rotations," *Clinical Neurophysiology*, vol. 116, no. 8, pp. 1808–1825, 2005.
- [32] J. Dien, W. Khoe, and G. R. Mangun, "Evaluation of PCA and ICA of simulated ERPs: Promax vs. Infomax rotations," *Human Brain Mapping*, vol. 28, no. 8, pp. 742–763, 2007.
- [33] P. Comon and C. Jutten, "Handbook of Blind Source Separation," in *Independent component analysis and applications*, Academic press, 2010.
- [34] F. Cong, I. Kalyakin, Z. Chang, and T. Ristaniemi, "Analysis on subtracting projection of extracted independent components from EEG recordings," *Biomedizinische Technik/Biomedical Engineering*, vol. 56, no. 4, pp. 223–234, 2011.
- [35] F. Cong, I. Kalyakin, and T. Ristaniemi, "Can back-projection fully resolve polarity indeterminacy of independent component analysis in study of event-related potential?," *Biomedical Signal Processing and Control*, vol. 6, no. 4, pp. 422–426, 2011.
- [36] S. Makeig, T. P. Jung, A. J. Bell, D. Ghahremani, and T. J. Sejnowski, "Blind separation of auditory event-related brain responses into independent components," *Proceedings of the National Academy of Sciences*, vol. 94, no. 20, pp. 10979–10984, 1997.
- [37] S. Makeig, M. Westerfield, T. P. Jung et al., "Functionally independent components of the late positive event-related potential during visual spatial attention," *Journal of Neuroscience*, vol. 19, no. 7, pp. 2665–2680, 1999.
- [38] O. Bertrand and C. Tallon-Baudry, "Oscillatory gamma activity in humans: a possible role for object representation," *International Journal of Psychophysiology*, vol. 38, no. 3, pp. 211–223, 2000.
- [39] C. S. Herrmann, M. Grigutsch, and N. A. Busch, "11 EEG oscillations and wavelet analysis," *Event-related potentials: A methods handbook*, p. 229, 2005.
- [40] C. S. Herrmann, S. Rach, J. Vosskuhl, and D. Strüber, "Time-frequency analysis of event-related potentials: a brief tutorial," *Brain Topography*, vol. 27, no. 4, pp. 438–450, 2014.
- [41] S. J. Kiebel, C. Tallon-Baudry, and K. J. Friston, "Parametric analysis of oscillatory activity as measured with EEG/MEG," *Human Brain Mapping*, vol. 26, no. 3, pp. 170–177, 2005.
- [42] C. Tallon-Baudry, O. Bertrand, C. Delpuech, and J. Pernier, "Stimulus specificity of phase-locked and non-phase-locked 40 Hz visual responses in human," *Journal of Neuroscience*, vol. 16, no. 13, pp. 4240–4249, 1996.
- [43] S. Glim, Y. O. Okazaki, Y. Nakagawa, Y. Mizuno, T. Hanakawa, and K. Kitajo, "Phase-amplitude coupling of neural oscillations can be effectively probed with concurrent TMS-EEG," *Neural Plasticity*, vol. 2019, Article ID 6263907, 13 pages, 2019.
- [44] A. Ahnaou, R. Biermans, and W. H. I. M. Dringenburg, "Cholinergic mechanisms of target oddball stimuli detection: the late "P300-like" event-related potential in rats," *Neural Plasticity*, vol. 2018, Article ID 4270263, 15 pages, 2018.
- [45] E. Mas-Herrero, P. Ripollés, A. HajiHosseini, A. Rodríguez-Fornells, and J. Marco-Pallarés, "Beta oscillations and reward processing: coupling oscillatory activity and hemodynamic responses," *NeuroImage*, vol. 119, pp. 13–19, 2015.
- [46] J. Canny, "A computational approach to edge detection," *IEEE Transactions on Pattern Analysis and Machine Intelligence*, vol. 6, pp. 679–698, 1986.
- [47] C. Hory, N. Martin, and A. Chehikian, "Spectrogram segmentation by means of statistical features for non-stationary signal interpretation," *IEEE Transactions on Signal Processing*, vol. 50, no. 12, pp. 2915–2925, 2002.
- [48] Ž. Milanović, N. Saulig, and I. Marasović, "Signal feature recognition in time-frequency domain using edge detection algorithms," in *2019 4th International Conference on Smart and Sustainable Technologies (SpliTech)*, Split, Croatia, 2019 IEEE.
- [49] N. Saulig, Ž. Milanović, and C. Ioana, "A local entropy-based algorithm for information content extraction from time-frequency distributions of noisy signals," *Digital Signal Processing*, vol. 70, pp. 155–165, 2017.
- [50] Q. Xu, S. Varadarajan, C. Chakrabarti, and L. J. Karam, "A distributed canny edge detector: algorithm and FPGA implementation," *IEEE Transactions on Image Processing*, vol. 23, no. 7, pp. 2944–2960, 2014.
- [51] G. Höltje and A. Mecklinger, "Feedback timing modulates interactions between feedback processing and memory encoding: evidence from event-related potentials," *Cognitive, Affective, & Behavioral Neuroscience*, vol. 20, no. 2, pp. 250–264, 2020.
- [52] M. Paul, C. Bellebaum, M. Ghio, B. Suchan, and O. T. Wolf, "Stress effects on learning and feedback-related neural activity depend on feedback delay," *Psychophysiology*, vol. 57, no. 2, p. e13471, 2020.
- [53] X. Zhang, Y. Lei, H. Yin, P. Li, and H. Li, "Slow is also fast: feedback delay affects anxiety and outcome evaluation," *Frontiers in Human Neuroscience*, vol. 12, p. 20, 2018.
- [54] Y. Wu and X. Zhou, "The P300 and reward valence, magnitude, and expectancy in outcome evaluation," *Brain Research*, vol. 1286, pp. 114–122, 2009.
- [55] T. Aktürk, Ü. İsoğlu-Alkaç, L. Hanoğlu, and B. Güntekin, "Age related differences in the recognition of facial expression: evidence from EEG event-related brain oscillations," *International Journal of Psychophysiology*, vol. 147, pp. 244–256, 2020.
- [56] J. Dien, "Evaluating two-step PCA of ERP data with geomim, infomax, oblimin, promax, and varimax rotations," *Psychophysiology*, vol. 47, no. 1, pp. 170–183, 2010.
- [57] J. Dien, "Addressing misallocation of variance in principal components analysis of event-related potentials," *Brain Topography*, vol. 11, no. 1, pp. 43–55, 1998.
- [58] J. Dien, K. M. Spencer, and E. Donchin, "Localization of the event-related potential novelty response as defined by

- principal components analysis,” *Cognitive Brain Research*, vol. 17, no. 3, pp. 637–650, 2003.
- [59] H. Jia, W. Peng, and L. Hu, “A novel approach to identify time-frequency oscillatory features in electrocortical signals,” *Journal of Neuroscience Methods*, vol. 253, pp. 18–27, 2015.
- [60] C. Tallon-Baudry and O. Bertrand, “Oscillatory gamma activity in humans and its role in object representation,” *Trends in Cognitive Sciences*, vol. 3, no. 4, pp. 151–162, 1999.
- [61] G. Pfurtscheller and F. H. Lopes da Silva, “Event-related EEG/MEG synchronization and desynchronization: basic principles,” *Clinical Neurophysiology*, vol. 110, no. 11, pp. 1842–1857, 1999.
- [62] C. S. Herrmann and R. T. Knight, “Mechanisms of human attention: event-related potentials and oscillations,” *Neuroscience & Biobehavioral Reviews*, vol. 25, no. 6, pp. 465–476, 2001.
- [63] W. Mumtaz, P. L. Vuong, A. S. Malik, and R. B. A. Rashid, “A review on EEG-based methods for screening and diagnosing alcohol use disorder,” *Cognitive Neurodynamics*, vol. 12, no. 2, pp. 141–156, 2018.
- [64] M. Wacker and H. Witte, “Time-frequency techniques in biomedical signal analysis,” *Methods of Information in Medicine*, vol. 52, no. 4, pp. 279–296, 2013.
- [65] A. E. Hendrickson and P. O. White, “Promax: a quick method for rotation to oblique simple structure,” *British Journal of Statistical Psychology*, vol. 17, no. 1, pp. 65–70, 1964.
- [66] A. Delorme and S. Makeig, “EEGLAB: an open source toolbox for analysis of single-trial EEG dynamics including independent component analysis,” *Journal of Neuroscience Methods*, vol. 134, no. 1, pp. 9–21, 2004.
- [67] M. B. Richman, “Rotation of principal components,” *Journal of Climatology*, vol. 6, no. 3, pp. 293–335, 1986.

# **PIV**

## **MULTI-DOMAIN FEATURES OF THE NON-PHASE-LOCKED COMPONENT OF INTEREST EXTRACTED FROM ERP DATA BY TENSOR DECOMPOSITION**

by

Guanghui Zhang, Chi Zhang, Shuo Cao, Xue Xia, Xin Tan, Lichengxi Si, Chenxin Wang, Xiaochun Wang, Chenglin Zhou, Tapani Ristaniemi, and Fengyu Cong  
2020

Brain Topography 33, 37–47, <https://doi.org/10.1007/s10548-019-00750-8>

Reproduced with kind permission of Springer Nature.





# Multi-domain Features of the Non-phase-locked Component of Interest Extracted from ERP Data by Tensor Decomposition

Guanghui Zhang<sup>1,2</sup> · Chi Zhang<sup>1</sup> · Shuo Cao<sup>3</sup> · Xue Xia<sup>4</sup> · Xin Tan<sup>1</sup> · Lichengxi Si<sup>1</sup> · Chenxin Wang<sup>1</sup> ·  
Xiaochun Wang<sup>4</sup> · Chenglin Zhou<sup>4</sup> · Tapani Ristaniemi<sup>2</sup> · Fengyu Cong<sup>1,2</sup>

Received: 22 June 2019 / Accepted: 10 December 2019 / Published online: 26 December 2019  
© The Author(s) 2019

## Abstract

The waveform in the time domain, spectrum in the frequency domain, and topography in the space domain of component(s) of interest are the fundamental indices in neuroscience research. Despite the application of time–frequency analysis (TFA) to extract the temporal and spectral characteristics of non-phase-locked component (NPLC) of interest simultaneously, the statistical results are not always expectedly satisfying, in that the spatial information is not considered. Complex Morlet wavelet transform is widely applied to TFA of event-related-potential (ERP) data, and mother wavelet (which should be firstly defined by center frequency and bandwidth (CFBW) before using the method to TFA of ERP data) influences the time–frequency results. In this study, an optimal set of CFBW was firstly selected from the number sets of CFBW, to further analyze for TFA of the ERP data in a cognitive experiment paradigm of emotion (Anger and Neutral) and task (Go and Nogo). Then tensor decomposition algorithm was introduced to investigate the NPLC of interest from the fourth-order tensor. Compared with the TFA results which only revealed a significant difference between Go and Nogo task condition, the tensor-based analysis showed significant interaction effect between emotion and task. Moreover, significant differences were found in both emotion and task conditions through tensor decomposition. In addition, the statistical results of TFA would be affected by the selected region of interest (ROI), whereas those of the proposed method were not subject to ROI. Hence, this study demonstrated that tensor decomposition method was effective in extracting NPLC, by considering spatial information simultaneously as the potential to explore the brain mechanisms related to experimental design.

**Keywords** ERP · Mother wavelet · Tensor decomposition · Time–frequency analysis · Non-phase locked

---

Handling Editor: Dezhong Yao.

✉ Fengyu Cong  
cong@dlut.edu.cn

Guanghui Zhang  
zhang.guanghui@foxmail.com

Chi Zhang  
chizhang@dlut.edu.cn

Shuo Cao  
caoshuo@dlut.edu.cn

Xue Xia  
Ssummer0909@hotmail.com

Xin Tan  
ggodsb@gmail.com

Lichengxi Si  
dgslcx@mail.dlut.edu.cn

Chenxin Wang  
QingJing1s@mail.dlut.edu.cn

Xiaochun Wang  
wangxiaochun@sus.edu.cn

Chenglin Zhou  
chenglin\_600@126.com

Tapani Ristaniemi  
tapani.ristaniemi@jyu.fi

<sup>1</sup> School of Biomedical Engineering, Faculty of Electronic Information and Electrical Engineering, Dalian University of Technology, Dalian 116024, China

<sup>2</sup> Faculty of Information Technology, University of Jyväskylä, 40100 Jyväskylä, Finland

<sup>3</sup> School of Foreign Languages, Dalian University of Technology, Dalian 116024, China

<sup>4</sup> School of Psychology, Shanghai University of Sport, Shanghai 200438, China

## Introduction

Electroencephalogram (EEG) has been extensively used in neuroscience since Berger Hans first recorded it from the human cerebral cortex in 1929 (Berger 1929). In early studies, most researchers mainly focused on the amplitude of an individual waveform in the time domain. With the introduction of computers, besides waveform, spectral and spatial characteristics of the component(s) of interest (COI) for group-averaged EEG/event-related-potential (ERP) data are analyzed (Luck 2014). They found that ERP components could be evoked from the related experiments, and have specific temporal, spectral and spatial characteristics. For instance, when words and other meaningful (or potentially meaningful) excitations include visual and auditory words, sign language signs, pictures, faces, environmental sounds, and smells are used for experimental stimuli, N400, a negative waveform which reaches a peak around 400 ms after stimulus onset and can extend the time window from 250 to 500 ms, can be discovered (Kutas and Federmeier 2000, 2011; Kutas and Hillyard 1980). Meanwhile, it is typically maximal over centro-parietal electrode sites. Therefore, all the temporal, spectral and spatial properties of ERP component(s) are useful for the investigation of brain mechanisms in cognitive processes and these properties may be coupled. Several techniques have been developed for ERP data processing and analyze to dig out the potential information in the cognitive processes, such as time domain analysis and time–frequency analysis (TFA).

Most previous studies focus on time domain analysis. The conventional method averages several single-trial data of the same stimulus in the time domain to obtain ERP components. The advantage of this method is that the energy of ERP is enhanced, with the amplitude of spontaneous EEG and noise extremely reduced (Cohen 2014). Some advanced signal processing and analyze methods also have been developed to extract COI from group-averaged ERP data such as Independent Component Analysis (ICA) (Hyvärinen 2013; Jung et al. 2000) and Principal Component Analysis (PCA) (Dien 2010a, b, 2012; Dien et al. 2005; Möcks and Verleger 1985; Kawaguchi et al. 2013). However, the main drawback of the time domain analysis is that it cannot reveal COI changes in the frequency domain over time so that the pivotal rhythm (or oscillation) information is neglected.

To extract the temporal and spectral characteristics of ERP component(s) simultaneously, some researchers use short-time Fourier transform (STFT) or wavelet transform algorithm (WTA) to convert time domain signals into time–frequency domain signals. There are two strategies for TFA of ERP data. One is evoked method in which multi-trial data are averaged before the computation of

the time–frequency transforms of averaged ERP data. The event-related oscillations (EROs) obtained by this type of TFA are extremely phase-locked to stimulus onset because of the simultaneous co-occurrence of enhanced EROs. The time locked and phase locked component (TLPLC) can be obtained and it is called evoked brain activity. The other one is based on averaging the time–frequency transforms of every single-trial. Both TLPLC and non-phase-locked component (NPLC) are summed up so that it refers to all-brain activities. And this strategy is considered as the induced method (Herrmann et al. 2004, 2014; Tallon-Baudry and Bertrand 1999). The induced method has two superiorities over time domain analysis or evoked method. The first one is that it can simultaneously exploit the temporal and spectral properties of an ERP component and reveal additional NPLC activity. For the other one, the results are non-negative, which means that it can avoid the amplitude of COI being cancelled out in the averaged ERP data, if they are randomly distributed for each single-trial in the time domain (Cong et al. 2015b). The TLPLC can be obtained by time domain analysis and evoked method, whereas NPLC is generated by averaging the time–frequency transforms of every trial and this type ERO is evoked by some high-order processes (David et al. 2006; Singer and Gray 1995). Meanwhile, as described in the study (David et al. 2006), TLPLC reflects some stimulus locked event related response, while NPLC might be evoked by nonlinear and autonomous mechanisms. In short, the neuronal processes and mechanisms of TLPLC and NPLC are different (David et al. 2006).

Since Tallon Baudry et al. proposed the NPLC-oriented TF method in 1996 (Tallon-Baudry et al. 1996), it has been widely used in the fields of cognitive neuroscience and medicine, such as Parkinson's disease (Wiesman et al. 2016), depression (Shaw et al. 2013), children sleep (Piantoni et al. 2013), and language cognition (Araki et al. 2016; Kielar et al. 2015; Wang et al. 2012). Hence, NPLC includes significant information of all-brain activities. However, the spatial information is still not utilized in TFA and sometimes statistically significant results cannot be obtained by TFA, which poses some challenges for the exploration of brain mechanisms. In such a context, we propose a NPLC-oriented tensor decomposition analysis of ERP data. Tensor decomposition exploits the interaction among modes. Firstly defined in the mathematics field (Hitchcock 1927), it has been extensively applied in the fields of psychometrics and chemometrics for multi-mode data analysis (Kroonenberg 2008; Smilde et al. 2004).

Aiming to overcome the shortcomings of time domain analysis and TFA, some researchers have attempted to use Canonical Polyadic decomposition (CPD) (Hitchcock 1927) to extract multi-domain features of COI simultaneously from high-order tensor composed of time–frequency results. Here, the high-order tensor is a fourth-order tensor. The order of

the fourth-order tensor represents the number of its “ways”, “dimensions”, “domains”, or “modes”, which includes four modes: frequency, time, channels/space, and subjects-stimuli/conditions (Zhou et al. 2016). The component is selected if its temporal, spectral, and spatial components are consistent with characteristics of COI in the time, frequency, and space domains, and then its multi-domain feature mode (the last mode) is applied to statistical analysis (Cong et al. 2012c, 2013, 2014). Despite the use of tensor decomposition algorithm to extract TLPLC of interest (Cong et al. 2012c), NPLC from all brain activities has not been investigated with tensor-based multi-mode analysis (more than three modes).

There are two problems to be solved before extracting NPLC. For one thing, when referring to TFA of ERP data, it is typically calculated by WTA (Herrmann et al. 2014; Tallon-Baudry and Bertrand 1999; Tallon-Baudry et al. 1996, 1997, 1998). Some researchers also use STFT for TFA of ERP data, but the central idea is similar to WTA (Hu et al. 2014). When WTA is used for TFA of ERP data, a mother wavelet should be firstly defined by a set of center frequency and bandwidth (CFBW). Since the differences of CFBW may result in divergent time–frequency results, different CFBW should be attempted for an optimal time–frequency result (Zhang et al. 2017). For another, NPLC is mixed together with other components (Jung et al. 2000). The key problem is how to separate NPLC from mixed signals. This study is dedicated to the

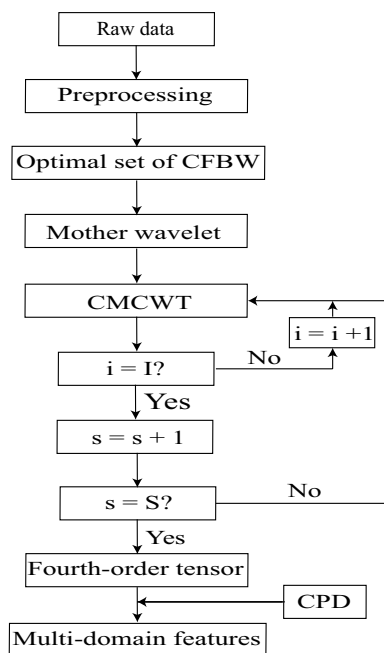


**Fig. 1** The flow of tensor-based method for ERP data analysis.  $S$  is the number of subjects-stimuli/conditions;  $I$  represents the number of channels

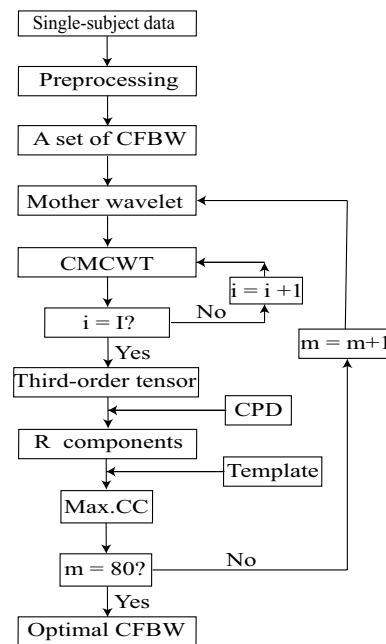


**Fig. 2** Optimal CFBW set selection.  $I$  and 80 are the number of channels and total number of sets of CFBW, respectively.  $\text{Max.CC}$  represents maximum correlation coefficient

investigation of these issues and the following steps are used for implementing the idea of NPLC-oriented tensor decomposition analysis. After ERP data preprocessing, CFBW are optimized by selecting from 80 sets of CFBW to define a mother wavelet for complex morlet continuous wavelet transform (CMCWT), which is used to solve the first problem as mentioned above (as shown in Fig. 2). The induced method was conducted to convert the time domain signals of every participant into the time–frequency domain signals, so that the fourth-order tensor was formed. Subsequently, the temporal components, spectral components, spatial components, and features of subjects-stimuli/conditions mode of NPLC are extracted simultaneously by CPD from the fourth-order tensor (to solve the second problem as mentioned above). Finally, a comparison was made of the diversity between NPLC extracted by CPD and TFA in the temporal component, spectral component, spatial component, and repeated measure analysis of variance (rm-ANOVA) results (the flow of data processing and analyze as shown in Fig. 1).

## Methods

### Participants and EEG Data Acquisition

Fifteen college students were recruited to participate as paid volunteers from Shanghai University of Sports in China.

Seven were females and eight were males (Mean age: 20.8; Std: 1.4). All the participants were right-handed, presented with normal or corrected to normal visual acuity and they did not know or see the experimental paradigm before the experiment. Previous studies reported that anger appeared to be an important factor in human behavior (Denny and Sieemer 2012) and the emotion Go/Nogo task was used in a great number of studies to explore the underlying mechanisms (Goldstein et al. 2007; Shafritz et al. 2006; Verona et al. 2012; Yu et al. 2014). Following this line, in this study, all participants were required to participate in emotion (Anger and Neutral) Go/Nogo task. The details of the experiment materials and the paradigm can be found in our previous research (Xia et al. 2018). EEG recordings at 64 locations were collected according to the standard 10–20 system. The EEG data were referenced online against the FCz electrode and grounded at the AFz electrode. Meanwhile, a vertical electrooculogram was obtained below the left eye, and the horizontal electrooculogram was obtained at the outer canthus of the right eye. Impedances were less than 5 kΩ. The BrainAmp amplifier and BrainVision Recorder 2.0 system (Brain Products GmbH, Germany) were used to record electrical activity for each participant with a 500 Hz sampling rate and the data were filtered between 0.01 and 100 Hz by a BrainAmp amplifier.

## Data Preprocessing

The preprocessing of EEG was conducted in two sorts of software. Firstly, by the Analyzer 2.0 system (Brain Products), the FCz electrode was restored when the data were re-referenced offline to an average of both posterior ear papillae (TP9 and TP10) for each participant (Debener et al. 2012). Subsequently, using the EEGLAB toolbox (Delorme and Makeig 2004) running in the MATLAB environment (MathWorks, Natick, MA), the data preprocessing was performed offline. The EEG signals were filtered offline with a 45–55 Hz notch infinite impulse response (IIR) (Delorme and Makeig 2004; Guan et al. 2004; Kropotov 2010; Lopez-Calderon and Luck 2014; Nishida et al. 1993; Widmann et al. 2015) filter (to remove line noise), a high-pass IIR filter of 0.2 Hz and a low-pass IIR filter with 30 Hz, respectively. Furthermore, the filtered continuous recordings were epoched from 200 ms before the stimulus onset to 1000 ms after the stimulus onset. Epochs/trials whose maximum magnitude exceeded 100 μV were excluded (5.7% of epochs/trials were rejected) and then remaining epochs were baseline corrected. Considering the COI is below 30 Hz and in order to reduce the impact of low-frequency components, a band-pass filter with 3–30 Hz based on Fast Fourier Transformation (FFT) was applied to filter the single-trial data (Cong et al. 2015b). Taking into account the diversity of bad channels of each participant, 22 bad channels were

removed for all participants. They were identified based on the data distribution and variance of channels, by using the EEGLAB's function-pop\_rejchan (Delorme and Makeig 2004) and the FASTER toolbox (Nolan et al. 2010).

## Time–Frequency Analysis

### Complex Morlet Continuous Wavelet Transform

STFT and WTA are two common algorithms in the TFA of ERP data. STFT has been extensively utilized for TFA of ERP data since it is proposed by Potter in 1947 (Araki et al. 2016; Cohen 1989; Ehm et al. 2011; Fumuro et al. 2015; Kauppi et al. 2013). This method is to calculate the Fourier transform of the windowed signals, which are approximately stationary over the window. However, the length of the window is the same for all frequencies. If the length of the window is too long, it will lead to low time-resolution at higher frequencies and low frequency-resolution at lower frequencies. In contrast, when the window length is relatively shorter, it will present the opposite results. Compared with STFT, the wavelet transform uses short windows at high frequencies and long windows at low frequencies (Riou and Vetterli 1991; Peng and Chu 2004). That is to say, the wavelet transform is more adapted to TFA of non-stationary signals, for example, EEG/ERP data (Peng and Chu 2004). Therefore, WTA is used to achieve a trade-off between time-resolution and frequency-resolution in this study.

When the length of discrete sequence signal  $y(t)$  is  $T(t = 0, 1, 2, \dots, T - 1)$ , then the wavelet transform can be expressed as (Zhang et al. 2017):

$$Y(a, t_0) = \frac{1}{\sqrt{|a|}} \sum_{t=0}^{T-1} y(t) \Phi\left(\frac{t-t_0}{a}\right). \quad (1)$$

In the above formula,  $\Phi\left(\frac{t-t_0}{a}\right)$  is the mother wavelet.  $a$  and  $t_0$  are called scaling and shifting parameters, respectively. In this study, the complex Morlet Wavelet is defined as the mother wavelet (Tallon-Baudry and Bertrand 1999; Tallon-Baudry et al. 1996, 1997, 1998; Bertrand and Tallon-Baudry 2000; Simões et al. 2003; Lachaux et al. 2005; Li et al. 2019; Xia et al. 2019):

$$\Phi(t, f_c) = \frac{1}{\sqrt{\pi f_b^2}} e^{i2\pi f_c t} e^{\frac{-t^2}{2f_b^2}}, \quad (2)$$

where  $f_b$  and  $f_c$  stand for bandwidth and center frequency, respectively. And a gaussian shape respectively in the time domain and frequency domain around its  $f_c$  can be obtained (Zhang et al. 2017).

A wavelet family is characterized by a constant ratio (Tallon-Baudry et al. 1996):

$$K = \frac{f_c}{f_{bf}} = 2\pi f_b f_c. \quad (3)$$

In this formula,  $f_{bf} = \frac{1}{2\pi f_b}$ ,  $K$  should be more than 5 (Zhang et al. 2017).

Given an ERP data  $\mathbf{x}_{c,n}(t)$ ,  $c$  and  $n$  are the number of the electrodes/sensors and trials, respectively. The definition of induced method can be given (Herrmann et al. 2005) by the following equation:

$$ERSP_{av}(t,f) = \frac{1}{N} \sum_{n=1}^N |\mathbf{X}_{c,n}(t,f)|^2. \quad (4)$$

In Eq. 4,  $|\mathbf{X}_{c,n}(t,f)|^2$  represent the power values of ERP data in  $c$ th electrode and  $n$ th trial.

### Selection of an Optimal Set of CFBW for CMCWT

As shown in our previous study (Zhang et al. 2017), different parametric settings may result in divergent time–frequency results. CMCWT [the MATLAB function (Daubechies 1992; Mallat 1999)] was used under the MATLAB environment for the TFA of ERP data with an optimal set of CFBW selected from a number of sets of CFBW (as shown in Fig. 2). The specific steps are as below.

Eighty sets were generated through different combinations of center frequency ( $f_c$ ) and bandwidth ( $f_b$ ) under the constraint of  $K > 5$ .  $K$  is the constant ratio in Eq. 3. The combinations are as follows: when  $f_{b1} = 0.1, f_c = 9, 10$ , respectively; when  $f_{b2} = 0.2, f_c = 5, 6, 7, 8, 9, 10$ , respectively; when  $f_{b3} = 0.3, f_c = 3, 4, 5, 6, 7, 8, 9, 10$ , respectively; when  $f_{b4} = 0.4, f_c = 3, 4, 5, 6, 7, 8, 9, 10$ , respectively; when  $f_{b5} = 0.5, f_c = 2, 3, 4, 5, 6, 7, 8, 9, 10$ , respectively; when  $f_{b6} = 0.6, f_c = 2, 3, 4, 5, 6, 7, 8, 9, 10$ , respectively; when  $f_{b7} = 0.7, f_c = 2, 3, 4, 5, 6, 7, 8, 9, 10$ , respectively; when  $f_{b8} = 0.8, f_c = 2, 3, 4, 5, 6, 7, 8, 9, 10$ , respectively; when

$f_{b9} = 0.9, f_c = 1, 2, 3, 4, 5, 6, 7, 8, 9, 10$ , respectively; when  $f_{b10} = 1, f_c = 1, 2, 3, 4, 5, 6, 7, 8, 9, 10$ , respectively.

The CFBW in each set was applied to the TFA (see “Complex Morlet Continuous Wavelet Transform” section) of the same single subject data under one condition.

Each set of CFBW corresponded to a time–frequency representation (TFR) and topography (obtained by averaging the same region of interest, the time window from 300–600 ms and the frequency range from 3 to 7 Hz for all sets of CFBW) obtained by TFA. Meanwhile, third-order tensor including frequency, time, and channels can be composed by the time–frequency results of all sets of CFBW, respectively.

A typical topographical distribution of time–frequency results was referred to as the template. For instance, when  $f_b = 1$ , the value of  $f_c$  can be respectively set as 1, 2, 3, 4, 5, 6, 7, 8, 9, and 10. The topographical distribution of  $f_{c_4} = 4$  was finally chosen as the template  $T_{template}(f_{b10}, f_{c_4})$ , based on the comparison of its topography and TFR with those of other sets of CFBW. That is to say, the time-resolution and frequency-resolution of its TFR are better than other sets of CFBW, and the template could represent most of the topographic maps of all sets of CFBW. After defining  $f_{c_n}$ , the correlation coefficients (CCs) between the template ( $T_{template}$ ) and spatial components  $s_r(f_{b10}, f_{c_n})$  obtained by CPD were calculated by the following equations ( $R$  components were extracted in each mode based on the method as described in our previous studies (Cong et al. 2012a, 2015a), the detail of extracted number of every set of CFBW is shown in Table 1).

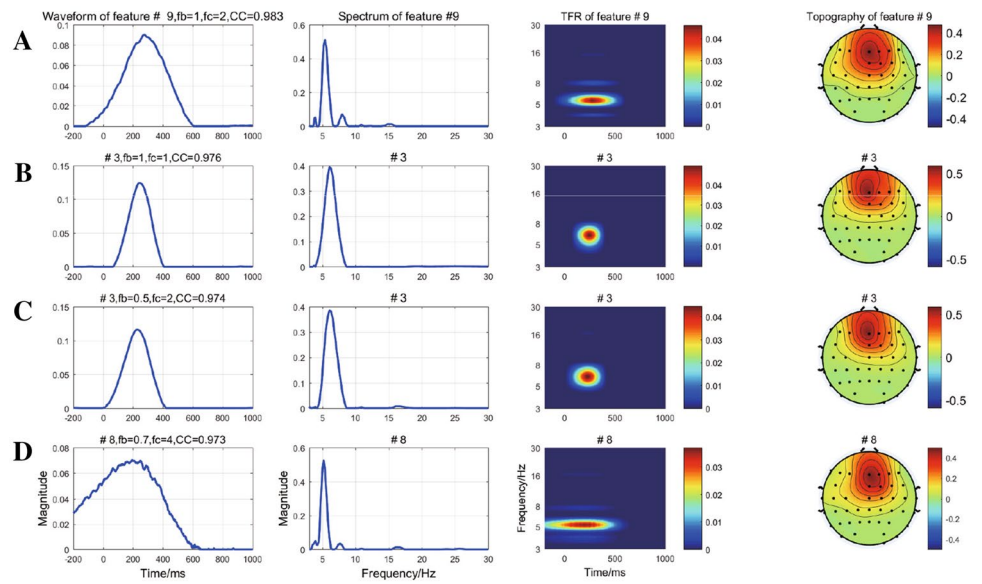
$$Y(f_{b10}, f_{c_n}, r) = \rho(s_r(f_{b10}, f_{c_n}), T_{template}(f_{b10}, f_{c_4})), \quad (5)$$

where  $r = 1, 2, \dots, R; n = 1, 2, \dots, 10$ ;  $Y$  is the CC of each component for every set of CFBW.

**Table 1** The extracted number in each mode of every set of CFBW

$f_c$	$f_b$										
		0.1	0.2	0.3	0.4	0.5	0.6	0.7	0.8	0.9	1
1	—	—	—	—	—	—	—	—	—	36	28
2	—	—	—	—	35	45	25	42	35	32	
3	—	—	51	43	32	34	28	25	45	45	
4	—	—	28	50	45	42	30	36	46	42	
5	—	25	44	46	25	35	25	25	40	25	
6	—	37	52	35	20	45	40	30	30	32	
7	—	34	37	30	42	40	28	42	42	45	
8	—	26	26	36	31	36	36	30	45	28	
9	25	40	44	25	40	25	35	40	33	30	
10	45	36	38	24	42	35	35	48	30	45	

**Fig. 3 a–d** The multi-domain components with the first four maximum CCs of four sets of CFBW ( $f_b = 1, f_c = 2$ ;  $f_b = 1, f_c = 1; f_b = 0.5, f_c = 2$ ;  $f_b = 0.7, f_c = 4$ ), respectively



$$\rho(s_r, T_{\text{template}}) = \frac{\sum_{i=1}^I (s_r^i - \bar{s}_r)(T_{\text{template}}^i - \bar{T}_{\text{template}})}{\sqrt{\left(\sum_{i=1}^I s_r^i - \bar{s}_r\right)^2} \sqrt{\sum_{i=1}^I (T_{\text{template}}^i - \bar{T}_{\text{template}})^2}}, \quad (6)$$

where  $\rho \in (-1, 1)$  represents the CC between  $s_r$  and  $T_{\text{template}}$ ;  $I$  is the number of channels;  $T_{\text{template}}^i$  and  $s_r^i$  are the value of each channel for  $T_{\text{template}}$  and  $s_r$ , respectively;  $\bar{T}_{\text{template}}$  and  $\bar{s}_r$  are the mean value of  $T_{\text{template}}$  and  $s_r$ , respectively.

Subsequently, the maximal CC for each set of parameters was chosen as:

$$q(f_{b10}, f_{c_n}, r) = \max(Y(f_{b10}, f_{c_n}, 1), Y(f_{b10}, f_{c_n}, 2), \dots, Y(f_{b10}, f_{c_n}, R)). \quad (7)$$

Then, the corresponding  $r$ th components with the maximum CC were obtained. The same procedures were applied to the other sets of CFBW.

Finally, an optimal set of CFBW was selected. Take the multi-domain components of the first four maximum CCs of four sets of CFBW as example, as shown in Fig. 3. Comparing the corresponding waveforms of the maximum CCs of the first four sets of CFBW, the set of  $f_b = 0.7, f_c = 4$  was firstly discarded, because the COI was evoked after the stimulus onset. Then, we considered that the period of waveform of COI was relatively narrow in the time domain (usually not more than one second) and there were few irrelevant spikes for waveform and spectrum of multi-domain features extracted by CPD.  $f_b = 1$  and  $f_c = 1$  were used to define the mother wavelet.

## Tensor Decomposition Algorithm

In an ERP experiment, there should be at least three modes including time, channels/space, and subjects-stimuli/conditions. When the time-domain data are converted into the time-frequency domain, a fourth-order tensor including time, frequency, channels/space, and subjects-stimuli/conditions can be formed. Moreover, EEG data are used to identify common activities over subjects. It is necessary and interesting to study the interaction among modes, such as time, frequency, and channels/space modes. Here, CPD (Hitchcock 1927; Cong et al. 2015a) is applied to extract COI from the high-order tensor.

Given an  $N$ th-order tensor  $\underline{X} \in \mathcal{R}^{I_1 \times I_2 \times \dots \times I_N}$ , the CPD can be defined as:

$$\underline{X} \approx \sum_{r=1}^R \underline{u}_r^{(1)} \circ \underline{u}_r^{(2)} \circ \dots \circ \underline{u}_r^{(N)} + \underline{E} = \hat{\underline{X}} + \underline{E} \approx \hat{\underline{X}}. \quad (8)$$

In Eq. 8,  $\hat{\underline{X}}$  approximates the high-order tensor  $\underline{X}$ ;  $\underline{E} \in \mathcal{R}^{I_1 \times I_2 \times \dots \times I_N}$  is a  $N$ th-order error tensor, whose sizes of all dimensions are the same as  $\underline{X}$ ;  $\|\underline{u}_r^{(n)}\|_2 = 1$  ( $n = 1, 2, \dots, N-1$ ).  $\underline{U}^{(n)} = [\underline{u}_r^{(1)} \circ \underline{u}_r^{(2)} \circ \dots \circ \underline{u}_r^{(N)}]$  represents a component matrix for mode  $n$ , and  $n = 1, 2, \dots, N$ .

In this study, the fourth-order tensor consisted of the time-frequency results. It can be extracted by CPD (Cong et al. 2014, 2012d):

$$\underline{X} \approx \sum_{r=1}^R \underline{u}_r^{(f)} \circ \underline{u}_r^{(t)} \circ \underline{u}_r^{(s)} \circ \underline{f}_r = \underline{I} \times_1 \underline{U}^{(f)} \times_2 \underline{U}^{(t)} \times_3 \underline{U}^{(s)} \times_4 \underline{F}. \quad (9)$$

In the above formula,  $\underline{I}$  is a diagonal tensor, the value of every element of its super-diagonal is equal to one; the component matrix  $\underline{F}$  contains the multi-domain features of  $R$

brain activity ( $R$  components are extracted in each mode), and each column corresponds to one feature. The component matrix corresponds to the  $r$ th components in the time domain ( $\mathbf{u}_r^{(t)}$ ), frequency domain ( $\mathbf{u}_r^{(f)}$ ) and space domain ( $\mathbf{u}_r^{(s)}$ ), respectively. Those components reveal the properties of the  $r$ th multi-domain feature in the domains as well (Cong et al. 2015a, 2012a). In the CPD, the  $r$ th temporal component,  $r$ th spectral component, and  $r$ th spatial component are interrelated, but neither of them is associated with other multi-domain components (Cong et al. 2015a). Meanwhile, combining with the generative mechanisms of NPLC of interest, CPD is selected to extract NPLC of interest from the fourth-order tensor. According to Eqs. 1 and 4, the time–frequency transforms are obtained by calculating the product of the constant and the sum of the square of the absolute value of the convolution between signals and the mother wavelet. Therefore, the elements of the high-order tensor are nonnegative in the study. In our previous study (Cong et al. 2014), the fourth-order tensor (the size of last mode is conditions by groups by subjects) is formed to find the discrepancy of cognitive processes between the two groups under every condition. Likewise, our interest is to identify the differences between emotion factor under Go/Nogo tasks by calculating statistical results of the features of last mode extracted from the fourth-order tensor (frequency by time by channels/space by subjects-stimuli/conditions:  $30 \times 600 \times 42 \times (15 \times 4)$ ).

## Results

### Time–Frequency Analysis

Combining the previous studies (Benvenuti et al. 2017; Harper et al. 2014; Karakaş et al. 2000; Kirmizi-Alsan

et al. 2006; Pandey et al. 2016) with the time–frequency representations (TFRs) and topographies of all conditions of the present data, we selected the Fz, FCz electrodes for analysis of the theta oscillation (range 3–7Hz) between 300 and 600ms. Then multivariate rm-ANOVAs were computed on theta oscillation using emotion (Anger and Neutral), task (Go and Nogo) as within-subject factors. Figure 4a–c displayed the grand averaged TFR of every condition at Fz and FCz, topography of the theta oscillation, and the corresponding mean power of every condition, respectively. In order to show the corresponding power of theta oscillation of every participant under each condition, the scatter plots with boxplots were displayed in Fig. 4d as well.

The results illustrated that the main effect of task was significant ( $F_{(1,14)} = 10.378, p = 0.006, \eta_p^2 = 0.426$ ). However, the interaction effect between emotion and task was insignificant ( $F_{(1,14)} = 0.007, p = 0.936, \eta_p^2 = 0.001$ ). Similarly, there was no significant main effect between anger and neutral condition ( $F_{(1,14)} = 2.816, p = 0.116, \eta_p^2 = 0.167$ ).

Through visual inspection of the TFR and the mean power of each condition or stimulus for TFA results, the power of Nogo task (mean:  $721.45 \mu V^2$ ; std:  $78.81 \mu V^2$ ) was significantly higher than that of Go task (mean:  $542.91 \mu V^2$ ; std:  $62.40 \mu V^2$ ). In addition, the anger condition (mean:  $647.70 \mu V^2$ ; std:  $66.32 \mu V^2$ ) also elicited stronger power than that of neutral condition (mean:  $616.65 \mu V^2$ ; std:  $65.90 \mu V^2$ ).

In order to demonstrate that the statistical results are affected by the selected ROI for TFA compared with those of the proposed method, the ANOVA results of another RIO (time window: from 200 to 700 ms; frequency range: 3–7 Hz) were also shown. The main effect of emotion ( $F_{(1,14)} = 1.955, p = 0.1840, \eta_p^2 = 0.123$ ) and interaction effect between the two factors

**Fig. 4** **a** The grand averaged time–frequency representations (TFRs). **b** Topographical distributions of the theta oscillations at Fz and FCz with the time window of 300–600 ms. **c** The mean power of every condition. **d** The scatter plots with boxplots of the mean power of every condition. Anger-Go, go task of the anger-associated words; Anger-Nogo, Nogo task of the anger-associated words; Neutral-Go, go task of the neutral words; Neutral-Nogo, Nogo task of the neutral words; ‘\*\*’ represents  $p < 0.01$

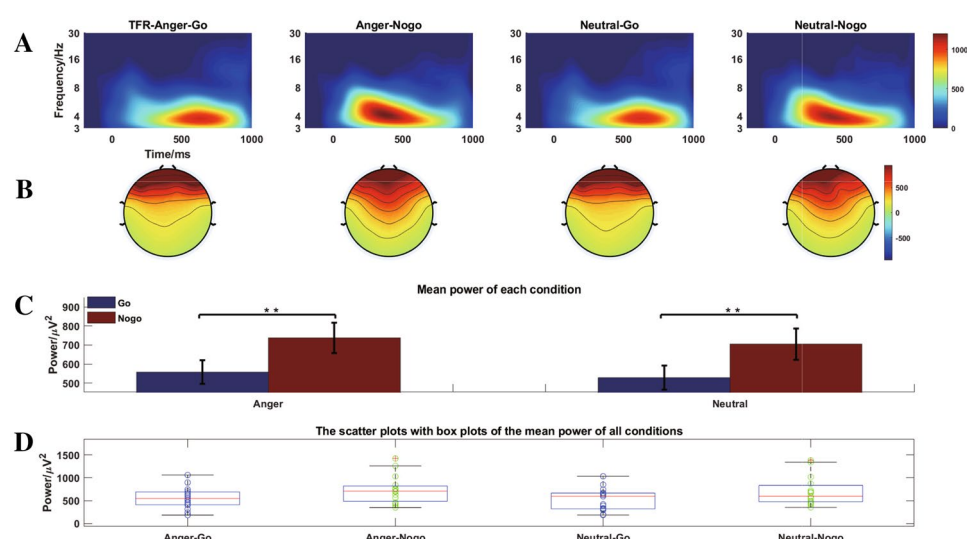
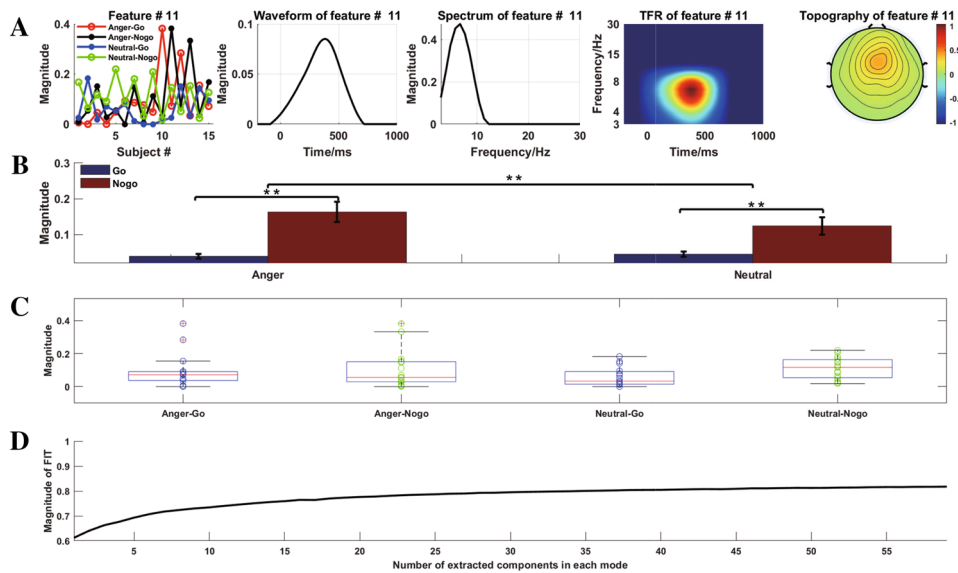


**Fig. 5** **a** Multi-domain features of NPLC of interest as well as the corresponding temporal, spectral, and spatial components were extracted from all brain activity. **b** The mean magnitude of every condition. **c** The scatter plots with boxplots of the mean magnitude of all conditions. **d** The magnitude of FIT, DIFFIT is performed on this curve. \*\*\* represents  $p < 0.01$



( $F_{(1,14)} = 0.023, p = 0.8810, \eta_p^2 = 0.002$ ) were insignificant, respectively. In addition, there was a significant main effect for tasks ( $F_{(1,14)} = 8.643, p = 0.0110, \eta_p^2 = 0.382$ ). The methods, which can be used to precisely determine the ROI of TFR of every condition according to the corresponding boundary, were not discussed in this study.

### Multi-domain Features of NPLC

Aiming at extracting the NPLC of interest, the results from each step of the tensor decomposition analysis of ERP are as following.

Using the CFBW confirmed in “[Selection of an Optimal Set of Parameters for CMCWT](#)” section ( $f_b = 1, f_c = 1$ ), the induced method was performed on all participants’ data for TFA. The sampling point is nonlinear distribution in the frequency domain, with 30 points set in the whole frequency band of interest (3–30 Hz).

The fourth-order tensor was formed by the time–frequency results.

According to the fit value as shown in Fig. 5d, 36 components were extracted in each mode. The detail of how to define the number of extracted components for CPD can be found in our previous studies (Cong et al. 2012c, 2013, 2014, 2012b).

We considered the temporal, spectral and spatial properties of NPLC of interest as shown in “[Time–Frequency Analysis](#)” section. Its latency fell in the range from 300 to 600 ms in the time domain, the peak of corresponding spectrum is below 8Hz, and its peak amplitudes are distributed in the frontal–central cortex in the space domain. The 11th component was chosen (in Fig. 5a). In addition, the TFR in Fig. 5a was based on the outer product of the temporal and spectral components.

When the multi-domain features were determined, two-way (emotion and task) repeated measurement statistical test were performed to investigate the between-task differences under emotion condition (Anger and Neutral) with 0.05 as the level of significance, and Greenhouse Geisser correction was performed when necessary. The results showed that the interaction effect between emotion and task reaches a significant level ( $F_{(1,14)} = 10.607, p = 0.006, \eta_p^2 = 0.431$ ). There was a significant main effect of both emotion ( $F_{(1,14)} = 6.162, p = 0.026, \eta_p^2 = 0.306$ ) and task ( $F_{(1,14)} = 17.688, p = 0.001, \eta_p^2 = 0.558$ ). Through post hoc analysis, the results demonstrated that the power of anger condition was larger than that of neutral stimuli in the Nogo task ( $p = 0.005$ ), not in the Go task ( $p = 0.367$ ). By contrast, there was a significant main effect of task conditions under both anger ( $p < 0.001$ ) and neutral condition ( $p = 0.005$ ). Thus, this study found that the power of NPLC oscillation obviously increases in anger words when compared to neutral words in the Nogo task as shown in Fig. 5b. In addition, the scatter plots with boxplots were also shown in Fig. 5c such that the feature of every participant in every condition can be observed.

### Conclusion and Discussion

Using CPD to separate the multi-domain features of NPLC of interest, this study investigated the differences between tensor decomposition analysis and TFA of ERP data. The tensor-based results were more discriminative than those derived from TFA. The method based on tensor decomposition showed not only the significant main effect of task condition, but also significant interaction effect between emotion and task. The main effect of emotion was found

to reach a significant level. Moreover, the proposed method ensured that statistical analysis results do not change with ROI. This manifested that the derived features fulfill expectations in this study, and it should be fundamental for the extension of our proposed method for the analysis of other EEG/ERP data.

In this study, the time–frequency results are used by averaging the time–frequency transforms of each single-trial data to separate the multi-domain features of NPLC of interest, and it is different from those methods which obtain COI by averaging multi-trial waveforms in time domain and calculating the time–frequency transforms of averaged ERP data. Moreover, there are several methods to form a high-order tensor to extract the information of short ERPs data simultaneously in the time, frequency, space, and participants modes. For example, in order to study the properties of NPLC at the single-trial level, the fourth-order tensor can be comprised of frequency by time by channels by subjects-trials. Particularly, the third-order tensor is constructed including temporal, spectral, and spatial information, because the time-locked characteristics of NPLC in different single-trial are not deterministic. Few strictly time-locked characteristics of NPLC are preserved.

Furthermore, CPD is a group analysis method that performs on the high-order tensor of brain activity collected from different participants and stimuli/conditions (Zhou et al. 2016). It assumes that all subjects share the same information of components in the time domain, frequency domain, and space domain, while the variance in signatures of all participants is revealed by those common components (Cong et al. 2015a). As we all know, the EEG/ERP data of one subject in each condition/stimulus can form one block tensor. In other words, for one subject's data, the block tensor can be a third-order tensor (time by channels by stimuli/conditions) or fourth-order tensor (frequency by time by channels by stimuli/conditions), so multi-participant data can form multi-block data. Therefore, coupled/constrained matrix and tensor factorizations can be applied to extract common and individual components and/or build links between them (Zhou et al. 2016).

There are several drawbacks for using CPD and TFA to extract the NPLC of interest from ERP data. One limitation is the small number of subjects were recruited to participate in the experiment in this study. The ERP data were only collected from 15 participants. Another one is the method to extract NPLC by tensor decomposition has not been employed in other ERP data. Additionally, in Fig. 4a, the grand averaged TFRs clearly display that the theta oscillation of interest of every condition has a specific and visible boundary and the ROIs of the four conditions are different. Hence, the same ROI for all conditions used for statistical analysis in the research is unreasonable and arbitrary. The techniques, such as edge detection method based on Canny,

Marr–Hildreth, Deriche, Sobel, and Laplacian algorithms, can be used to precisely mark the edge of ERO of interest of every condition respectively in the TFR (Milanović et al. 2019). In this study, the tensor decomposition was used to extract the multi-domain features of NPLC simultaneously for an expected statistical results, evidencing that this method is promising with substantial potentials in neuroscience applications.

**Acknowledgements** Open access funding provided by University of Jyväskylä (JYU). This work was supported by National Natural Science Foundation of China (Grant Nos. 91748105, 81471742, and 61703069) and the Fundamental Research Funds for the Central Universities [DUT2019] in Dalian University of Technology in China, and the scholarships from China Scholarship Council (No. 201806060165).

**Open Access** This article is licensed under a Creative Commons Attribution 4.0 International License, which permits use, sharing, adaptation, distribution and reproduction in any medium or format, as long as you give appropriate credit to the original author(s) and the source, provide a link to the Creative Commons licence, and indicate if changes were made. The images or other third party material in this article are included in the article's Creative Commons licence, unless indicated otherwise in a credit line to the material. If material is not included in the article's Creative Commons licence and your intended use is not permitted by statutory regulation or exceeds the permitted use, you will need to obtain permission directly from the copyright holder. To view a copy of this licence, visit <http://creativecommons.org/licenses/by/4.0/>.

## References

- Araki T, Hirata M, Yanagisawa T, Sugata H, Onishi M, Watanabe Y, Ogata S, Honda C, Hayakawa K, Yorifuji S et al (2016) Language-related cerebral oscillatory changes are influenced equally by genetic and environmental factors. *Neuroimage* 142:241–247
- Benvenuti SM, Buodo G, Palomba D (2017) Appetitive and aversive motivation in dysphoria: a time-domain and time-frequency study of response inhibition. *Biol Psychol* 125:12–27
- Berger H (1929) Über das elektrenkephalogramm des menschen. *Eur Arch Psychiatry Clin Neurosci* 87(1):527–570
- Bertrand O, Tallon-Baudry C (2000) Oscillatory gamma activity in humans: a possible role for object representation. *Int J Psychophysiol* 38(3):211–223
- Cohen L (1989) Time-frequency distributions—a review. *Proc IEEE* 77(7):941–981
- Cohen MX (2014) Analyzing neural time series data: theory and practice. MIT Press, Cambridge
- Cong F, Phan AH, Zhao Q, Huttunen-Scott T, Kaartinen J, Ristaniemi T, Lyytinen H, Cichocki A (2012a) Benefits of multi-domain feature of mismatch negativity extracted by non-negative tensor factorization from eeg collected by low-density array. *Int J Neural Syst* 22(06):1250025
- Cong F, Phan AH, Zhao Q, Nandi AK, Alluri V, Toivainen P, Poikonen H, Huotilainen M, Cichocki A, Ristaniemi T (2012b) Analysis of ongoing EEG elicited by natural music stimuli using nonnegative tensor factorization. In: 2012 proceedings of the 20th European signal processing conference (EUSIPCO). IEEE, pp 494–498
- Cong F, Phan AH, Zhao Q, Wu Q, Ristaniemi T, Cichocki A (2012c) Feature extraction by nonnegative tucker decomposition from EEG data including testing and training observations. In:

- International conference on neural information processing. Springer, pp 166–173
- Cong F, Zhou G, Zhao Q, Wu Q, Nandi AK, Ristaniemi T, Cichocki A (2012d) Sequential nonnegative tucker decomposition on multi-way array of time-frequency transformed event-related potentials. In: 2012 IEEE international workshop on machine learning for signal processing. IEEE, pp 1–6
- Cong F, Phan AH, Astikainen P, Zhao Q, Wu Q, Hietanen JK, Ristaniemi T, Cichocki A (2013) Multi-domain feature extraction for small event-related potentials through nonnegative multi-way array decomposition from low dense array EEG. *Int J Neural Syst* 23(02):1350006
- Cong F, Zhou G, Astikainen P, Zhao Q, Wu Q, Nandi AK, Hietanen JK, Ristaniemi T, Cichocki A (2014) Low-rank approximation based non-negative multi-way array decomposition on event-related potentials. *Int J Neural Syst* 24(08):1440005
- Cong F, Lin QH, Kuang LD, Gong XF, Astikainen P, Ristaniemi T (2015a) Tensor decomposition of eeg signals: a brief review. *J Neurosci Methods* 248:59–69
- Cong F, Ristaniemi T, Lyytinen H et al (2015b) Advanced signal processing on brain event-related potentials: filtering ERPs in time, frequency and space domains sequentially and simultaneously. World Scientific, Singapore
- Daubechies I (1992) Ten lectures on wavelets, vol 61. SIAM, Philadelphia
- David O, Kilner JM, Friston KJ (2006) Mechanisms of evoked and induced responses in MEG/EEG. *Neuroimage* 31(4):1580–1591
- Debener S, Minow F, Emkes R, Gandras K, De Vos M (2012) How about taking a low-cost, small, and wireless eeg for a walk? *Psychophysiology* 49(11):1617–1621
- Delorme A, Makeig S (2004) Eeglab: an open source toolbox for analysis of single-trial eeg dynamics including independent component analysis. *J Neurosci Methods* 134(1):9–21
- Denny KG, Siemer M (2012) Trait aggression is related to anger-modulated deficits in response inhibition. *J Res Personal* 46(4):450–454
- Dien J (2010a) The ERP PCA toolkit: an open source program for advanced statistical analysis of event-related potential data. *J Neurosci Methods* 187(1):138–145
- Dien J (2010b) Evaluating two-step pca of erp data with geomin, info-max, oblimin, promax, and varimax rotations. *Psychophysiology* 47(1):170–183
- Dien J (2012) Applying principal components analysis to event-related potentials: a tutorial. *Dev Neuropsychol* 37(6):497–517
- Dien J, Beal DJ, Berg P (2005) Optimizing principal components analysis of event-related potentials: matrix type, factor loading weighting, extraction, and rotations. *Clin Neurophysiol* 116(8):1808–1825
- Ehm W, Bach M, Kornmeier J (2011) Ambiguous figures and binding: EEG frequency modulations during multistable perception. *Psychophysiology* 48(4):547–558
- Fumuro T, Matsuhashi M, Miyazaki T, Inouchi M, Hitomi T, Matsumoto R, Takahashi R, Fukuyama H, Ikeda A (2015) Alpha-band desynchronization in human parietal area during reach planning. *Clin Neurophysiol* 126(4):756–762
- Goldstein M, Brendel G, Tuescher O, Pan H, Epstein J, Beutel M, Yang Y, Thomas K, Levy K, Silverman M et al (2007) Neural substrates of the interaction of emotional stimulus processing and motor inhibitory control: an emotional linguistic go/no-go fMRI study. *Neuroimage* 36(3):1026–1040
- Guan C, Zhu X, Ranganatha S, Thulasidas M, Wu J (2004) Robust classification of event-related potential for brain-computer interface. In: Proceedings of 2nd international conference on advances in medical signal information processing (MEDSIP), pp 321–326
- Harper J, Malone SM, Bernat EM (2014) Theta and delta band activity explain n2 and p3 ERP component activity in a go/no-go task. *Clin Neurophysiol* 125(1):124–132
- Herrmann CS, Lenz D, Junge S, Busch NA, Maess B (2004) Memory-matches evoke human gamma-responses. *BMC Neurosci* 5(1):13
- Herrmann CS, Grigutsch M, Busch NA (2005) 11 EEG oscillations and wavelet analysis. Event-related potentials: a methods handbook, p 229
- Herrmann CS, Rach S, Vosskuhl J, Strüber D (2014) Time-frequency analysis of event-related potentials: a brief tutorial. *Brain Topogr* 27(4):438–450
- Hitchcock FL (1927) The expression of a tensor or a polyadic as a sum of products. *J Math Phys* 6(1–4):164–189
- Hu L, Xiao P, Zhang Z, Mouraux A, Iannetti GD (2014) Single-trial time-frequency analysis of electrocortical signals: baseline correction and beyond. *Neuroimage* 84:876–887
- Hyvärinen A (2013) Independent component analysis: recent advances. *Philos Trans R Soc A Math Phys Eng Sci* 371(1984):20110534
- Jung TP, Makeig S, Westerfield M, Townsend J, Courchesne E, Sejnowski TJ (2000) Removal of eye activity artifacts from visual event-related potentials in normal and clinical subjects. *Clin Neurophysiol* 111(10):1745–1758
- Karakas S, Erzengin ÖU, Başar E (2000) A new strategy involving multiple cognitive paradigms demonstrates that erp components are determined by the superposition of oscillatory responses. *Clin Neurophysiol* 111(10):1719–1732
- Kauppi JP, Parkkonen L, Hari R, Hyvärinen A (2013) Decoding magnetoencephalographic rhythmic activity using spectrospatial information. *NeuroImage* 83:921–936
- Kawaguchi H, Kume T, Kobayashi T (2013) A background EEG removal method combining PCA with multivariate empirical mode decomposition for event-related potential measurements. *IEEJ Trans Electri Electron Eng* 8(S1):S53–S60
- Kielar A, Panamsky L, Links KA, Meltzer JA (2015) Localization of electrophysiological responses to semantic and syntactic anomalies in language comprehension with MEG. *NeuroImage* 105:507–524
- Kirmizi-Alsan E, Bayraktaroglu Z, Gurvit H, Keskin YH, Emre M, Demiralp T (2006) Comparative analysis of event-related potentials during Go/NoGo and CPT: decomposition of electrophysiological markers of response inhibition and sustained attention. *Brain Res* 1104(1):114–128
- Kroonenberg PM (2008) Applied multiway data analysis, vol 702. Wiley, Hoboken
- Kropotov JD (2010) Quantitative EEG, event-related potentials and neurotherapy. Academic Press, Cambridge
- Kutas M, Federmeier KD (2000) Electrophysiology reveals semantic memory use in language comprehension. *Trends Cogn Sci* 4(12):463–470
- Kutas M, Federmeier KD (2011) Thirty years and counting: finding meaning in the N400 component of the event-related brain potential (ERP). *Annu Rev Psychol* 62:621–647
- Kutas M, Hillyard SA (1980) Reading senseless sentences: brain potentials reflect semantic incongruity. *Science* 207(4427):203–205
- Lachaux JP, George N, Tallon-Baudry C, Martinerie J, Hugueville L, Minotti L, Kahane P, Renault B (2005) The many faces of the gamma band response to complex visual stimuli. *Neuroimage* 25(2):491–501
- Li X, Zhang G, Zhou C, Wang X (2019) Negative emotional state slows down movement speed: behavioral and neural evidence. *PeerJ* 7:e7591
- Lopez-Calderon J, Luck SJ (2014) Erplab: an open-source toolbox for the analysis of event-related potentials. *Front Hum Neurosci* 8:213
- Luck SJ (2014) An introduction to the event-related potential technique. MIT press, Cambridge

- Mallat S (1999) A wavelet tour of signal processing. Elsevier, Amsterdam
- Milanović Ž, Saulig N, Marasović I (2019) Signal feature recognition in time-frequency domain using edge detection algorithms. In: 2019 4th international conference on smart and sustainable technologies (SpliTech). IEEE, pp 1–5
- Möcks J, Verleger R (1985) Nuisance sources of variance in principal components analysis of event-related potentials. *Psychophysiology* 22(6):674–688
- Nishida S, Nakamura M, Shibasaki H (1993) Method for single-trial recordings of somatosensory evoked potentials. *J Biomed Eng* 15(3):257–262
- Nolan H, Whelan R, Reilly R (2010) Faster: fully automated statistical thresholding for EEG artifact rejection. *J Neurosci Methods* 192(1):152–162
- Pandey AK, Kamarajan C, Manz N, Chorlian DB, Stimus A, Porjesz B (2016) Delta, theta, and alpha event-related oscillations in alcoholics during Go/NoGo task: neurocognitive deficits in execution, inhibition, and attention processing. *Prog Neuropsychopharmacol Biol Psychiatry* 65:158–171
- Peng Z, Chu F (2004) Application of the wavelet transform in machine condition monitoring and fault diagnostics: a review with bibliography. *Mech Syst Signal Process* 18(2):199–221
- Piantoni G, Astill RG, Raymann RJ, Vis JC, Coppens JE, Van Someren EJ (2013) Modulation of gamma and spindle-range power by slow oscillations in scalp sleep EEG of children. *Int J Psychophysiol* 89(2):252–258
- Rioult O, Vetterli M (1991) Wavelets and signal processing. *IEEE Signal Process Mag* 8(ARTICLE):14–38
- Shafritz KM, Collins SH, Blumberg HP (2006) The interaction of emotional and cognitive neural systems in emotionally guided response inhibition. *Neuroimage* 31(1):468–475
- Shaw A, Brealy J, Richardson H, Muthukumaraswamy SD, Edden RA, Evans CJ, Puts NA, Singh KD, Keedwell PA (2013) Marked reductions in visual evoked responses but not  $\gamma$ -aminobutyric acid concentrations or  $\gamma$ -band measures in remitted depression. *Biol Psychiatry* 73(7):691–698
- Simões C, Jensen O, Parkkonen L, Hari R (2003) Phase locking between human primary and secondary somatosensory cortices. *Proc Natl Acad Sci* 100(5):2691–2694
- Singer W, Gray CM (1995) Visual feature integration and the temporal correlation hypothesis. *Annu Rev Neurosci* 18(1):555–586
- Smilde AK, Bro R, Geladi P et al (2004) Multi-way analysis with applications in the chemical sciences. Wiley Online Library, Hoboken
- Tallon-Baudry C, Bertrand O (1999) Oscillatory gamma activity in humans and its role in object representation. *Trends Cogn Sci* 3(4):151–162
- Tallon-Baudry C, Bertrand O, Delpuech C, Pernier J (1996) Stimulus specificity of phase-locked and non-phase-locked 40 Hz visual responses in human. *J Neurosci* 16(13):4240–4249
- Tallon-Baudry C, Bertrand O, Delpuech C, Pernier J (1997) Oscillatory  $\gamma$ -band (30–70 Hz) activity induced by a visual search task in humans. *J Neurosci* 17(2):722–734
- Tallon-Baudry C, Bertrand O, Peronnet F, Pernier J (1998) Induced  $\gamma$ -band activity during the delay of a visual short-term memory task in humans. *J Neurosci* 18(11):4244–4254
- Verona E, Sprague J, Sadeh N (2012) Inhibitory control and negative emotional processing in psychopathy and antisocial personality disorder. *J Abnorm Psychol* 121(2):498
- Wang L, Jensen O, Van den Brink D, Weder N, Schoffelen JM, Magyari L, Hagoort P, Bastiaansen M (2012) Beta oscillations relate to the N400m during language comprehension. *Hum Brain Mapp* 33(12):2898–2912
- Widmann A, Schröger E, Maess B (2015) Digital filter design for electrophysiological data—a practical approach. *J Neurosci Methods* 250:34–46
- Wiesman AI, Heinrichs-Graham E, McDermott TJ, Santamaria PM, Gendelman HE, Wilson TW (2016) Quiet connections: reduced fronto-temporal connectivity in nondemented parkinson's disease during working memory encoding. *Hum Brain Mapp* 37(9):3224–3235
- Xia X, Wang X, Zhang G (2018) Anger weakens behavioral inhibition selectively in contact athletes. *Front Hum Neurosci* 12:463
- Xia X, Zhang J, Wang X, Wang X (2019) The approach behavior to angry words in athletes—a pilot study. *Front Behav Neurosci* 13:117
- Yu F, Ye R, Sun S, Carretié L, Zhang L, Dong Y, Zhu C, Luo Y, Wang K (2014) Dissociation of neural substrates of response inhibition to negative information between implicit and explicit facial go/no-go tasks: evidence from an electrophysiological study. *PLoS ONE* 9(10):e109839
- Zhang G, Tian L, Chen H, Li P, Ristaniemi T, Wang H, Li H, Chen H, Cong F (2017) Effect of parametric variation of center frequency and bandwidth of morlet wavelet transform on time-frequency analysis of event-related potentials. In: Chinese intelligent systems conference. Springer, pp 693–702
- Zhou G, Zhao Q, Zhang Y, Adali T, Xie S, Cichocki A (2016) Linked component analysis from matrices to high-order tensors: applications to biomedical data. *Proc IEEE* 104(2):310–331



**PV**

**SIGNAL PROCESSING TECHNIQUES FOR EVENT-RELATED  
POTENTIALS: FROM SINGLE-WAY TO MULTI-WAY  
COMPONENT ANALYSIS**

by

Guanghui Zhang, Xueyan Li, Xiulin Wang, Wenya Liu, Yongjie Zhu, Xiaoshuang  
Wang, Reza Mahini, Rao Fu, Zheng Chang, Timo Tiironen, and Fengyu Cong  
2021

To be submitted

Reproduced with kind permission of Authors.

